Title

Development Method For an Astronaut-Powered Laundry Machine

Author

Arends, Andrew

Publication Date

2024

Peer reviewed|Thesis/dissertation

Development Method For an Astronaut-Powered Laundry Machine

By

Andrew Robert Arends

Thesis

Submitted in partial satisfaction of the requirements for the degree of

Master of Science

in

Mechanical and Aerospace Engineering

in the

Office of Graduate Studies

of the

University of California

Davis

Approved:

Stephen K. Robinson, Chair

Donald L. Margolis

Donald P. Land

Committee in Charge

2024

Contents

List of Figures

List of Tables

Abstract

Development Method For an Astronaut-Powered Laundry Machine

Without a precedent to laundering clothes off-Earth, a preliminary solution is required to develop a spaceflight laundry machine capable of operating in various gravity fields. With this thesis' proposed solution, human exercise to power an agitating bladder, a closed-loop hydraulic system, and a wastewater sensor suite provide a desirable environment for quantifying waste-mass transfer away from textiles while minimizing textile damage. Bond Graph Theory is used to model the proposed solution and to evaluate how human-power and valve configurations affect the system's cleaning performance. Bond Graph simulation results reveal preliminary performance metrics and hardware significantly impacting the machine's performance. A human-powered laundry machine prototype and model are essential for maturing the technology to Spaceflight readiness.

Acknowledgments

Thank you, Dr. Mark Sivik, from the Procter & Gamble Company, for your insight on detergent research.

To my mother, father, and brother, I want to express my gratitude for all the support and encouragement you have shown me over the years as I worked on this thesis and made difficult career and life decisions.

Thank you to all the Human/Robotics/Vehicle/Integration and Performance Laboratory members at the University of California, Davis, for their scientific and engineering excellence that contributed to this thesis and the communal environment they created.

Chapter 1

Introduction

1.1 Motivation

From language to preferred diets and workout regimens, human spaceflight programs have addressed fundamental behaviors of humans, except for a frequent activity thousands of years old. Laundering textiles is inherently human and something essential to human life. Leaving Earth's gravity for prolonged periods rapidly deteriorates the human body, requiring astronauts to exercise for multiple hours during a twenty-four-hour period to avoid long-term health risks and maintain in-flight performance. An extended exercise period saturates textiles with perspiration, dead skin, and other bodily fluids. Exposure to human excretions for prolonged periods also poses a health risk to the human body. Future spaceflight operations must address storing contaminate-saturated textiles and donning clean textiles while off-Earth to mitigate health issues.

The dirty textiles go where the humans go. Off-Earth surface activities, such as showering and horizontal sleeping, will require laundering towels and sheets. Multi-day transits between planetary bodies and future Low Earth Orbit (LEO) tourism programs must also address contaminated garments. Spaceflight textiles consume volume, add mass, and require the forethought of handling and replacing once soiled. From a logistical spaceflight stance, it is not practical to continually discard and resupply exercise clothing during an extended duration mission. During a 3-year mission to Mars without textile laundering, each crew member may go through about 210 kg (460 lbs.) of textiles, with attendant launch and transport costs.[1] Furthermore, the prolonged impacts of lunar and martian regolith on spaceflight

textiles have yet to be observed, which makes current deep-space textile logistics planning conservative and uncertain.

This thesis proposes using human exercise as power input, wastewater recycling, adjustable agitation rates, and feedback metrics for textile cleanliness to address the generation of soiled textiles off-Earth, regardless of the local gravity field.

1.2 Research Questions

Our guiding research questions to build a fundamental development method for machine design are:

1. What factors are required to launder textiles on Earth?
2. What are the characteristics of laundry mass dynamics?
3. How to measure general textile cleanliness?
    (a) What are cleanliness metrics?
    (b) How do we measure the metrics?
4. Machine design in the context of the spaceflight environment.

Chapter 2

Literature Review

2.1 Overview

There is no precedent to reliably laundering textiles off-Earth; however, the collective human knowledge of laundering textiles has identified a few core aspects of the laundering environment for off-Earth living. The objective of laundering clothing is to transport waste matter away from textiles. Traditional laundering environments combine water, heat, mechanical agitation, and chemicals in a complex combination of time-dependent rate-driven relationships. Contaminants naturally diffuse out of textiles submerged in water, and more waste can be removed (dispersed) by deforming textile weaves with mechanical power from hydrodynamics, abrasion, and fiber flexing. The mechanical actions promote the rolling-up of oils off textiles, penetration and chemical degradation of attached particulates, and the solubilization and emulsification of the washing fluid. Hard and pre-contaminated water plays a significant role in the overall laundering efficiency regardless of water, energy, chemical, and textile combination. After a long washing period without replacing the washing fluid, the redeposition rate of waste from the water back onto the textiles is negligible.[2–9] Furthering the complexity of laundry, the waste-textile combination is an essential factor in the contaminate mass dynamics.

Depending on how waste enters and interacts with textiles, specific laundering environments (i.e., machine configurations) become more impactful. Textile wastes are either soluble, saponifiable, emulsifiable, or inert. Soluble waste readily dissolves in water, saponifiable waste contains lipids that react with alkalis to become soluble soaps, and emulsifiable waste

does not react with alkalis and is often petroleum-based. Inert waste consists of abrasive particles such as lunar regolith. Waste-mass enters fiber matrices through the siphoning of dirty water and textile-waste collisions. Waste is held in place by Van der Waal's forces, chemical bonds, and the location of waste relative to fabric cores (the microfibers at the center of fiber bundles). Water dislodges waste primarily with kinetic impacts and dipole moments. The closer the waste is to the fabric cores, the further away the waste is from the water flow path, thereby lowering the probability of waste detaching from textiles during the laundering process - the general laundering length scales and this Stagnate Core phenomenon are illustrated in Figure 2.1 and 2.3 respectively. In addition, if large pores are present in the textile's fabric weave, as shown in Figure 2.1, water flow increases through the textile and increases the likelihood of waste removal.

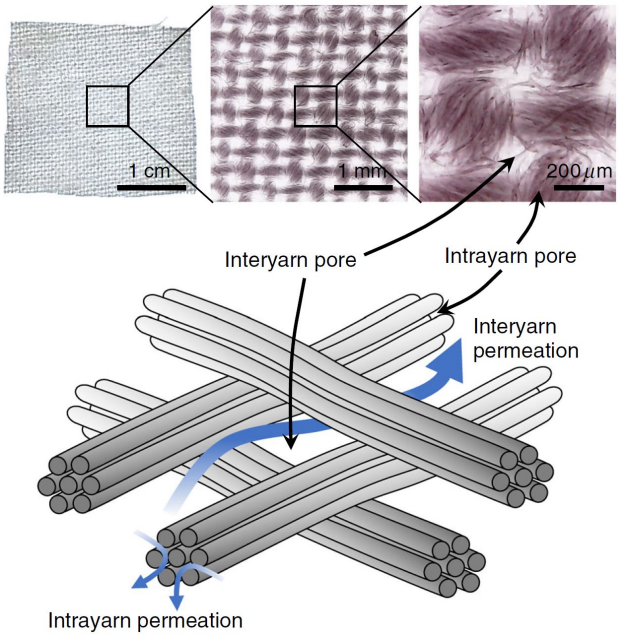

Figure 2.1: Typical length scales of textile weaves, pores, and fabric bundles with dense inner cores.[10]

Textile material properties influence washing fluid absorption, abrasion resistance, and flexibility. Materials that swell reduce the water flow path area and the waste's overall diffusion and dispersion rate. Regardless of configuration, an average rate of waste removal can be determined over time (see Section 2.3). Deviations from the relationship occur due to the changing laundering environment (e.g., adding detergent, rinsing with cold water, or

having impulse agitation instead of continuous); regardless, most waste removal occurs within the first twenty minutes of laundering.[6–9] No work found in literature addresses how altered gravitational fields will impact a laundering process and the end cleanliness of laundered textiles.

In a constant 1-g field without a pressure differential, gravitational forces overcome stagnant water surface tension forces, and the free surface of the resting water can be assumed to be normal to the gravity vector. The reduction of the gravity vector magnitude enables the surface tension of stagnated water to be the dominating force.[11] Because gravitational fields generate a potential energy field for matter, calibrated systems perform suboptimally if the gravity field changes, i.e., the head acting on hydraulic reservoirs changes, the pipe fluid dynamics change, the equilibrium point of mass-spring-damper systems changes, and the loading from masses change. Because the local gravity field directly affects mass dynamics, material stresses, and strains, biomechanics, and bioprocesses in living organisms change in spaceflight, leading to organism (astronaut) atrophy.

Over extended periods of non-Earth gravity levels, simple exercise machines counter human body atrophy. The prominent degradation of human bodies in spaceflight occurs in the first four months, with the cardiovascular, musculoskeletal, and muscle systems being impacted the most by the removal of Earth's gravity.[12] Humans' legs, hips, and lower back are especially susceptible to reduced bone tissue and muscle density, strength, and volume due to the lack of loading on the legs while off-Earth. Aerobic and resistive exercise can improve red blood cell count and skeletal structure to combat cell atrophy. Countering atrophy is vital to promoting adequate in-flight crew mission performance, safe Earth reentry, and post-flight recovery.[12–16] Due to the importance of exercise off-Earth and spaceflight resource management, exercise machines gain mechanical robustness from simple low-volume and mass designs for maintenance, usage, and vibration isolation. Many Spaceflight exercise machines struggle to achieve a relatively low-mass and volume configuration. Frequent spaceflight exercise produces liquid perspiration and other waste that contaminate and produce biohazard-ridden textiles that are not laundered, which is why off-Earth laundering is needed.

This review discusses laundry mechanics, textile cleanliness evaluation methods, and

capturing human-power in spaceflight. First, References [10, 17–20] suggest high-frequency fiber flexing and clean flowing water being the best promotors of waste transfer off textiles. Next, to quantify general cleanliness during a laundering process, References [21–27] suggest observations of electrolyte, organic, and particulate waste transported away from textiles. Lastly, considerations to convert human energy to mechanical work in spaceflight are explored.[1,11–16,28–30]

2.2 Laundry Mechanics

Textile agitation in the laundering environment is needed to remove a majority of waste-mass because agitation is how most energy enters the system; however, agitation methods have different waste-removing capabilities. References [10, 17, 18] evaluate and compare the four most common laundering textile agitation methods (swelling, hydrodynamics, abrasion, and fiber flexing) using the same cleanliness quantification method (fluorescent microscopy). The main difference between abrasion and fiber flexing is the direction of the applied force with respect to the fabric core axis. As shown in Figure 2.2, abrasive agitation has most of the applied force off-set and parallel to the fabric core axis, thereby generating a shearing force along the core. Fiber flexing has most of the applied force along the fabric core axis thereby generating a buckling-type response. In an ideal buckling, all fibers will bend so they do not interact with neighboring fibers. Therefore, the ideal agitation method has ideal buckling (fiber flexing) and no abrasion - real agitation applications generate both phenomena.

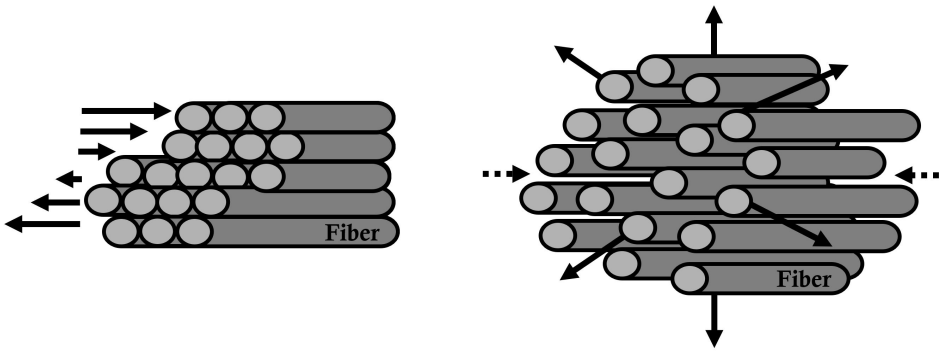

Figure 2.2: Abrasion (Left) and ideal fiber buckling phenomena (Right) on fabric cores.

Fiber-flexing is the best promoter of contaminate removal in non-detergent environments with and without pre-soaking (a method to either have a time-dependent or independent textile pore size, which affects initial contamination dispersion rates). References [19] and [20] expand on the idea of agitating with high-frequency inputs to promote a higher rate of waste transfer by controlling the frequency at which the fibers are flexing. The controlled agitation methods conclude that rapidly pushing and pulling the fiber matrix at high frequencies (over one kilohertz) with clean rinsing water encourages textiles to efficiently expel waste attached to the inner fiber cores in only a few minutes.

Although Ref. [17] evaluated abrasion agitation with a Tribometer in a controlled environment, the cleanliness results depended heavily on the water temperature, and textile damage results were not reported, which was unexpected and reaffirmed Ref. [18] and [10]'s trade space on controlled agitation. In general, abrasive water-textile impacts and textile fiber flexing break van der Waal's forces holding inert particulates and promote the rolling up and release of liposoluble (saponifiable and/or emulsifiable) waste.[18] Although Ref. [18] concluded that soaking and hydrodynamics do not cause significant fiber flexing or abrasion, Ref. [10] found that clean water promotes a highly favorable concentration gradient for waste transfer away from fibers comparable to hydrodynamics. Both Refs. [17] and [18] note the potential textile damage of highly abrasive laundering, but they do not mention damage potential from high-frequency flexing of the fibers.

Unlike agitators and impellers, ultrasonic laundering controls fiber flexing; Refs. [19] and [20] agree that the asymmetrical collapse of pressure waves near the textile during ultrasonic laundering compresses and stretches the fibers in a buckling-type motion. As a result, ultrasonics promotes waste dispersion into the water, but most energy goes into deforming the textiles and not displacing a bulk of wastewater from textiles.[19] Ref. [20] addresses the high-frequency abrasion concerns of Ref. [19] by performing a detailed inspection of the textile's structure before and after laundering. Ref. [20] found that ultrasonic-laundered fibers had better tensile strength retention in both the warp (transverse weave) and weft (longitudinal) directions with minimal abrasive and cavitation damage compared to commercial agitation machines. Reducing textile damage is another important consequence to consider in the laundering environment. As shown in Figure 2.3, high-frequency flexing textile fibers increase

their water contact area over a longer period, increasing the area and opportunity for waste to transfer off the textile into the nearby water.

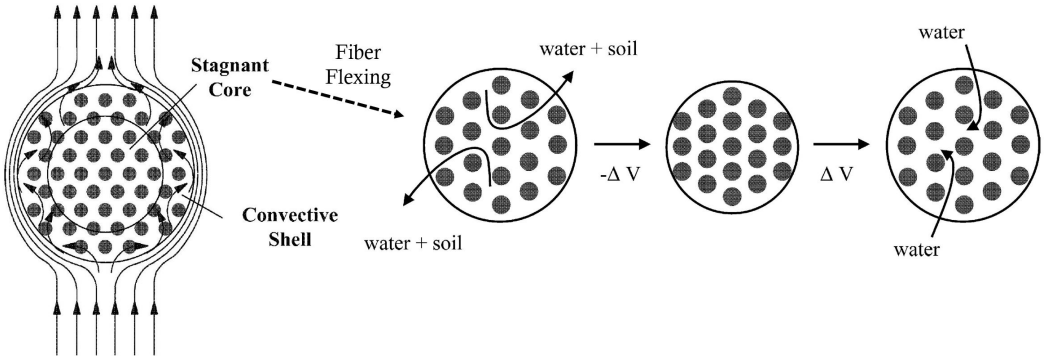

Figure 2.3: Fiber bundle convection regions and fiber response to flexing (the changing of available volume for contaminate transfer into water). Image modified from [19].

In summary, Refs. [10, 17–20] showed that waste transfer depends on how the textiles are being deformed (axial or shearing force) and water cleanliness. Refs. [10, 19, 20] expand upon Refs. [17] and [18] by concluding that high-frequency fiber flexing (axial loading) rapidly pushes and pulls fibers in such a way that waste transfer rates increase and textile damage decreases compared to other traditional mechanical agitations. However, Refs. [2–10, 17–21] do not acknowledge the waste-removing ability of fiber flexing at high frequencies with a continuous clean crossflow to promote waste transfer and transport, and they used limited textile-waste combinations due to the cleanliness quantification method.

2.3 Cleanliness Quantification

Different combinations of water quantity and temperature, agitation method and duration, and added detergents all impact the laundering environment and, therefore, the cleanliness of textiles. The rate-dependent environment makes the quantification of textile cleanliness nontrivial. References [21–25] discuss laboratory reflectance, irradiation, and image analysis methods that quantify the amount of waste remaining on a single type of fabric or textile after laundering. To address the shortcomings of labor-intensive analysis of waste-textile combinations, References [19, 26, 27] evaluate cleanliness through generalized methods targeting waste's chemical characteristics in a textile bulk instead of single article combinations. Understanding the chemical properties of waste embedded in textiles leads to

observing wastewater for cleanliness quantification.

Different wavelengths of light used in spectroscopy and microscopy methods can be used to quantify how much specific waste is on a textile; Ref. [21–25] show how different models can be used at different wavelengths to quantify the cleanliness of a single waste-textile combination. The Kubelka–Munk equation based on reflectance (visible light microscopy) measurements is a widely used model and it requires the dying of textile waste and knowledge of textile-waste combinations to calibrate measurements.[10,17,18,21,24,25]

Alternatively, irradiating waste with near-infrared, ultraviolet, or x-ray wavelengths for quantification can be done without dying waste beforehand. Nonetheless, textile-waste combinations are also needed to calibrate measurement systems. Irradiation can also damage textiles after prolonged exposure.[21,22,24,25] A noninvasive measurement approach can be made with image analysis due to the periodic nature of textile structures and image converting algorithms. It is possible to undertrain algorithms with improper textile-sensor alignment and combination.[23,24] Another noninvasive measurement method was derived by Reference [26] to observe ozone decomposition rates within an agitation chamber containing a bulk of textiles. Reference [26] found that the decomposition rate of ozone is proportional to the amount of organic waste within the chamber; however, regardless of the model fit, ozone is consumable, leaves a residual smell on textiles, does not clean textiles, and does not interact with non-organic molecules. Keeping with practicality, References [10, 17, 18, 21–25]'s cleanliness quantification methods of a single article are also not favorable because typical laundering consists of a bulk of textiles, often containing a few different materials with different and unsteady contaminate removal rates.

The mass of the contaminants must enter the laundering water for the textiles to become cleaner, so observing laundry wastewater may serve as a viable cleanliness quantification method. Figure 2.4 shows all the time-dependent laundering elements affecting the contaminate removal rate. A primary contaminant expected in the spaceflight environment is perspiration due to crew exercise requirements. Perspiration consists of salts, proteins, and lipids; therefore, a method to quantify the amount of salt, biofluid, and inert particulates in the wastewater may provide the necessary information to determine how clean a bulk of clothes is becoming during the laundering process.

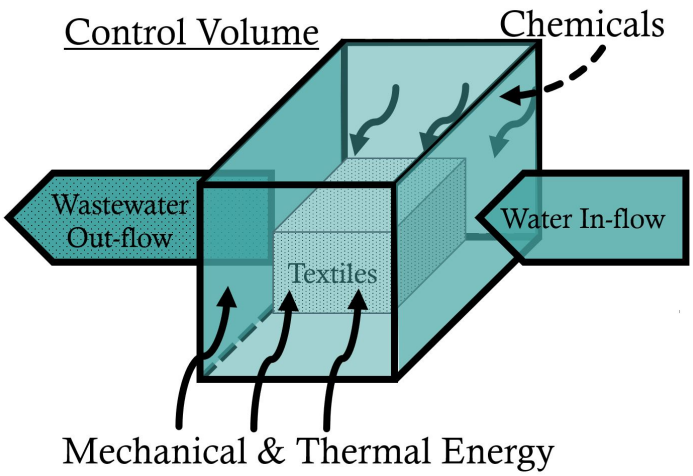

Figure 2.4: Laundry control volume showing all the time-dependent variables affecting the contaminate mass removal rate

References [19, 26, 27] outline ways to quantify the electrolytes and organic waste in wastewater. Reference [27] found that off-the-shelf technology could quantify small concentrations of cortisol and amine biomarkers (common organic molecule structures in human-produced biofluids) in a saline solution (wastewater) with an ultraviolet spectrometer without preparing the sample for analysis as you would with laboratory equipment. Although a linear relationship between biofluid concentration and absorbance was determined, there was no mention of the sample flowing through the optical path. Reference [27]'s method would also incorporate the abundance of particulates that occlude the ultraviolet light. Another consideration in this wastewater monitoring method is that References [21, 22, 24–27] did not attempt to quantify waste removal while laundering.

A generalized relationship between the laundering environment and time-to-cleanliness is needed to determine when equilibrium (i.e., no more contaminates removed from textiles for the given laundering environment) is reached. Reference [6–8] use a log-log relationship, Equation 2.1, to describe the amount of waste removed during laundering where $\bar{c}$ is the average concentration of waste removed, $\frac{\Delta c}{\Delta t}$ is the change in concentration over time, k is the waste removal rate coefficient normalized to $\frac{\Delta c}{\Delta t}$, and n is the kinetic order (a term derived by [6–8]). Equation 2.1 cannot always be physically realized because waste values may combine different units (e.g., Volts from a conductivity sensor and pH from a pH meter) for convenience, and n is not always an integer. Therefore, $\bar{c}$ must be unitless.

$$\overline{c} = \left(\frac{1}{k} \cdot \frac{\Delta c}{\Delta t}\right)^{\frac{1}{n}} \tag{2.1}$$

Although derived from domestic machine agitation, specific textile contamination methods, and specific textile-waste combinations, the general first-order kinetics equation (Equation 2.1) still holds across other experiments.[6–8] The change in waste concentration over time can be calculated with water monitoring sensors (e.g., conductivity, turbidity, hardness, pH). In general, the kinetic order depends on the textile-soil combination, the agitation method, the amount of energy imparted on the textiles, how the textiles were contaminated, and the absorptivity of the textile. Various experiments empirically found that the kinetic order ranges from 0.85 to 1.24.[6–8] The main uncertainty with this model is with the waste removal rate coefficient because it is a function of time and the same factors as the kinetic order. Continual water monitoring and calculating of a waste removal rate model may reduce the uncertainty during the laundering process; however, other time-dependent factors must be considered in the context of the laundering machine and environment (This is explored further in Section 4.5 within the context of a proposed solution).

In closing, there are many methods to quantify the cleanliness of laundered textiles, with some methods providing more practical applications. For example, References [21, 22, 24, 25] provided high-accuracy methods at the expense of labor and textile damage, while References [19, 26, 27] generalized the quantification from measuring the waste transport out of textiles. Overall, conductivity measurement combined with irradiated wastewater observation may provide the best solution in modeling and quantifying textile bulk cleanliness during a laundering process with [6–8]'s generalized time-to-cleanliness equation. Still, the spaceflight environment may further limit cleanliness quantification sensing and modeling.

2.4 Spaceflight Application

Laundering textiles on Earth started with humans exerting power, and off-Earth laundering can take a similar approach. Frequent exercise is required off-Earth; References [28–30] review the design of off-Earth exercise machines and their ability to keep humans healthy. Last, Refs. [1, 11–16] are reviewed with Ref. [28–30] in the context of applicable spaceflight engineering and operations principles. The synthesis of off-Earth exercise and generating fa-

vorable laundering environments offers a preliminary solution to spaceflight laundering with human-power in alternating gravity fields.

Currently, there are many spaceflight exercise machines in use and development. Reference [29] evaluates the International Space Station's (ISS) Advanced Resistive Exercise Device (ARED), while References [28, 30] explore compact pully driven exercise machines. Although the ARED can exercise twenty different muscle groups and provide a two-point skeletal loading, it is far too large and power-consuming for current exploration vehicles, and it does not have an aerobic exercise component.[29] Reference [30] evaluates a similar two-point skeletal loading system with a resistive bar attached to pulleys; likewise, there is no aerobic capability. Reference [28]'s Miniature Exercise Device - 2 is a compact motor and pully device for aerobic and resistive exercise capable of getting the user to achieve a maximum heart rate for an extended period; however, the resistive component cannot effectively load skeletons. Regardless of the mechanism, the context of spaceflight dictates the hardware needed to capture and convert human power.

A general spaceflight exercise hardware framework emerges from References [1, 11–16, 28–30]. Due to the critical health risks of musculoskeletal atrophy, exercise machines must have robust, simple, and serviceable designs. From the user's perspective, the interface and machine operation should be intuitive. The exercise motion envelope and machine stowage volume need to be as small as possible, and vibration isolation systems may be needed.[1,11–16,28–30] Each topic mentioned thus far in capturing human-power sets a context to design and evaluate a human-powered spaceflight textile laundering machine. None of the reviewed articles mention converting human-power in spaceflight into hydraulic- and electrical-power.

2.5 Conclusion

A combined exercise and textile laundering machine to maintain human health in space is possible in the context of current research. Compared to domestic machine agitation methods, high-frequency fiber flexing improves waste transfer from textiles and reduces textile weave damage. Clean water rinsing also promotes a high rate of waste transfer. A minimal resource consumption solution to quantify cleanliness uses conductivity sensors and

an appropriate wavelength spectrometer to analyze textile wastewater in real time until an equilibrium state is reached.[21–27] Lastly, in spaceflight, the simultaneous working out and laundering conserves astronaut time within a twenty-four-hour period, and the device performs two health risk reduction activities within a small volume that can travel with an astronaut wherever they go.[1,11–16,28–30] Without a precedent to compare, a preliminary machine and accompanying model are needed to evaluate a development method to launder textiles off-Earth with human-power.

Chapter 3

Proposed Solution

Designing a spaceflight exercise and textile laundering machine requires evaluation of the Literature Review, insight into determining spaceflight engineering design requirements, and forethought of how the machine will be treated throughout its lifetime. The machine presented and evaluated in this thesis *does not* address the detergent aspect of laundry due to the complexity and heritage of laundry chemistry. It is assumed that if any chemicals enter the machine in the future, the compounds will be compatible with hydraulic material, fibers, and sensors. High-temperature water (+80°F) will also be neglected in the laundering methods because it is a main driver of chemical reactions. What follows are initial design decisions and conceptual layout (Figure 3.1) for a preliminary spaceflight exercise and textile laundering machine, which will be evaluated with Bond Graph Theory in Chapter 4.

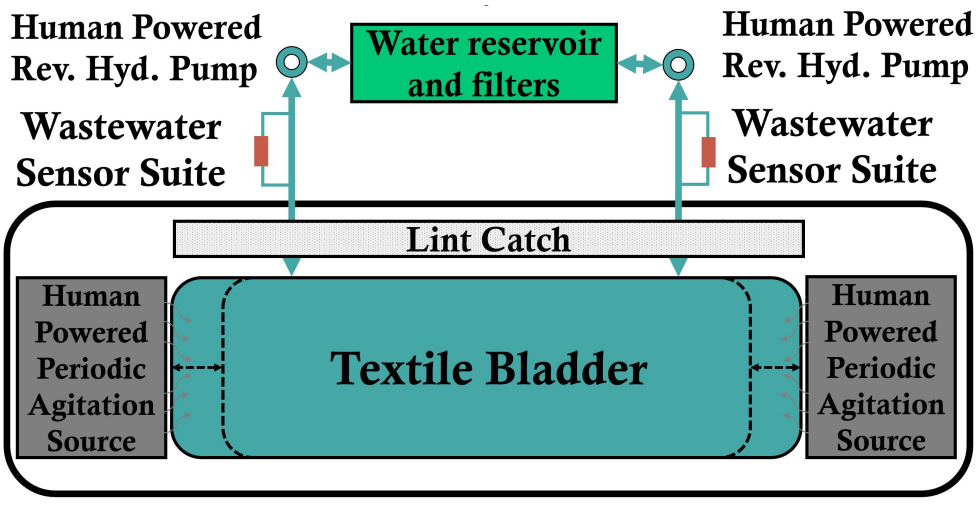

Figure 3.1: Spaceflight exercise and textile laundering machine concept diagram.

3.1 Problem Statement

The problem is how to effectively and sustainably launder clothes during spaceflight. Earth-based laundering provides a foundation for understanding the basics of removing waste mass from fabrics, but the context (a one-g environment) of laundry is not sufficient to design a spaceflight machine. To address this problem, this thesis documents technology development for a spaceflight exercise and laundering machine by simultaneously developing a prototype and mathematical model.

3.2 Spaceflight Approach

Current lunar exploration plans outline the different spacecraft and habitats humans will live in while traveling to and from the Moon. In addition, there are multiple LEO space stations under development for tourism. Each spacecraft, habitat, and station have unique habitable volumes, Environmental Control and Life Support Systems, and available resources during a mission. Therefore, an initial laundering machine for spaceflight should be a standalone machine to reduce design complexity, ensure nominal operation regardless of habitable volume, and enable machine transport between different spacecraft, habitats, and stations. The constant resource across all the space environments is crew time, which is scheduled according to maintenance and mission-related tasks.

A consequence of frequent astronaut exercise is deposits of salt, sebum, perspiration, and dead skin onto textiles. A machine that simultaneously acts as an exercise and laundering machine has the potential to counter human atrophy, mitigate the risk of crew exposure to biohazard-ridden textiles, and reduce the logistical allocations of clean textiles on resupply efforts at no extra cost to astronaut time during nominal operation. The machine is expected to travel with astronauts during their spaceflight experience, so the machine needs to operate nominally in various gravity fields without significant alterations, regardless of workout regimen or power input. For 2024-related near-term goals, the gravity environments are Earth, the Moon, and microgravity. A robust and straightforward exercise machine can be designed around pedals, and simple off-the-shelf devices can convert rotary motion into translational motion, electrical potentials, and hydraulic pressure differentials. The arms and upper body of the user are the primary targets due to physically demanding extravehicular activities.

3.3 Laundering Methods

Controlling fluids in microgravity is not trivial, so wetting and wringing textiles in microgravity may also not be trivial. In the proposed design, a flow-through flexible bladder ensures all textiles are submerged in water before laundering. A flexible bladder can be filled with water and textiles simultaneously, even if the volume of textiles changes. A flexible bladder can also compress the textiles within to wring out wastewater. In addition, the ability for water to flow through the bladder may produce favorable waste concentration gradients between the textile and water. To further the favorable concentration gradients, the water system will include a reservoir and filters to hold clean water and remove the waste-mass entering the water from laundering. Last, the value of water in human spacecraft cannot be underestimated, so the water system is also designed to be closed-loop - negating the water exiting the system from damp clothes and the eventual system *top-off* to maintain laundering performance. Furthermore, the laundering water system filters should be designed to be replaced. Replacement of filters is expected when the sorbents are saturated and or the main textile contaminates change (e.g., perspiration, a soluble compound, is the expected primary contaminate in lunar orbit while lunar regolith, an inert compound, is the expected primary contaminate on the lunar surface).

The frequency of filter replacement is dependent on many factors. A primary factor is the amount of contaminants and lint in the water, which depends on the agitation method and fiber type. As noted in Section 2.2, an efficient combination of fiber flexing and abrasion can be achieved with ultrasonic agitation with piezoelectric transducers. Ultrasonics is a practical method for on-Earth laundering, but it may not be well suited for spaceflight applications because it consumes lots of electrical-power, generates lots of vibration, and requires specialized equipment to repair and replace.

All considered, ultrasonic agitation may not fit well into spaceflight resource allocation and maintenance practices. Instead, a mechanical agitation device is proposed to mimic the pressure waves of ultrasonic agitators but at a much lower frequency. Dubbed here as *periodic agitation*, such an agitation method consists of traditional mechanisms to convert rotary motion into oscillating motion with low amplitudes and frequencies above two Hertz (limit determined by domestic machine agitation rates[19]) to generate fiber-flexing pressure

waves with no electrical-power and maintenance similar to bicycle repair with common hand tools. The initial periodic agitation method, which is explained further in Section 4.2, consists of the water-textile bladder mounted on a tilt plate mechanism driven by a crank-follower mechanism with an adjustable shock absorber so users can adjust the machine to meet exercise and laundering needs.

3.4 Wastewater Monitoring

All the waste removed from textiles must enter the washing water, which means that quantifying waste-mass in the water informs how clean a bulk of textiles are becoming. Equation 2.1 can be used with the wastewater observation approach to model the amount of contaminates removed from textiles because it was derived from previous theoretical work and empirical data. The kinetic order (n) of the equation will remain empirically bound, and the unknowns of the model are the waste removal rate coefficient and the change in waste concentration over time.

The main uncertainty with this model is with the waste removal rate coefficient (k) because it is a function of time and the same factors as the kinetic order. In other words, the waste removal rate highly depends on the laundering environment's small and large temporal and spatial scales. Continual monitoring and calculating the waste removal rate may reduce the uncertainty during the laundering process; however, other time-dependent factors must be considered. Without chemical aids in this proposed solution, the agitation method and power input significantly determine the waste removal rate coefficient.[6–8] Fundamentally, cleaning imparts momentum on waste to overcome binding forces; the periodic agitation and crossflow through the agitation bladder are the sources of momentum imparted on textile waste. Therefore, the agitation and hydraulic system dynamics significantly affect the waste removal rate coefficient. Another dependency of the waste removal rate coefficient is that the water flowing through the agitation bladder transports waste away from textiles, changing the waste concentration gradients near textiles and the probability of waste detaching from textiles. Lastly, the volume of textiles within the agitation bladder also affects the waste removal rate coefficient because the agitation bladder is of a relatively fixed volume and filled with water during all laundering cycles; therefore, with fewer textiles, there is more water

interacting with the textiles to remove waste.

Equation 3.1 is an initial approach to combining all the factors affecting the waste removal rate coefficient in the context of the proposed solution. Overall, a single value in Hertz is determined, normalized, and scaled to the change in concentration over time measurements. First, three ratios are multiplied: the ratio of textile volume to agitation chamber volume, the ratio of water volume flux to agitation chamber volume in Hertz, and the ratio of mechanical momentum to hydraulic momentum interacting with textiles. The ratios identify how much energy is added to the textiles and the water. The known variables, which can be measured with appropriate sensors and devices, needed to calculate the waste removal rate coefficient are the volume of the agitation chamber, the volume of textiles in the flow path, the volumetric flowrate of water through the agitation chamber, the tilt plate momentum, and the water momentum in the agitation chamber. The only unknown is the exponent (k_s); this exponent is used to scale the rate value to the magnitude of the contaminate measurement and it requires experimentation to determine. The exponent is expected to be affected by the material properties of all the fibers within a bulk of textiles, the intensity of water-textile surface tension forces generated by the local gravity field, unobserved time-and-rate dependent laundering phenomena, and the fusion of the known variables.

$$k = \left(\left(\frac{\text{Textile Volume}}{\text{Chamber Volume}} \right) \left(\frac{\text{Water Volume Flux}}{\text{Chamber Volume}} \right) \left(\frac{\text{Mechanical Momentum}}{\text{Hydraulic Momentum}} \right) \right)^{k_s} \quad (3.1)$$

The last part of the general cleanliness model, Equation 2.1, is the change in waste concentration over time ($\frac{\Delta c}{\Delta t}$). Measuring the concentration of waste in the water is determined by the chemical characteristics of the waste. Salt deposits on textiles are expected, and due to the high solubility of salt, a conductivity sensor can be used to quantify the relative concentration of dissolved salt (electrolytes). Human-produced organic waste is typically highly water soluble and contains primary amine groups; an appropriate wavelength can be selected for wastewater spectroscopy. Appropriate wavelength irradiation provides enough activation energy to interact with primary amine groups; the chemical bonds absorb the emitted radiation. The Beer-Lambert Law, Equation 3.2, can then quantify the abundance of particulates (e.g., dead skin, lint, and regolith) that occlude and primary amine groups (e.g., perspiration, sebum, and microbes) that absorb emitted radiation by calculating the

absorbance as a function of emission and detected intensity on the other side of a flow cell, as shown in Figure 3.2.

$$\text{Absorbance} = log_{10}\left(\frac{\text{Emmitted Intensity}}{\text{Detected Intensity}}\right) \tag{3.2}$$

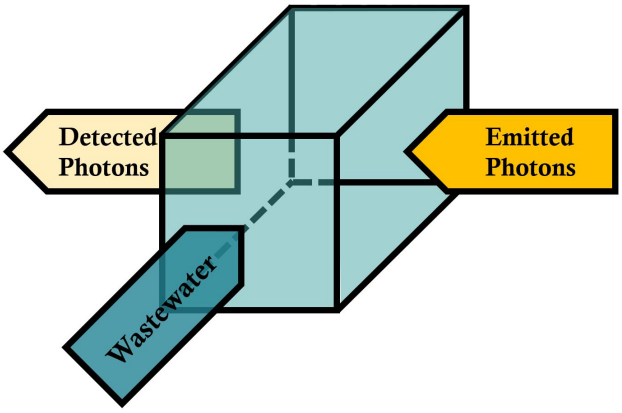

Figure 3.2: Flow cell utilizing the Beer-Lambert Law.

To address spaceflight human- and electrical-power requirements and rapid device development desires, commercial off-the-shelf (COTS) hardware is selected to observe and measure the waste-mass entering the washing water. COTS conductivity sensors can be created with nichrome wire and an analog-to-digital converter. COTS diode spectrometers that target primary amine groups consist of a single wavelength Light-emitting Diode (LED) between 180-320 nm[27], a photon detector operating in the same wavelength range as the LED, and an analog-to-digital converter. The specific LED and photon detector wavelengths presented in this solution can be serviced and replaced. The spectrometer housing includes dark chambers to reduce outside photon interference, electronic protection from water, and lenses and windows with more than 90% transmittance at 1 nm to focus the emitted photons through the water and onto the sensor detection area. The combination of flow rate, acceleration, rotation speed, water conductivity, and water absorbance measurements provide the data needed to quantify the cleanliness of a bulk of textiles during a laundering process. Figure 3.3 shows a preliminary layout of the sensors needed to quantify cleanliness. All the sensors used in the prototype machine are summarized in Table 5.1 of Section 5.2

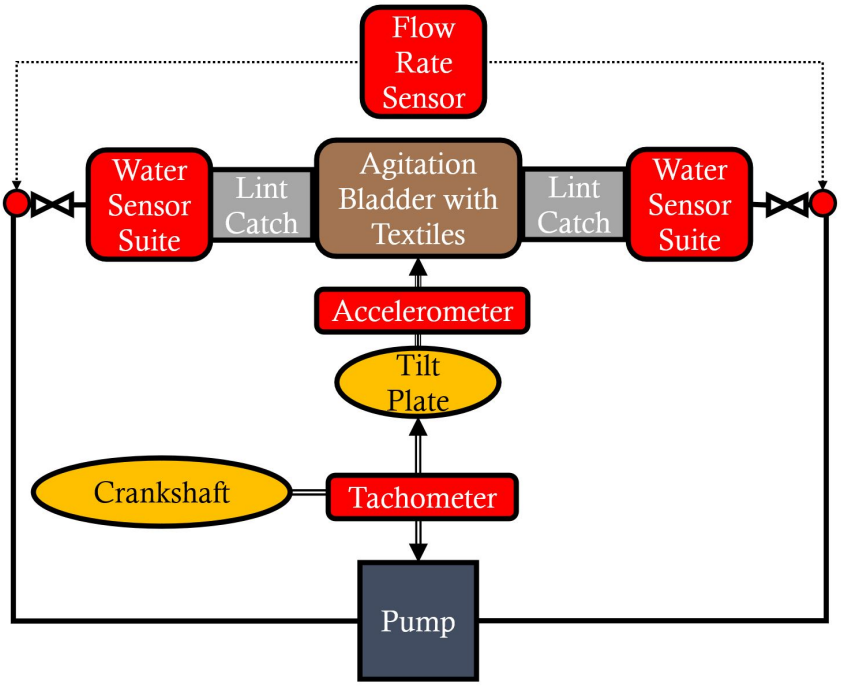

Figure 3.3: Concetpual system layout for determining textile cleanliness. Sensors in red.

Chapter 4

System Concepts and Modeling

4.1 Bond Graph Theory Overview

The device concept takes human power as an input and converts the power into chemical concentration gradients and mechanical, electrical, and hydraulic power sources to launder textiles. Bond Graph Theory[31] models the device's coupled mechanical, electrical, hydraulic, and chemical properties to inform concurrent device design and hardware selection. Understanding how humans power and configure the device is essential to predicting textiles' overall waste removal rate. The Bond Graph model can be adjusted and verified from hardware acquisition, device manufacturing, and sensor data collection to produce an accurate waste removal rate model. Modeling can also be used to inform astronauts about their current laundering efforts and indicate if the laundering processing should be changed. Furthermore, because humans are unique in their physical abilities and body functions (before and after microgravity alterations), a machine and model capable of adapting to these conditions is a goal of this technology development process.

Bond Graph (BG) modeling is a graphical method built from the first principles of energy conservation that shows the flow of information and energy between system elements.[31]The BG technique produces a topological graph that uses interconnected elements to generate the system's codable first-order differential state space. The elements are linear, nonlinear, differential, and/or algebraic equations solved with computer code to obtain time and frequency domain responses. The BG method reduces the time needed to derive entire sets of equations for a dynamic or static system while producing symbolic and numeric transfer

functions for a concurrent controller and hardware design and selection. Only a few BG symbols model entire systems; each symbol interacts with power. Traditional BG power is composed of two conjugate variables defined by the International System of Units: an effort ("across variable") and a flow ("through variable") where the product of the variables has the units of power in Watts.

Figure 4.1 shows the most common symbol, a power bond. The horizontal line joins two elements, the arrowhead indicates the direction of positive power, and the vertical line is a causal stroke. The causal stroke indicates the direction of the effort signal and dictates the element's consecutive relation. Causal strokes cannot be assigned until the entire system is modeled and simplified; this is an essential step because equations are derived depending on the model's causality.

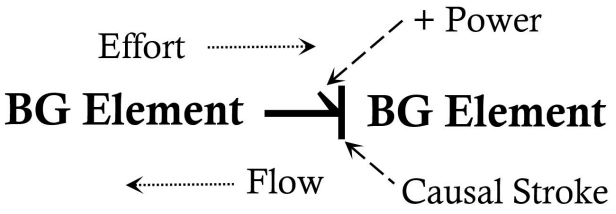

Figure 4.1: Bond Graph Power Bond Structure

Domain	Effort (e)	Flow (f)	Momentum(p)	Displacement(q)
Mechanical Translation	Force **N**	Velocity $\frac{m}{s}$	Momentum **N·s**	Displacement **m**
Mechanical Rotation	Torque **N·m**	Angular Velocity $\frac{rad}{s}$	Angular Momentum **N·m·s**	Angle **rad**
Electrical	Voltage **V**	Current **A**	Flux Linkage **V·s**	Charge **C**
Hydraulic	Pressure $\frac{N}{m^2}$	Volumetric Flow Rate $\frac{m^3}{s}$	Pressure Momentum $\frac{N \cdot s}{m^2}$	Volume m^3
Chemical	Chemical Potential $\frac{J}{mol}$	Molar Flow $\frac{mol}{s}$		Molar Mass $\frac{g}{mol}$

Table 4.1: Bond graph power domain state variables with units in bold.

A BG element's constitutive relation, or mathematical model ($\Phi()$ functions in Table 4.2), are functions of an inputted effort or flow, a generalized momentum (integral of effort), and/or displacement (integral of flow) state variable. Table 4.1 summarizes the different state variables used in BG Theory. BG elements are ideal and are either a power source, dissipator, conserver, converter, or junction. Ten additional BG elements commonly used are summarized in Table 4.2. BG models oscillate when inertia and compliance elements interact, motion decays occur when inertia and resistance elements interact, and energy dissipation occurs rapidly when compliance and resistance elements interact.[31]

Effort and flow source elements have one permissible causality because they enforce an effort or flow. Compliance and inertia elements utilize displacement and momentum variables in an integral or derivative causality. It is generally preferred that compliance and inertial

Element	Symbol	Description	Math Relationships
Effort Source	S_e	Enforces effort value over time	$e(t) = E(t)$
Flow Source	S_f	Enforces flow value over time	$f(t) = F(t)$
Resistor	R	Power dissipating	$e = \Phi_R(f)$ $f = \Phi_R^{-1}(e)$
Compliance	C	Power storing	$e = \Phi_C^{-1}(\int^t f\,dt)$ $f = \frac{d}{dt}\Phi_C(e)$
Inertia	I	Power storing	$e = \frac{d}{dt}\Phi_I(f)$ $f = \Phi_I^{-1}(\int^t e\,dt)$
Transformer	TF	Power Conserving and or Converting	$e_2 = m \cdot e_1$ $f_1 = m \cdot f_2$
Gyrator	GY	Power Conserving and or Converting	$f_1 = r \cdot e_2$ $f_2 = r \cdot e_1$
Zero-Junction	0	Common effort distributor	$\sum f_i = 0$
One-Junction	1	Common flow distributor	$\sum e_i = 0$
Active Bond	Information bond with zero power consumption.		

Table 4.2: Common Bond Graph elements.

elements are in integral causality. Because of power conservation and enforced relationships, the transducers and gyrators have two causality configurations. Zero-junctions may only have one causal stroke nearest the junction to enforce the common effort. One-junctions may only have one causal stroke away from the junction to enforce the common flow. A simulation can be coded with system diagrams, element constitutive relations, a causally correct BG, and an ordinary differential equation solver.

Things considered while modeling are that oversimplifying models may lead to poor results, no model can be exactly like a real system, it is the modelers' discretion to assign signs and determine how much system detail is required, and lastly, the initial state of the system and future time history of the input signal must be known. The construction, simplification, and use of multiple energy domain BG models require further explanation, reading, derivation, and examples outside this thesis' scope, but readings used to develop the following BG model can be found in References [31–38].[1]

4.2 Mechanical Domain

Many mechanical devices can be powered using the human-power assumption from Section 3.2. An initial mechanism to produce periodic agitation (the method discussed in Section 3.3) is an agitation plate, as shown in Figure 4.2. The plate must impart oscillatory momentum of at least 2 Hertz onto textiles submerged in washing fluid.[19] Although a shaker plate or linear actuator can produce higher frequency vibrations, the hydraulic connection points would experience more mechanical fatigue than a rotating connection point at the hinge. It is also assumed that more deformation of the agitation bladder causes a higher waste removal by imparting a load gradient across the textiles. Such gradients would produce localized regions of convection in the washing fluid. A tilting plate mechanism can impart momentum in two orthogonal directions; if washing fluid flows through the textiles in another orthogonal direction, washing fluid momentum is imparted on the textiles in three principal axes. Figure 4.3 shows a tilt plate mechanism BG with elements that have linear constitutive relations. Note that the inertia of the tilt plate (I: J_{tp}) depends on the volume of washing fluid in the bladder capacitor element (q_a).

[1] All the numeric and element information for the Bond Graph simulation for the astronaut-powered laundry machine can be found in Appendix A and B.

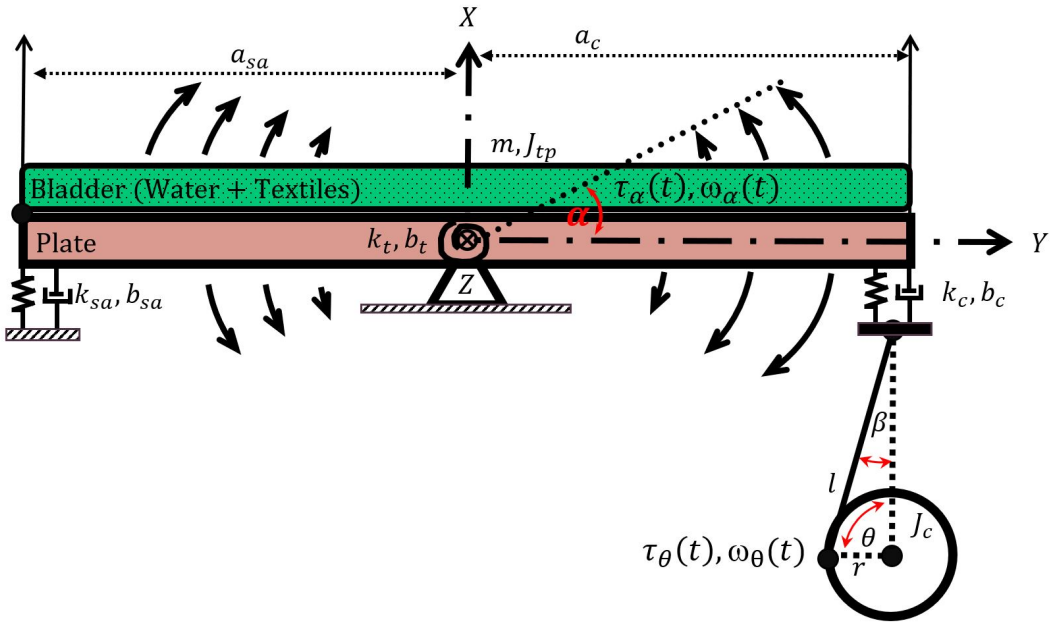

Figure 4.2: Tilt plate mechanism concept.

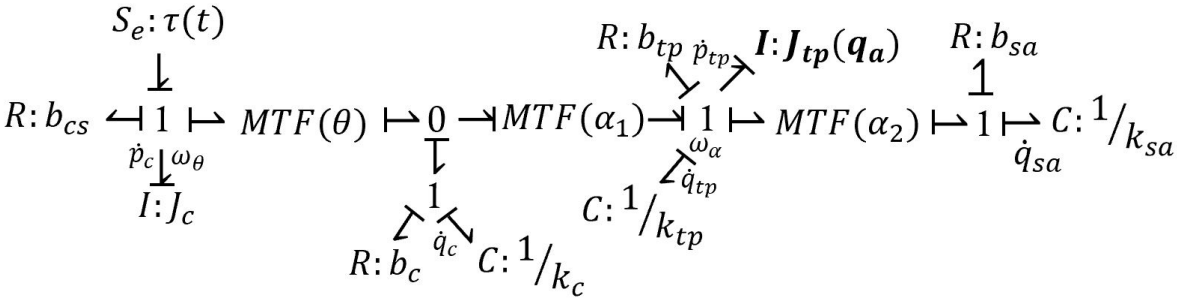

Figure 4.3: Bond Graph of the tilt plate mechanism concept.

4.3 Hydraulic Domain

The crankshaft of the mechanical domain may also be attached to a reversible hydraulic pump to power the system outlined in Figure 4.4. Hydraulic valves, porous plugs, and small passageways in the hydraulic system are modeled as energy-dissipating BG elements. The washing fluid filters can be modeled as a spherical particle-packed bed, and the lint catch as a cylindrical fiber-packed bed. Modified Ergun Equations can be used as constitutive relations to determine the pressure drop across the packed beds as a function of a uniform volumetric flow rate.[39] Pressure and volumetric flow rate measurements are needed to model the resistive functions and coefficients. Therefore, the washing fluid filters and lint catches of Figure 4.4 can be modeled as linear resistors in Figure 4.5 to reduce model complexity initially. The flexible agitation bladder is a compliant BG element dependent on the amount of textiles inside. Assuming the bladder is a thin-walled pressure vessel, the stress and strain relationship in the thin-walls can relate the bladder's volume change to the pressure change.[31] The reservoir and filters also act as a compliance BG element. The BG model reveals a parallel variable resistor structure, which aligns well with meeting user needs: these include a reservoir and filter loop to clean the washing fluid and an agitation bladder and reservoir loop to fill and remove washing fluid from the agitation bladder, and the valves can also be used to increase power feedback (exercise resistance) by choking the pump.

A few BG modeling assumptions need to be addressed before model adjustment and verification. First, fluid dynamics are not modeled because an analytical solution is not known for this system. Therefore, a finite-element method is used to model the fluid dynamics. Second, the flow is assumed and modeled as incompressible and quasi-one-dimensional due to each pipe segment's small cross-sectional area and length. Third, an *average* fluid velocity is used because the velocity profile is unknown spatially and temporally before gravity effects are considered. Fourth, resistance effects due to large area changes, wall friction, and pressure drops due to gravity are initially neglected until experimental data is available. Fifth, with the previous assumptions, a *Bernoulli resistance*[31] effect must be considered when fluid dynamic pressure is converted to static pressure at certain system regions. Fifth, the control volume does not have an inertial reference frame when considering micro-gravity effects. Last, it is assumed that the amount of trapped air is negligible.

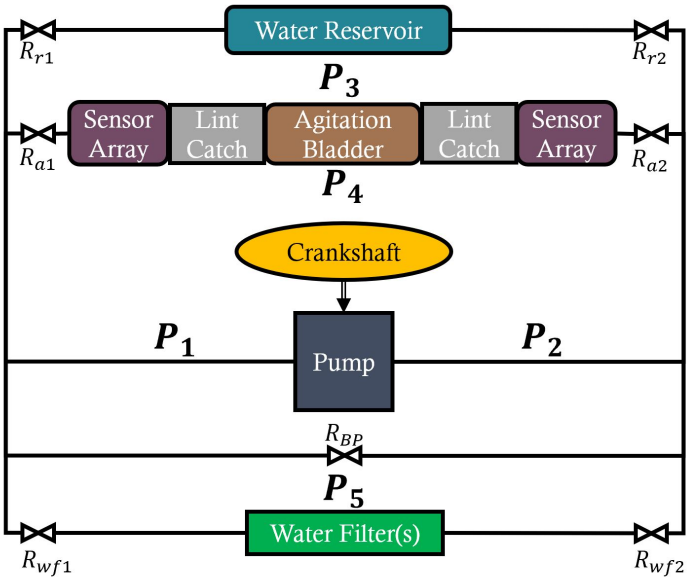

Figure 4.4: Hydraulic system concept.

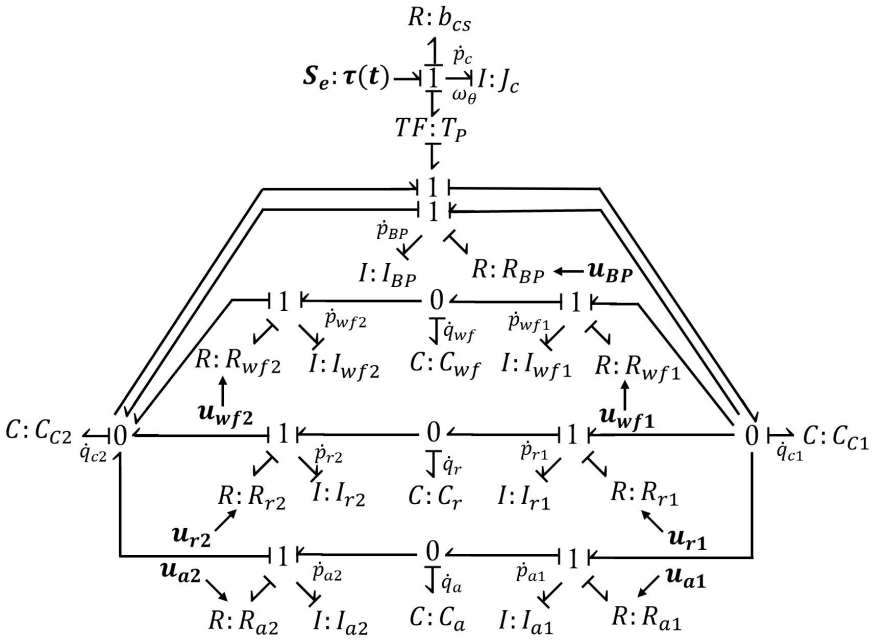

Figure 4.5: Bond Graph of the hydraulic system concept.

4.4 Electrical Domain

The crankshaft may also be attached to a permanent magnet generator to power the microcontroller pinout in Figure 4.7. Evaluating the electrical schematic reveals that a minimum of approximately 2W is required to power the entire electrical system. With a minimum flow requirement, it is of little impact if power-conserving elements are neglected in the initial Bond Graph. Therefore, only the resistive effects of the electronics will be considered in the construction of the electrical BG in Figure 4.6 at this time.

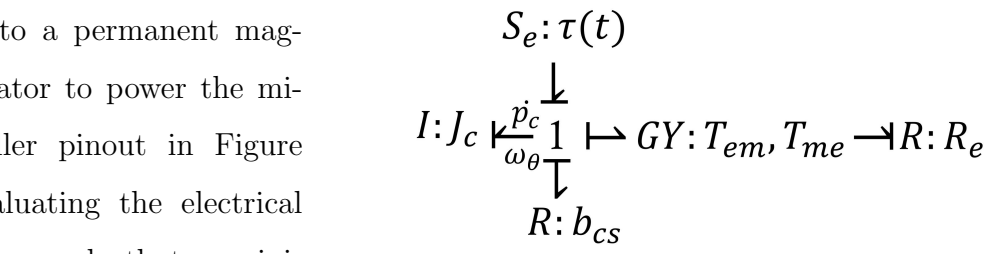

Figure 4.6: Bond Graph of the electrical system concept.

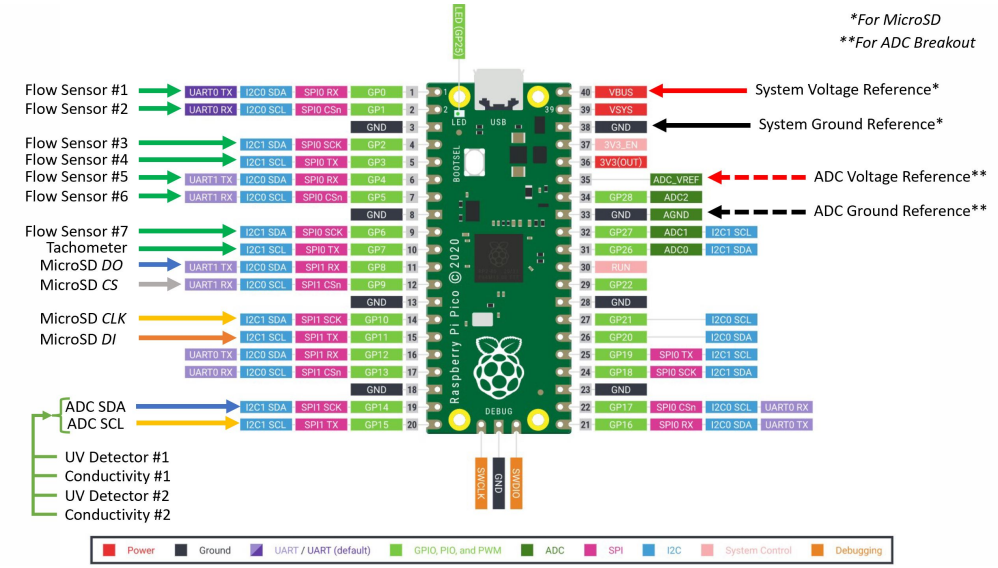

Figure 4.7: Microconroller pinout.

4.5 Chemical Domain

In addition to the chemical domain information in Table 4.1, chemical BGs use absolute temperature and pressure as efforts and the time derivative of entropy and volume as flows.[35] The information in Table 4.1 is determined using Gibbs Free Energy functions and assuming constant pressure and temperature. Chemical BGs use scalar flow to conserve mass within

the system, not moles of chemical species, which are used as transformer elements that interact with other BG elements. Chemical processes and reactions couple solvent diffusion, electrolyte interactions, and hydrodynamic dispersion, resulting in very complex BGs outside the scope of this BG application.[35] For this application, chemical BGs are used to determine the mass of waste dissolving into the washing fluid, with the textiles acting as a waste source and the filters acting as a waste sink. Figure 4.8 reports a basic diagram of the chemical domain.

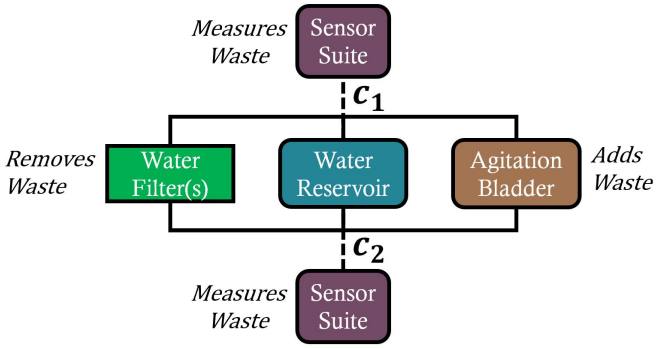

Figure 4.8: Chemical domain concept.

BG modeling issues arise when considering the state of a chemical process. The chemical reactions and processes dissipate energy as a function of reaction rate and chemical affinity, meaning that a multiport resistive BG element is required to complete the set of simulation equations and the causality of the BG model. It is also known that chemical reaction forward and reverse reaction rates are not always equal or linear when in far-off equilibrium conditions; this leads to an unsymmetrical resistor constitutive matrix Jacobian. Eventually, the reaction reaches equilibrium; in other words, the forward and backward reaction rates are equal, and the Jacobian of the chemical BG resistor constitutive matrix is symmetrical, indicating that the BG topology needs to change.[35] Reliability changing BG model topology during a simulation is also outside the scope of this application and is the primary justification for foregoing a traditional chemical BG branch in the machine's model.[31–38] Moreover, the complexity of the laundry environment also motivates the foregoing of chemical BGs. To overcome chemical BG modeling difficulty, Equation 2.1 can be derived to model the waste removal from textiles instead of using chemical domain constitutive relations, and Equation 3.1 can be used to determine the waste removal rate coefficient.

The BG variables needed to calculate the waste removal rate coefficient are the volume of the agitation chamber (V_A), the volume of textiles in the flow path (V_T), the volumetric flowrate of washing fluid through the agitation chamber (q_A), the tilt plate momentum (p_{tp}),

the washing fluid momentum in the agitation chamber (p_{a1}), and a scaling exponent (k_s) to account for textiles with various types of fabric, gravity effects, unknown time-and-rate dependent laundering processes, and the fusion of the data from the sensor suite. Active bonds extend from corresponding mechanical and hydraulic BG elements to transmit the required information to compute Equations 2.1 and 3.1. The final mean soil removal value is the average of Equation 2.1 with an upper (1.24) and lower (0.84) kinetic order value.[6–8] It is important to note that Equation 3.1 is specific to the laundering environments discussed so far, and currently, there are no datasets to reinforce the derived model.

4.6 Initial Model Simulation

All the sub-subsections and information outlined so far in Chapter 4 result in Figure 4.9, a BG of the exercise and textile laundering machine concept to relate human torque input to the rate of waste transported away from textiles in the agitation bladder. To generate a model response, the causality of the BG model needs to be assigned and evaluated. It can be seen in Figure 4.9 that all the effort source elements are outputting an effort, all the inertial and compliance elements are in their preferred integral causalities, all the transformers and gyrators comply with energy conservation and conversion, and all the junctions have the proper configurations for setting common efforts and flows. Although causality is assigned appropriately to the BG model, the model's behavior must be initiated and actuated with realistic values for a proper performance evaluation.[2]

It is assumed that there is no washing fluid in the agitation chamber when the machine starts because the bladder in Section 3.3 only contains clothes at the start. To account for this state, the initial simulation values need to reflect the amount of washing fluid in the bladder and reservoir; all state initial values can be found in Table A.3. The initial volume of washing fluid in the agitation bladder is the total volume (one gallon) of the bladder minus the volume of textiles (a full bladder without textiles is assumed to be the reference point). Likewise, the washing fluid reservoir has a net positive volume to reflect the fluid to be added to the agitation chamber. The input signal to the simulation reflects the torque

[2]The full derivation of Astronaut Powered Laundry Machine can be found in Appendix A, in addition to the BG element constitutive relations and parameters used in the simulation. The parameter values used for the initial simulation results in this Section (Figures 4.10, 4.11, 4.12, and 4.13) can be found in Table A.2.

generated by a human or other power source. Two types of input signals were used for an initial evaluation: constant and periodic. The constant signal reflects a mechanism that produces constant and continuous step-type torque through a Heaviside-type function. The periodic signal mimics human pedaling because, at an instant in the pedal's rotation, the human-exerted force vector is perpendicular and co-planar to the pedal's rotational axis. An underlying Heaviside-type function reflects the buildup to the maximum pedaling torque. The magnitude of the torque signals was determined by the distance between the center of rotation and pedal mounting location (approximately a foot-long moment arm) and a human's ability to push a ten-pound-force weight with each arm for an extended period.

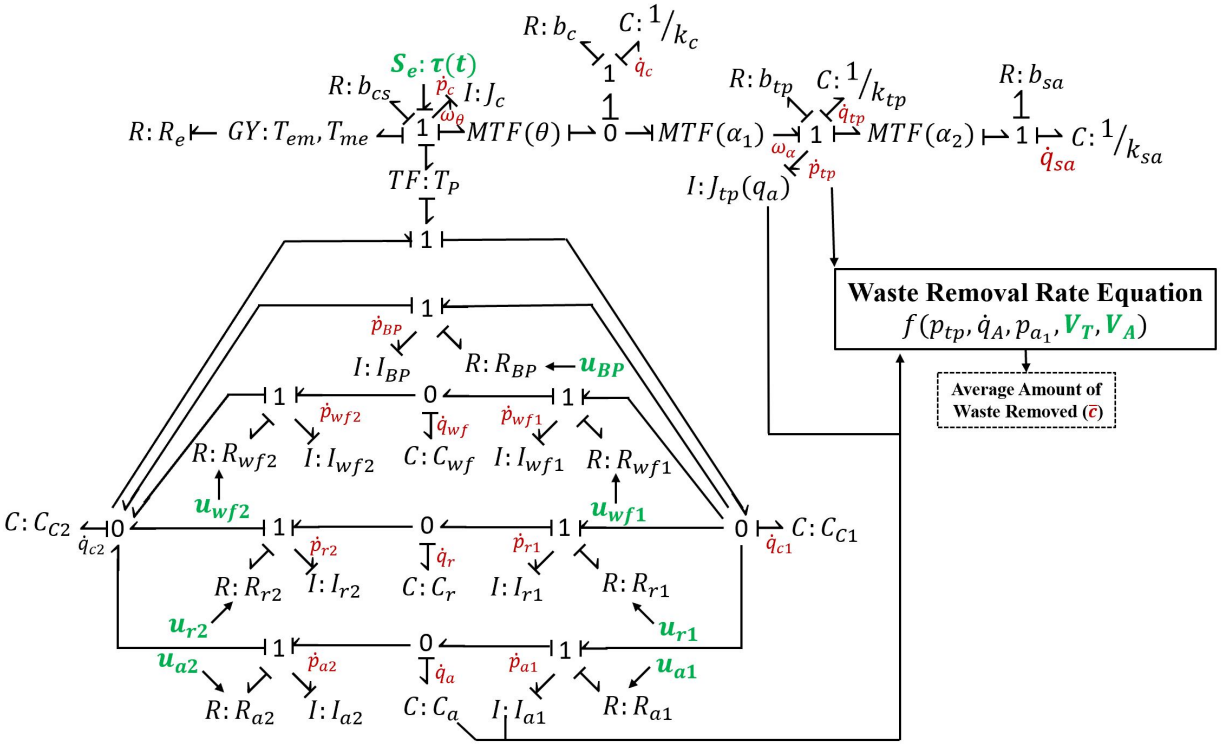

Figure 4.9: Bond Graph of an astronaut-powered laundry machine concept with inputs in green and outputs in red.

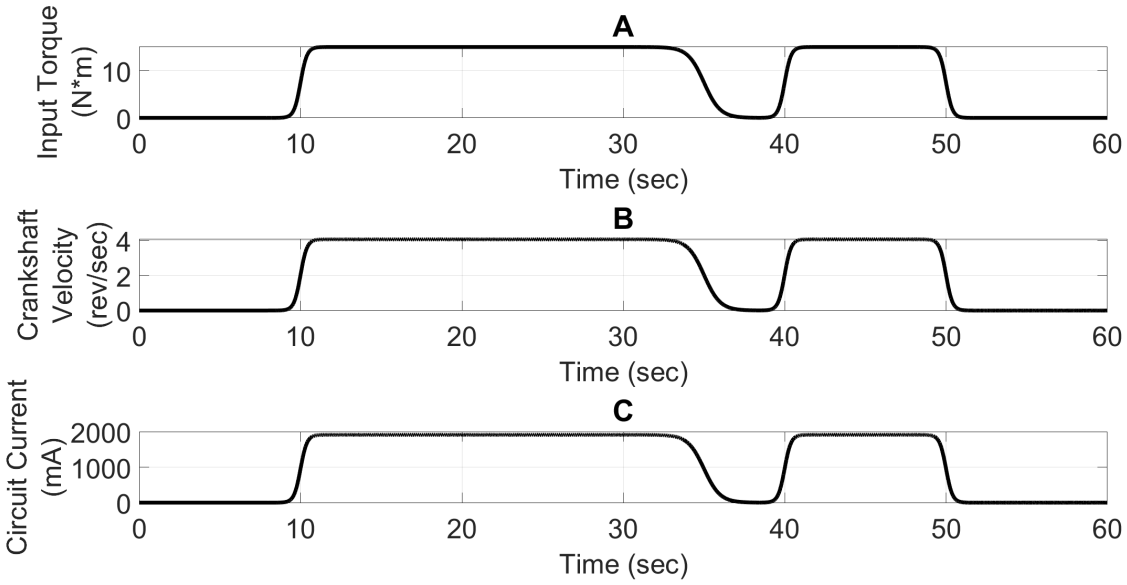

Figure 4.10: Bond Graph results for Heaviside-type Torque input, crankshaft speed, and electrical current outputs.

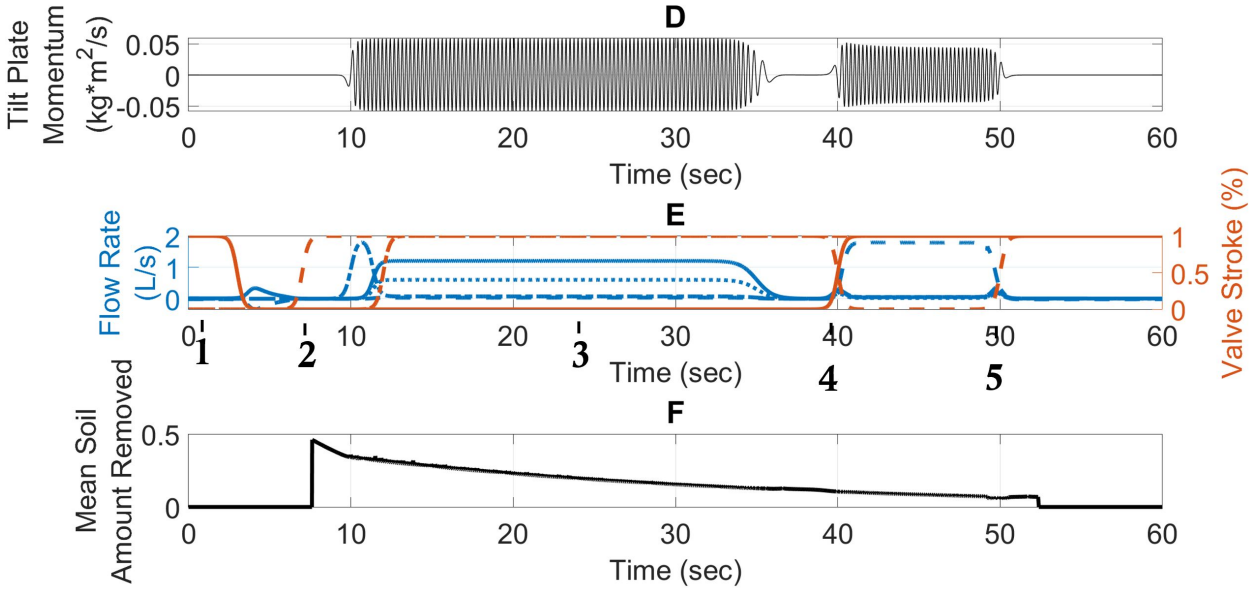

Figure 4.11: Bond Graph results for Heaviside-type Torque input: Tilt plate maximum momentum, flow rates for each flow path as a function of valve position, and generated electrical current outputs.

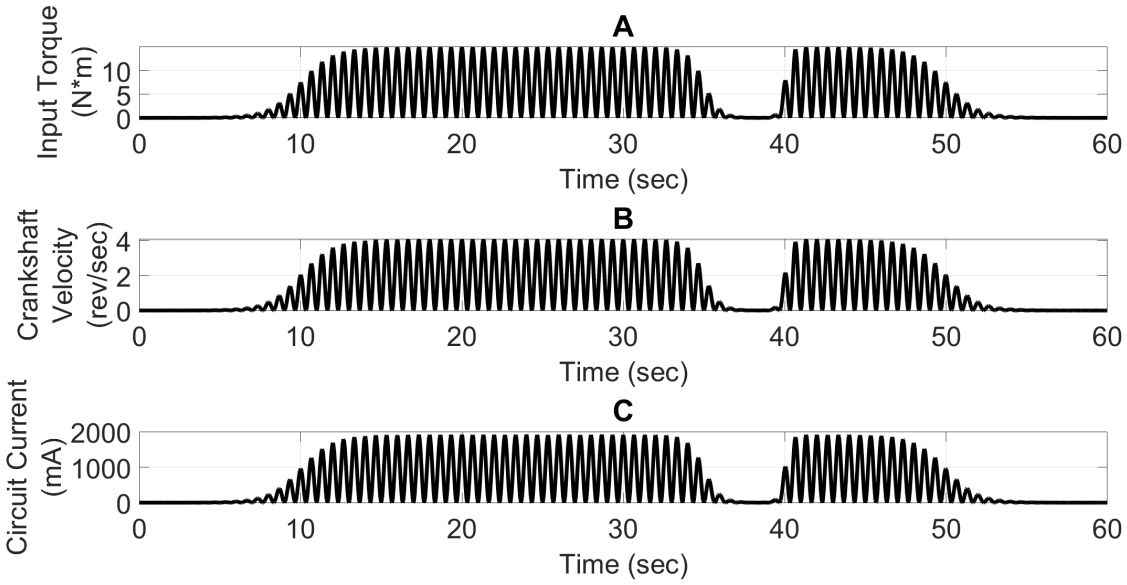

Figure 4.12: Bond Graph results for Sinusoid-Heaviside-type Torque input, crankshaft speed, and electrical current outputs.

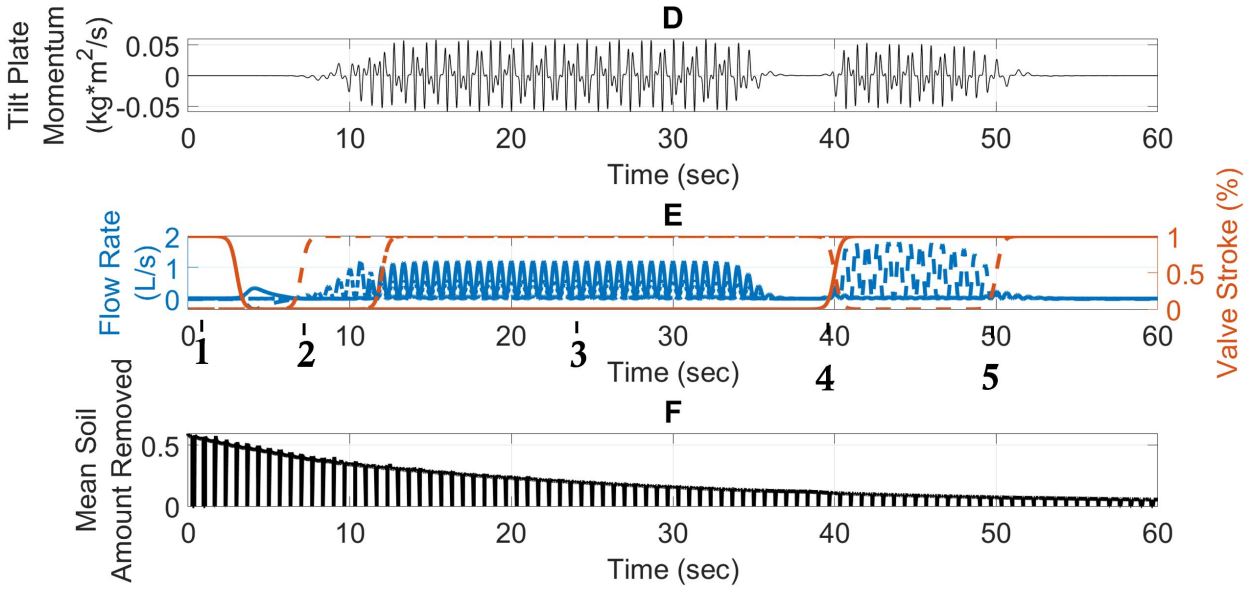

Figure 4.13: Bond Graph results from Sinusoid-Heaviside-type Torque input: Tilt plate maximum momentum, flow rates for each flow path as a function of valve position, and generated electrical current outputs.

The BG model can be simulated with initial, parameter, and torque values. MATLAB was used for the BG simulation, although any coding language with an ordinary differential equation solver can be used. The first step in evaluating the results is to check the BG simulation model for Bounded Input Bounded Output (BIBO) stability, which was done, and not presented, with parameters that mimic real-world values and the same sinusoid Heaviside-type function approximation for both forward and backward pedaling acting on a variety of valve configurations. Six different valve configurations were used in testing: one with all flow paths open, one with all flow paths closed, and one with a single flow path open while the others are closed - All results were BIBO stable. The valve configurations were also tested as initial conditions and then again as functions of time during a non-zero torque input - All results were BIBO stable. With a BIBO model, the machine performance indicators can be calculated: input torque in Newton meters, crankshaft speed in revolutions per second, electrical circuit current in milliamps, agitation plate angular momentum in Newton meter seconds, the flow rate of washing fluid in each flow path in liters per second with respect to value positions, and the mean soil concentration removed. Note that the exponential decay rate of the unitless mean soil amount removed has been modified to a one-minute simulation instead of the empirically expected fifteen to twenty minutes.[6–8]

Figures 4.10, 4.11, 4.12, and 4.13 are the results of an initial BG simulation for an astronaut-powered laundry machine. The main difference between the two sets of results is that the constant torque input set shows the max values achieved in the periodic set that oscillates between the value and zero. The produced crankshaft speed is reasonable and follows the torque signal shape, as expected from the BG structure. Similarly, the current produced is reasonable in shape. However, the magnitude depends on the arbitrarily selected generator coefficients; electrical results are expected to change after a prototype is developed and analyzed. Another difference between the two result sets is the momentum generated at the edge of the tilt plate. The constant torque produces a typical sinusoidal shape with a constant frequency and an underlying exponential growth and decay similar to the periodic torque input signal. Conversely, the periodic torque signal produces a superimposed sinusoidal shape with underlying exponential growth and decay. This result reveals that constant torque inputs achieve a higher magnitude of time-rate-of-change in momentum transfer. The

periodic torque signals produce a less uniform time-rate-of-change momentum transfer. It is unknown which shape is desired for textile agitation. So, the torque input signal impacts laundering performance and may dictate a preferred valving configuration for the washing fluid.

The phases of Subplot E in Figures 4.11 and 4.13 show the flow rates and value positions; the magnitudes and shapes are acceptable for this low pressure and flow area system. The phases of the figures are as follows: Phase 1 is the release of reservoir washing fluid (dashed blue) to fill the vacuum sealed agitation bladder (solid blue), Phase 2 is the closure of reservoir valves (dashed orange) and bypass value (dotted orange) as a torque signal is applied to the system at ten seconds, Phase 3 is the steady state operation of the machine under the applied torque signal, Phase 4 is the closure of filter valves (dashed orange), the opening of the reservoir valves (solid orange), and the closure of one agitation bladder value to draw washing fluid out of the textiles (dot-dash orange), and Phase 5 is the closure of the open agitation bladder valve (dashed orange) and final ramp down and reconfiguration of the system for the following user. The mean soil removed is the primary metric (cleanliness quantification) of this machine development method. It will require further analysis due to the model's uncertainty and other unaccounted chemical phenomena in the laundering process.

The next step in the device's development was to create a prototype, where more advantages of Bond Graph Theory manifest themselves. From the laundry machine BG model, the measurable states can be determined. The selection and placement of sensors in the system correspond to the energy domain under observation and the state variables present in a BG. The mechanical domain requires two sensors: an accelerometer on the edge of the agitation plate and an angular velocity sensor for the crankshaft. The hydraulic domain requires nine sensors - a flow meter near each valve and an absolute pressure transducer on each side of the hydraulic loop. The chemical domain sensors are selected to characterize the state of the wastewater. A diode spectrometer quantifies the abundance of organics and particulates in the washing fluid, and a conductivity sensor quantifies the salinity. The next advantage of Bond Graph Theory is the identification of parameters impacting the desired performance. In the context of the proposed machine, the goal is to launder clothes efficiently with a high

momentum transfer rate from the tilt plate and flowing washing fluid to the soil attachment points on textiles. The parameters that can be evaluated in a hardware context for prototype development to reach the desired goal are summarized in Table 4.3. The BG model sets the initial approach to prototype development; after prototype development, the laundry machine BG model will be updated to reflect the prototype to simulate more accurate responses and predictions.

Variable	**Units**	**Description**
Mechanical Domain		
a_a	m	Distance from tilt plate hinge to crank arm mount.
a_{sa}	m	Distance from tilt plate hinge to shock absorber mount.
J_c	$kg \cdot m^2$	Inertia of crank shaft.
l	m	Length of crank arm.
l_{tp}	m	Edge length of square tilt plate.
r	m	distance from crank arm mount to crankshaft center of rotation.
Hydraulic Domain		
A_P	m^2	Area of hydraulic piping.
V_A	m^3	Volume of agitation bladder.
V_R	m^3	Volume of reservoir.

Table 4.3: Bond Graph parameters identified as the main impacts on simulated and prototype machine performance.

Chapter 5

Prototype Development

5.1 Approach

The machine prototype used to verify assumptions and approaches in the design and modeling process follows the conceptual Bond Graph domains discussed in Chapter 4: Mechanical, Electrical, Hydraulic, and Chemical. First, sensors are selected for each domain to measure the states of the Bond Graph model within the respective domain. Second, the data processing methods are discussed. Third, the sensors are calibrated to known values based on calibrated sensors or benchtop experiments. Last, subsystem testing for functionality and observation.

5.2 Sensors

Each subsystem's sensors are reported in Table 5.1 and discussed below. Three technical criteria were used in the COTS sensor selection: power consumption, analog signal capabilities, and MicroPython capabilities. After collecting data on all available sensors, budgeting, vendor reliability, and community support were considered before purchase. The power consumption of the sensors is 1.369 W and the Raspberry Pi Pico microcontroller consumes a maximum of 550 mW - the max electrical-power consumption of the machine is 1.919 W.

Sensor	Comm. Type	Power	Frequency	Qty.
Mechanical Domain				
Tachometer	GPIO	25 mW	6.3 Hz	1
Hydraulic Domain				
Flow Meter	GPIO	5 mW	20 Hz	5
Electrical Domain				
ADC	I2C	1 mW	128 Hz	1
MicroSD	I2C	8 mW	40 MHz	1
Chemical Domain				
Cond. Sensor	ADC	5 mW	50 Hz	2
Spectrometer	ADC	0.65 W	50 Hz	2

Table 5.1: Sensors and other electronics present in the machine prototype.

5.2.1 Tachometer

The tachometer (Figure 5.1) consists of an infrared emitter and detector diode side-by-side pointing at the same object. The constant emission of infrared reflects off a striped paper wrapped around the crankshaft. Due to infrared absorption on black surfaces, the striping allows for a high signal retention on white alignment and a low signal retention on black alignment. At high crankshaft speeds, the detected frequency of the pulse-width-modulated signals also increases. The detected signal is sent to the microcontroller through General-purpose input/output (GPIO) pins.

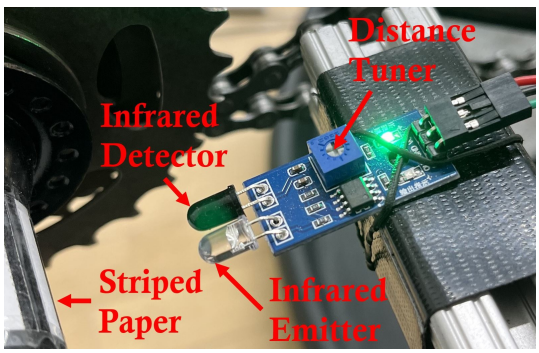

Figure 5.1: Machine prototype infrared tachometer.

5.2.2 Flow Meter

The flow meter (Figure 5.2) uses a mounted rotor (turbine) as a Hall sensor in the flow path. A circuit closes as the embedded rotor magnet passes an electromagnet outside the flow path. The pulsing circuit communicates with the microcontroller through GPIO pins.

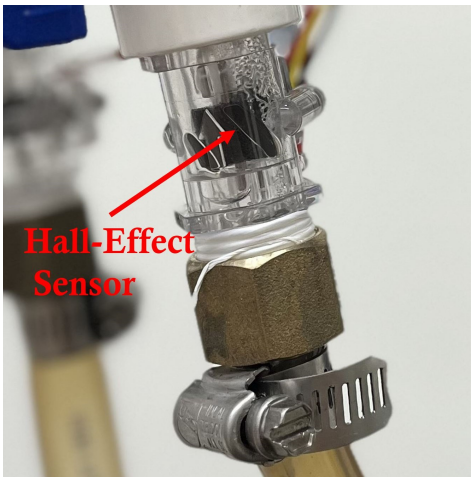

Figure 5.2: Machine prototype Hall Effect flow rate sensor.

5.2.3 ADC and MicoSD

An ADC (Figure 5.3a) breakout board communicates with the analog conductivity and diode spectrometer sensors. A microSD card (Figure 5.3b) breakout board stores the data generated during a laundry cycle. Breakout boards (small printed circuit boards converting analog signals to I2C signals for the microcontroller) reduce cable management complexity.

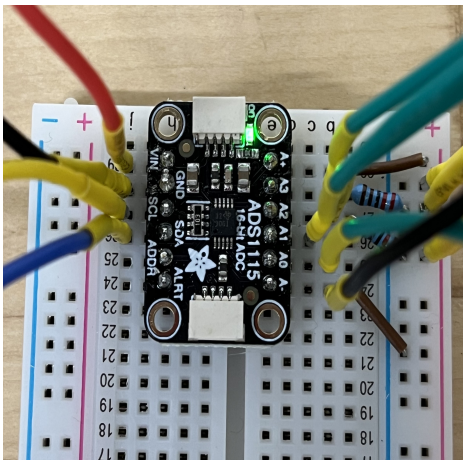

(a) Analog-to-digital converter.

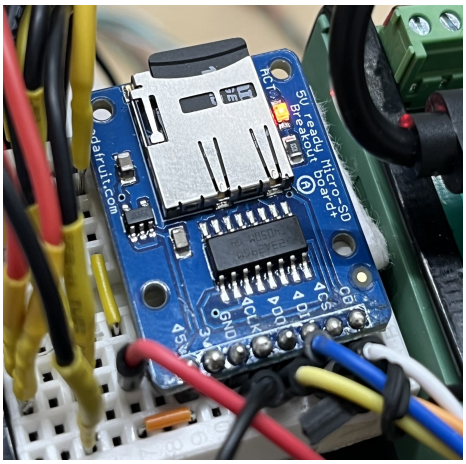

(b) MicroSD card reader.

Figure 5.3: Breakout board electronics used in the machine prototype.

5.2.4 Wastewater Sensor Suite

The conductivity sensor (Figure 5.4a) is hand-made and is composed of copper wire, a resistor, and two nichrome wire probes near each other that act as a voltage divider feeding into the ADC; the first resistance of the divider is dependent on the electrolytes within the water to connect the positive and negative nichrome wires.

The diode spectrometer is a light-emitting diode at 275 nm and an ultraviolet light detector breakout board that sends analog voltage signals to the ADC. The conductivity and diode spectrometer sensors are placed in a single body, making the Wastewater Sensor Suite (WSS), as shown in Figure 5.4b.

Figure 5.5 shows a diagram of the wastewater sensor suite. Three electrical devices and one optical device in the suite observe the half-inch diameter flow path. The suite was assembled using a waterproof marine adhesive sealant that is corrosion resistant (salts and oxidation) and ultraviolet light tolerant (will not become brittle after prolonged exposure). The conductivity sensor was placed inside a plastic housing, sealed, and placed in the suite housing to extend an eighth inch into the water, insulating the exposed nichrome wire from the aluminum housing. A through hole was created for the ultraviolet light path on two parallel faces of the housing. One face has the UV LED directly mounted and sealed to the housing (i.e., the protective window on the LED directly touches water). The other face has a countersunk hole for a 3D-printed mount for the UV detector breakout board and window. The optical device (circular UV window) is quartz glass capable of letting UV through infrared light pass with high transmittance (detectable photon intensity). The window also serves as a protective barrier between the wastewater and UV detector breakout board. The UV detector is placed behind the window facing the LED so that the diode spectrometer is normal to the flow path once the suite is assembled. The detector and window are adhered to the 3D-printed mount sealed in the countersunk hole. Once assembled, the housings are integrated into the machine with a suite on each side of the agitation bladder, as shown in the hydraulic system concept (Figure 4.4).

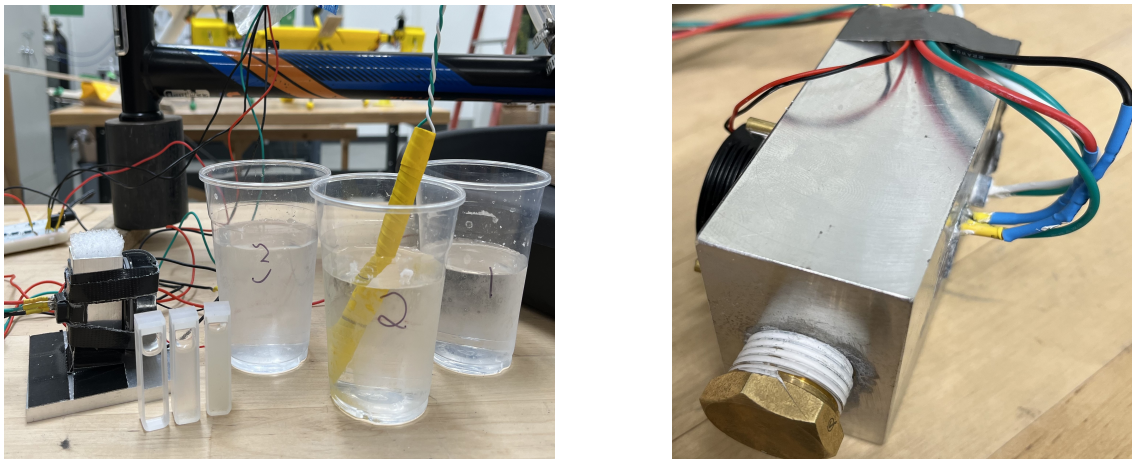

(a) Individual sensors **(b)** Single body sensor suite.

Figure 5.4: Wastewater sensor suite containing a conductivity sensor and ultraviolet light diode spectrometer used in the machine prototype.

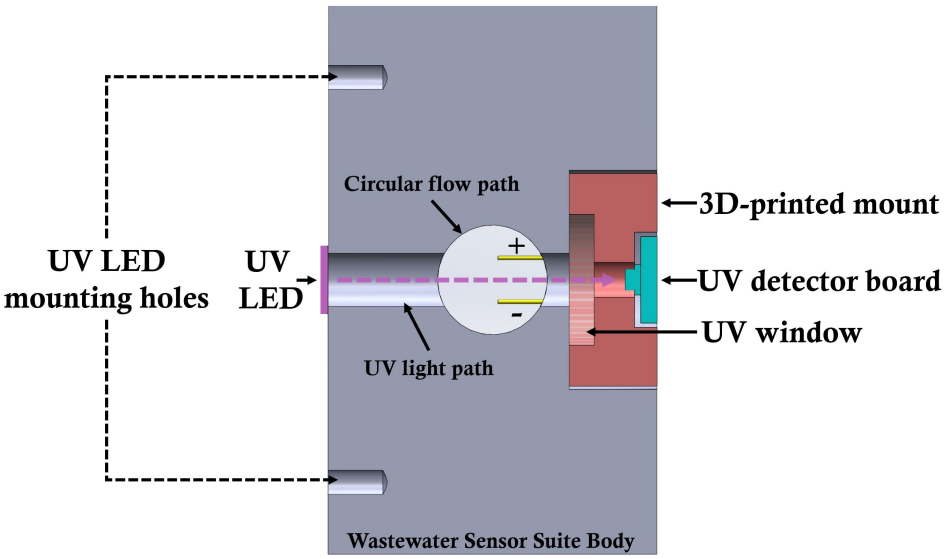

Figure 5.5: Cut-away diagram of the wastewater sensor suite (grey) containing a conductivity sensor (yellow) and ultraviolet light diode spectrometer (blue, red, and purple).

5.3 Data Processing

After each data set is recorded to the micoSD card, the card is removed from the Raspberry Pi Pico microcontroller and placed into a Windows 10 computer. The raw data sets are placed in a central raw data directory named from the MicroPython code running on the microcontroller. All directories on the Windows 10 computer are the turquoise blocks of Figure 5.6. R code is then used to manage and process the collected data; Appendix F

has the whole code. In Figure 5.6, the "Sensor Data" file contains each sensor's systematic error, filter window size, and confidence level quantile percentage (data set post-processing variables are summarized in Table 5.2).

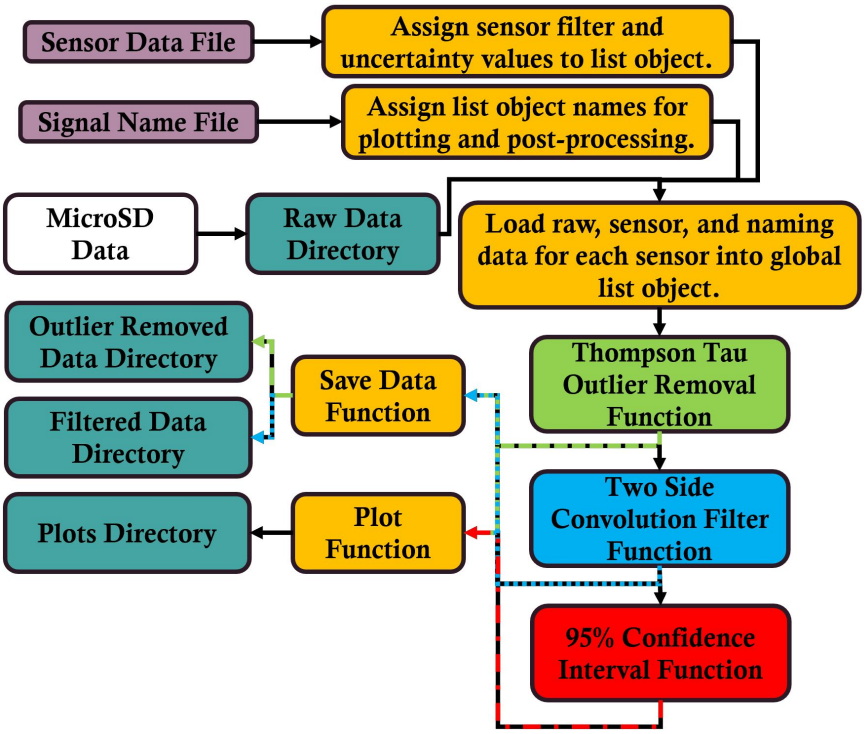

Figure 5.6: Flow chart for processing and plotting data from raw prototype signals.

Sensor	Filter Window Length	Systematic Error	Quantile Percent
Tachometer	6	0.1	50%
Flow Meter	5	0.03	21%
Cond. Sensor	20	0.1	5%
Spectrometer	20	0.1	5%

Table 5.2: Sensor data post-processing variables.

The "Signal Name" file contains string elements corresponding to plot legend names. The code combines the raw data, the "Sensor Data" file, and the "Signal Name" file into a single list object for manipulation. Each entry in the list is a different sensor data set. After the list is created, a modified Thompson Tau outlier removal test[40] is used on each data set by identifying potential outliers and testing them against a rejection region of a local

window mean. Due to the subjective nature of outlier removal, a check between data sets with and without outlier removal is necessary to ensure data is not manipulated to falsify results or produce an inaccurate bond graph model. Figure 5.7 and 5.8 are filtered data sets produced from the same raw data sets for the flow meters where the first graph does not remove outliers and the second one does. Comparing the raw and outlier removed data sets numerically with average flow rates across all trials reveals an average difference of -8.64e-4 milliliters per second. Therefore, the main result of using the Thompson Tau outlier removal method is a slight decrease in the mean value of the signal. This is expected when data points are removed, and it holds across unsteady, steady, and transient periods in data sets. With a small average difference in value from outlier removal, the data sets can then be filtered and have a 95% confidence interval determined for bond graph modification. A built-in R filter, a two-sided convolution function smoothing the data based on a moving window size, filters the data. The window sizes were manually adjusted for each sensor until smooth data sets were consistently produced. During the 95% Confidence Interval Function, systematic and random errors are present. No error propagation is considered because the data sets are not directly used to calculate variables with a high covariance. Because the data collected is not always steady, the standard deviation of the signals cannot be used to determine the random error. Instead, a quantile window specific to each sensor is used to calculate the random error. Quantile windows were also adjusted for each sensor until smooth data sets were consistently produced. The data sets are saved and plotted in each intermittent step of the data processing and will be used to modify the machine's Bond Graph model.

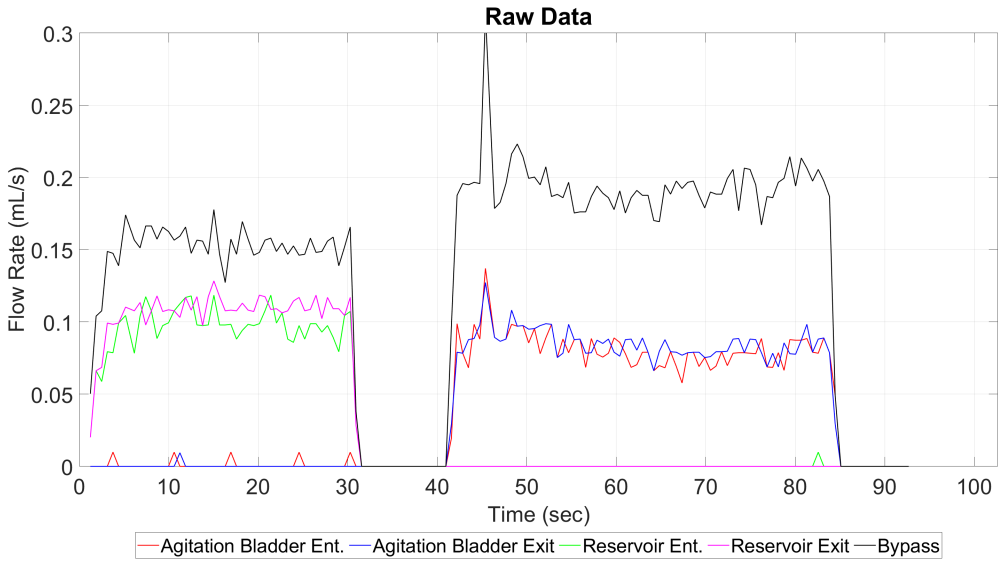

Figure 5.7: All flow meter signals processed without Thompson Tau outlier removal.

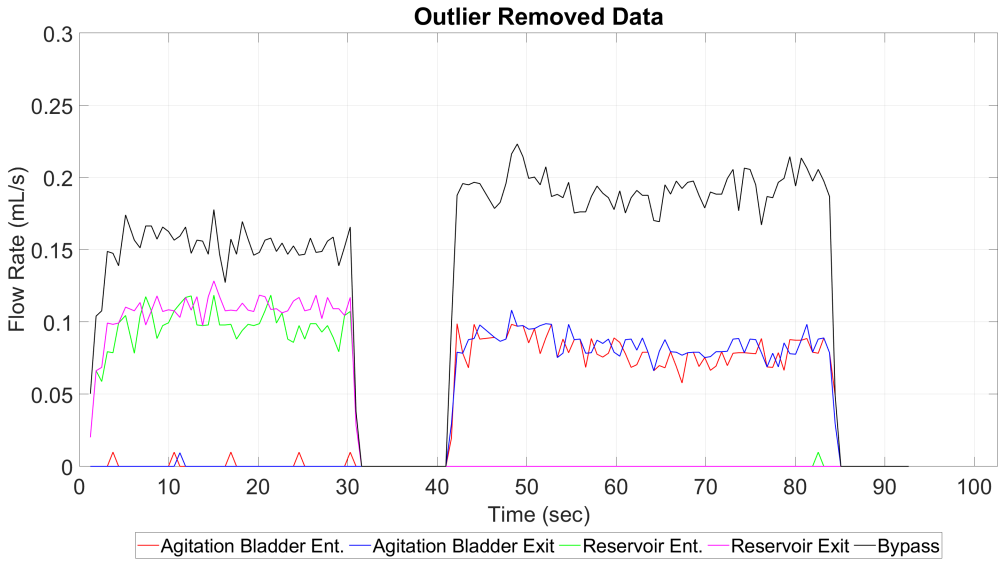

Figure 5.8: All flow meter signals processed with Thompson Tau outlier removal.

5.4 Sensor Calibration

Some sensors need to be calibrated to known values to avoid sensor aliasing and improve post-processing. The tachometer and flow meters must be calibrated because they have associated errors reported on their data sheets.

5.4.1 Tachometer

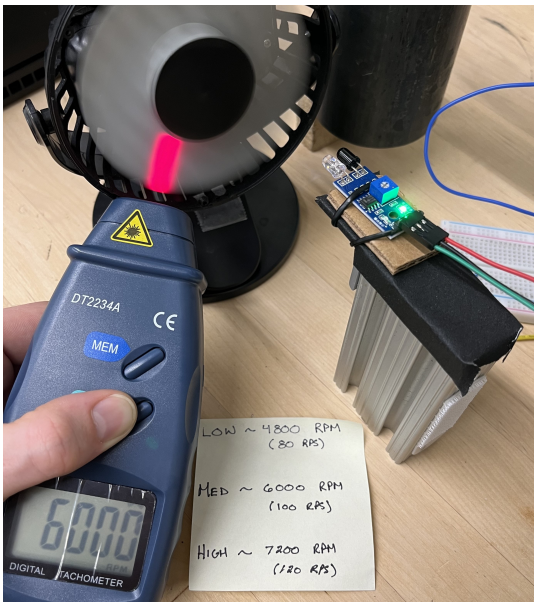

Figure 5.9: Machine prototype tachometer calibration experiment set-up.

For the tachometer, a variable speed fan and a National Institute of Standards and Technology calibrated tachometer, as shown in Figure 5.9, were used to record the fan's three speeds. The machine's tachometer was then used to measure the fan speed. The tachometer's data collection frequency and infrared diodes were then adjusted until all three fan speeds were read constantly across many trials. Figure 5.10 shows the calibration results.

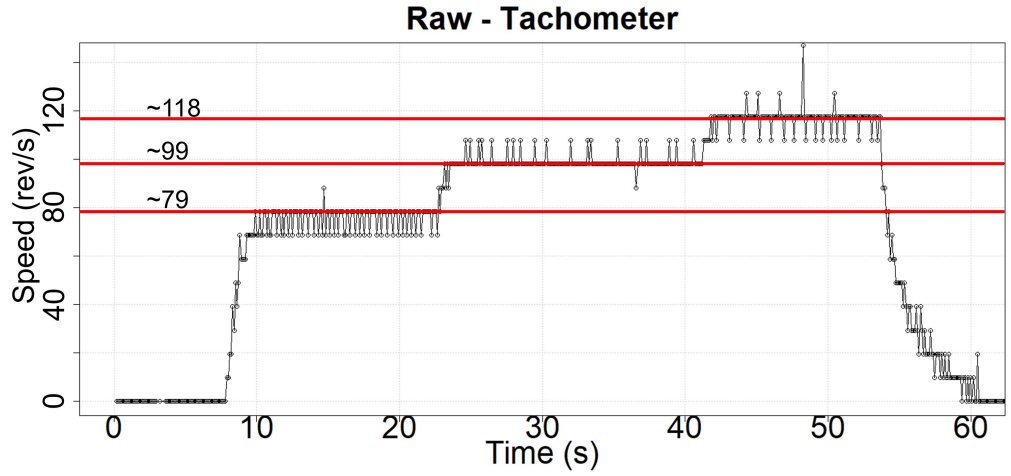

Figure 5.10: Machine prototype tachometer calibration experiment results. Red lines represent the tachometer sensed revolutions per second.

5.4.2 Flow Rate Sensors

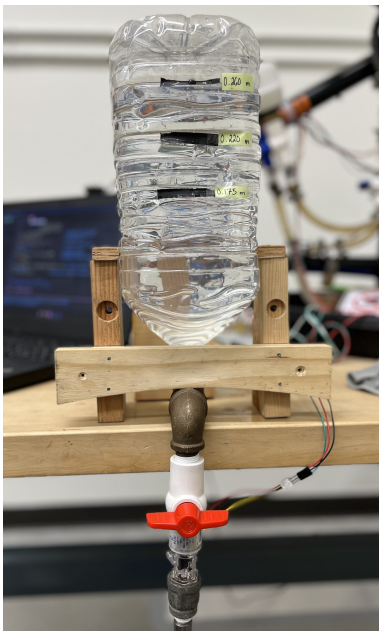

Figure 5.11: Machine prototype flow meter calibration experiment set-up.

Figure 5.11 shows a device to model Torricelli's Law for the flow rate sensors. Torricelli's law relates the ejection speed of a water stream out of a reservoir to the height of water in a reservoir. The flow rate of the ejecting stream is an exponentially decaying function, and the machine's flow rate sensors were placed in the device to measure the exit flow rate. The data collection rate of the flow meter was adjusted to the decaying function. The calibration results after applying a low pass filter are shown in Figure 5.12. The initial height of the reservoir was changed for each calibration trial, and the results show respective signals oscillating around the respective decay function, revealing accurate sensor measurements. Higher resolution signals could not be achieved due to the COTS hardware. Assuming no heavy concentration of particulates, the waste within the water should not impact the flow rate.

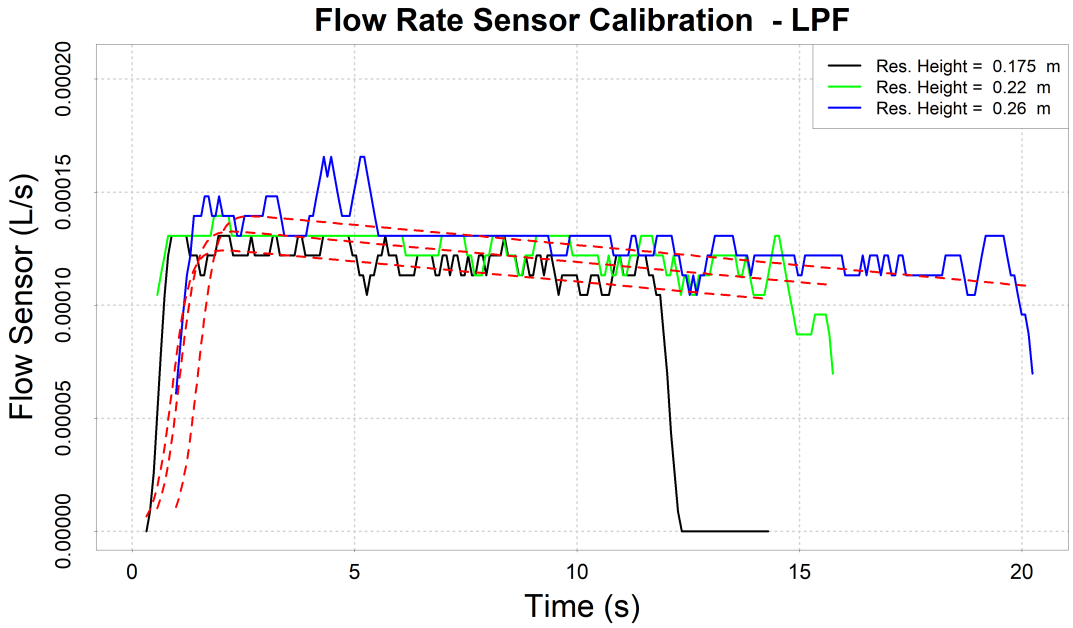

Figure 5.12: Machine prototype flow meter calibration experiment results after applying a low pass filter (LPF).

5.4.3 Wastewater Sensors

The wastewater sensors are normalized to a distilled water baseline and then compared to the other upstream wastewater sensors. The relative sensitivity of the sensors needs to be tested (e.g., what is the smallest change in electrolytes that the sensor can record). A sample of saturated salt water was used for the conductivity sensor to observe the change in the water's bulk electrical resistance. The sensor baseline was set to tap water conductance before the saturated salt water was added in small quantities to the fixed volume of water. Figure 5.13 shows the experiment results, which show that changes in electrolyte concentration can be detected at a high resolution. The results also have a time delay in the response, most likely due to the localized mixing and diffusion throughout the sample volume. The conductivity sensor acts as a voltage divider, so the length of copper wire, amount of solder, connection contacts, length of exposed nichrome wire, distance between the nichrome probes, and condition of resistors in the circuit all impact the measured voltage.

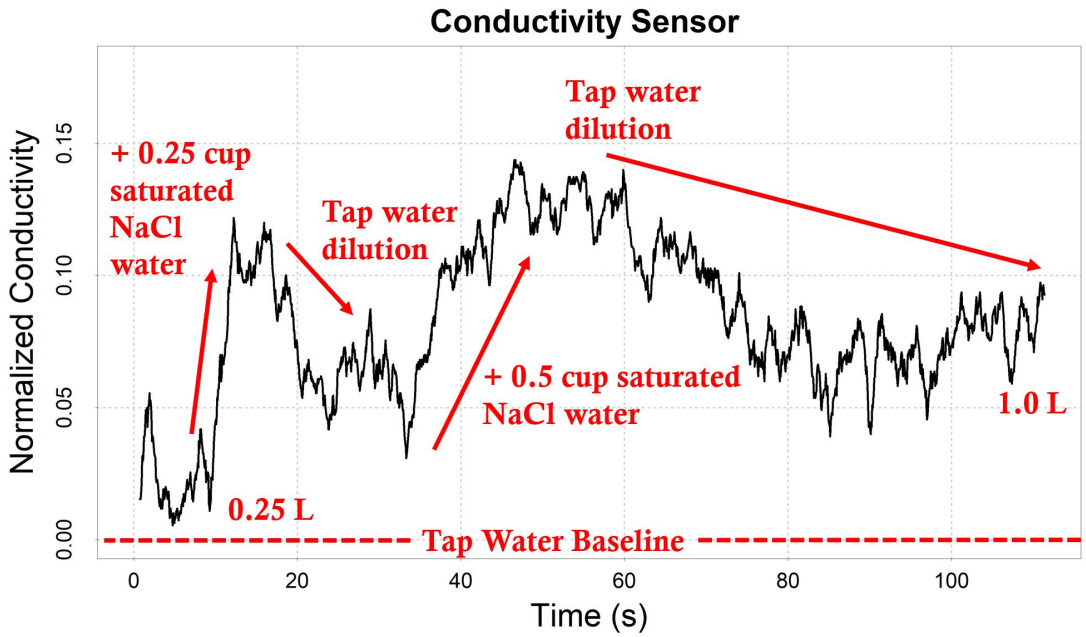

Figure 5.13: Machine prototype conductivity sensor calibration experiment results.

The main impact is the condition of the secondary resistance in the voltage divider because it controls the current intensity that interacts with the electrolytes in the water. The sensitivity of the conductivity sensor manufacturing plays a significant role in the reliability and ability to calculate the relative change in electrolyte concentration in the laundering process. To address the manufacturing issue, all conductivity sensors used in the machine were manufactured simultaneously to ensure all components came from the same batch (e.g., solder, resistors, connectors, wire) and constructed with an identical process that included intermittent steps to compare each sensor to one another.

For the diode spectrometer, samples of saliva diluted in distilled water were created to observe the relative change in detected absorbance using the Beer-Lambert Law (see Equation 3.2 and Section 3.4). After calibrating to local tap water, the three samples were sequentially placed into the spectrometer. Figure 5.14 shows the results of the discrete-sample testing. The near linear relationship between saliva by volume and absorbance reveals that the UV detector breakout board circuit is sensitive to a 1% change in bio-fluid concentration. Particulate testing in the spectrometer was not done. After the conductivity and diode spectrometer were tested, they were integrated into the single-body WSS. Two wastewater sensor suites were manufactured to measure the waste-mass exiting textiles.

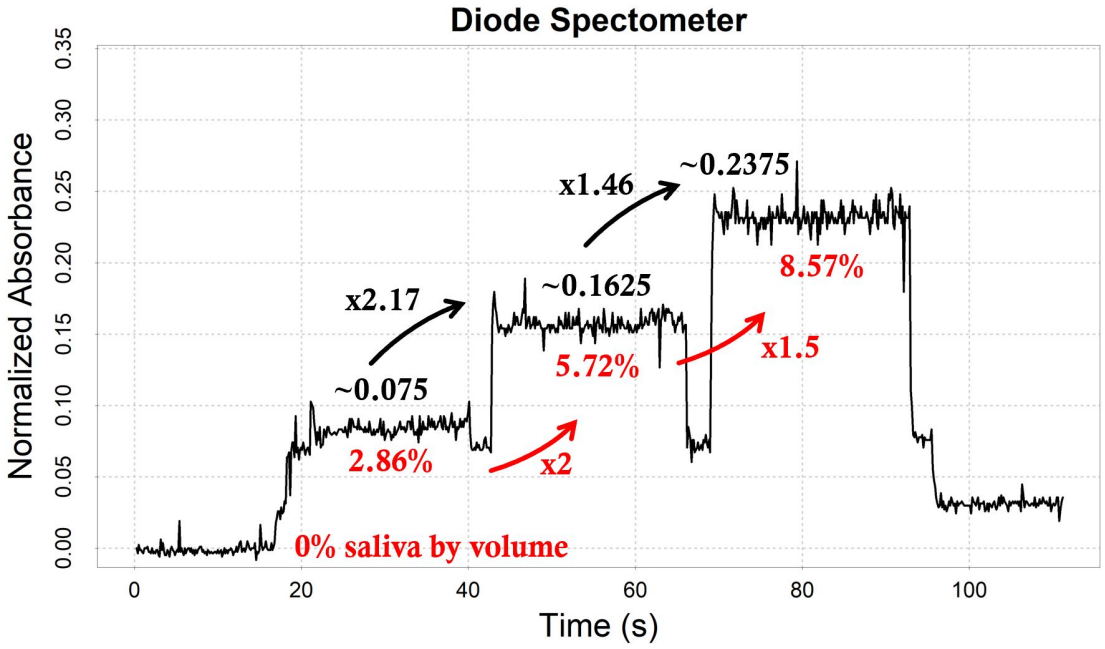

Figure 5.14: Machine prototype diode spectrometer calibration experiment results.

The two wastewater sensor suites were calibrated for experimental use by subtracting the sensed values of the same distilled water sample. The difference in sensed spectrometer amplitude readings was approximately 5e-9, and conductivity readings were approximately 3e-7 V. Two experiments were done to evaluate the WSS measurement system's performance. The first experiment contaminated distilled water with table salt and real saliva (low in electrolytes with bio-fluids). This was done to observe the diode spectrometer and conductivity sensor performance in an environment where each can only measure a single contaminant. The second WSS experiment contaminated distilled water with synthetic perspiration to observe a primary spaceflight textile contaminate, which requires both sensors to quantify relative concentration.

The first WSS experiment started with distilled water before adding salt in four centigrams and saliva in two percent by volume increments up to sixteen and eight, respectively. This resulted in the twenty-five samples ranging from uncontaminated to eight percent by volume saliva-water with sixteen centigrams of salt. The results from observing the twenty-five wastewater samples per sensor suite are shown in Figure 5.15 for the conductivity sensor

and Figure 5.16 for the diode spectrometer - Due to the slight difference in measurements, it appears that only one sensor suite was operational, however, there is another set of data under the visible lines. The conductivity results show that with higher saliva, the conductivity increases, which is accurate due to the electrolytes in saliva, and that conductivity increases with more dissolved electrolytes regardless of saliva concentration.

The diode spectrometer results reveal the expected trend of increased amplitude with more saliva and the unexpected trend that with higher dissolved salt, the amplitude also increases regardless of saliva concentration. The increasing detected abundance with higher salt may be due to the electrolytes clouding the water, obscuring the emitted ultraviolet light. With the expected results, a second experiment with synthetic perspiration can be done to evaluate the wastewater sensor suite further.

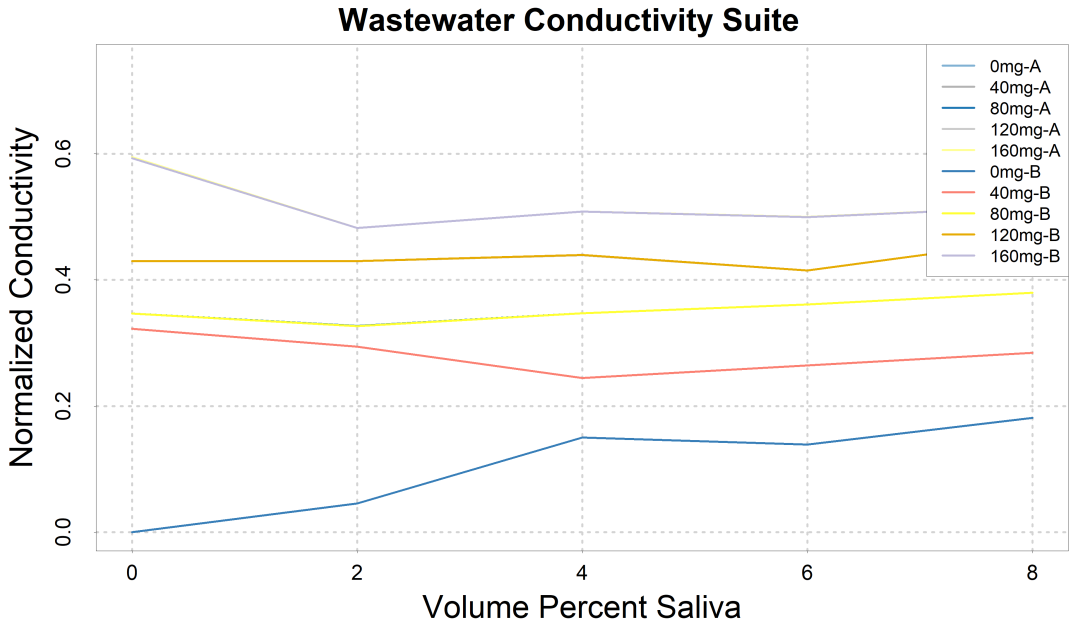

Figure 5.15: Machine prototype wastewater sensor suite conductivity calibration experiment for salt and saliva experiment.

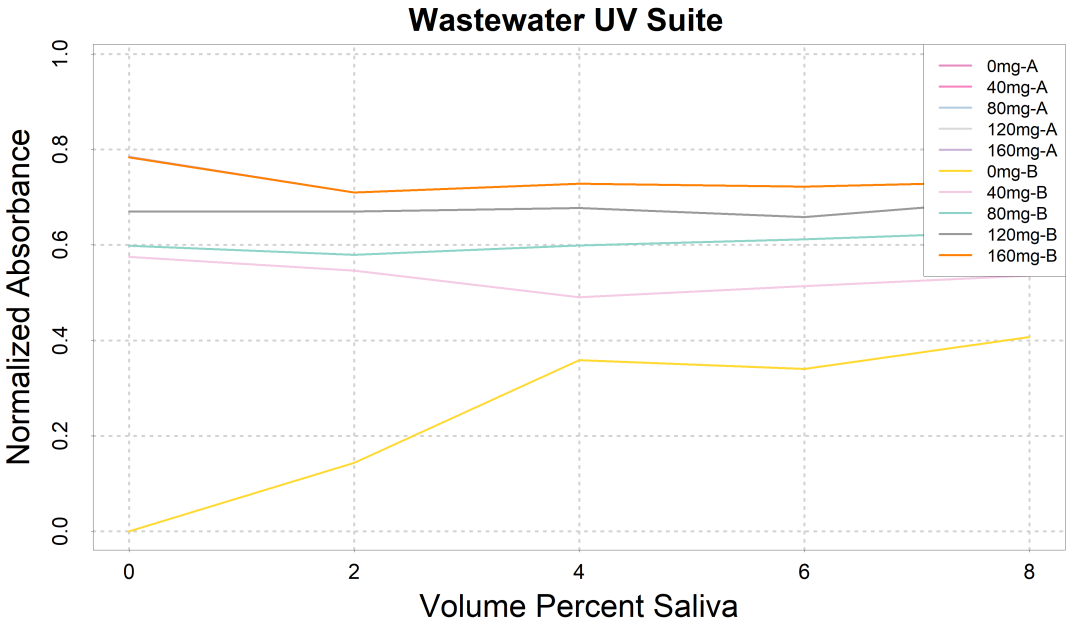

Figure 5.16: Machine prototype wastewater sensor suite diode spectrometer calibration experiment for salt and saliva experiment.

The second WSS experiment started with uncontaminated distilled water before adding synthetic perspiration in two percent by volume increments up to twenty percent. The ten samples are shown in Figure 5.17 for the conductivity sensor and Figure 5.18 for the diode spectrometer - Due to the slight difference in measurements, it appears that only one sensor suite was operational, however, there is another set of data under the visible lines. As the concentration of synthetic perspiration is lowered below 3%, the sensitivity of the sensors becomes relatively poor compared to sensitivity at higher contaminate concentrations. The linear rise of the detected conductivity and abundance with increasing synthetic perspiration concentration matches the first experiment's results and discrete benchtop testing results (Figure 5.13 and 5.14). These results and previous testing are deemed sufficient for wastewater sensor suite integration into the prototype machine, along with all the other sensors mentioned in this chapter.

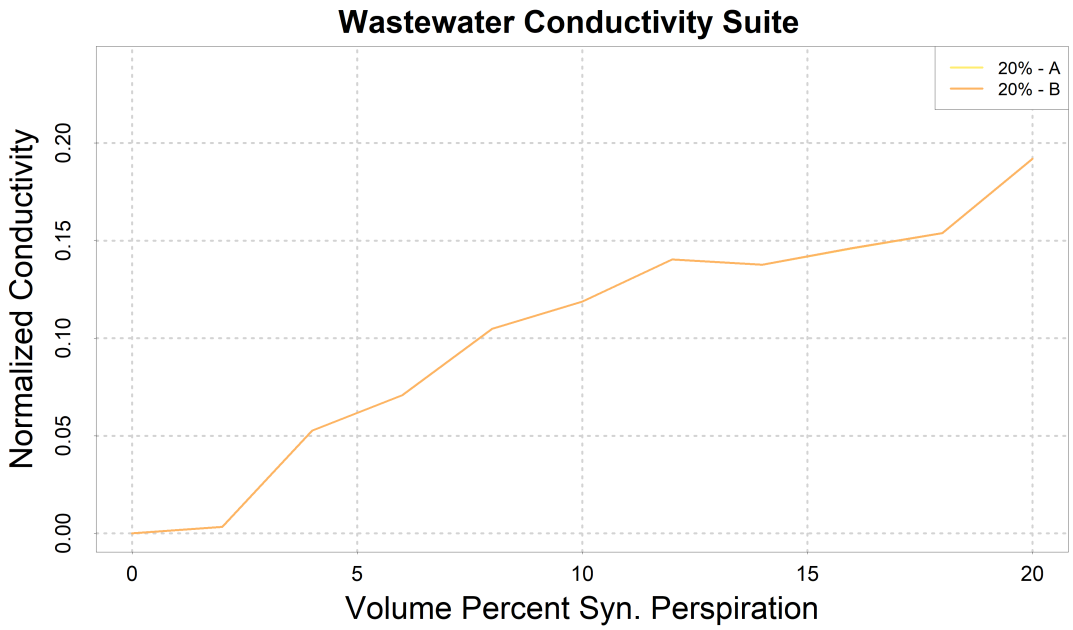

Figure 5.17: Machine prototype wastewater sensor suite conductivity calibration results for synthetic perspiration experiment.

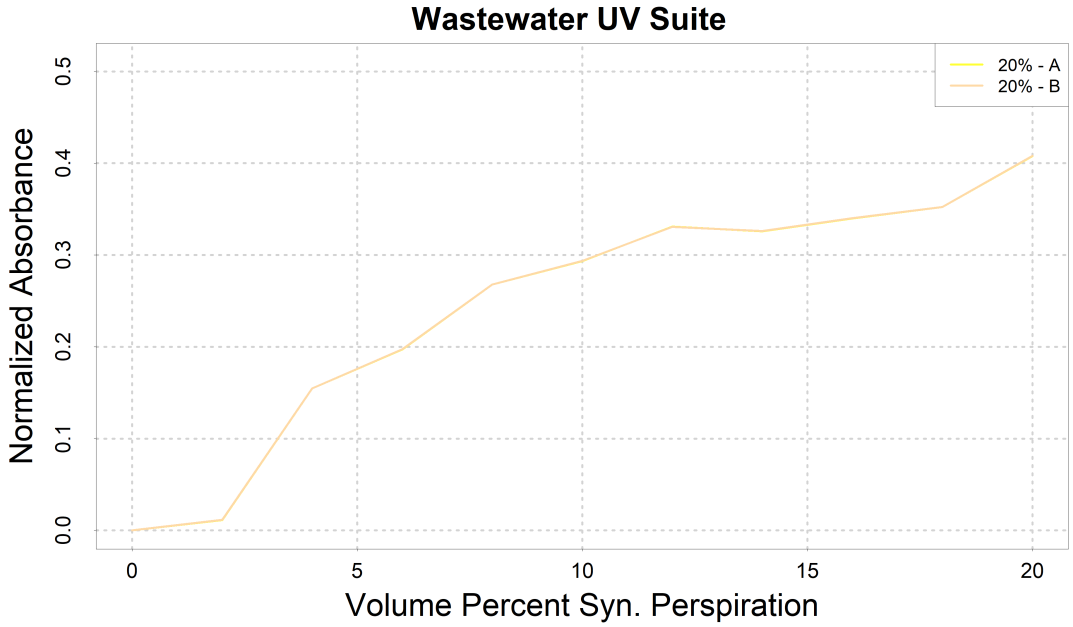

Figure 5.18: Machine prototype wastewater sensor suite diode spectrometer calibration results for synthetic perspiration experiment.

5.5 Prototype Machine Assembly

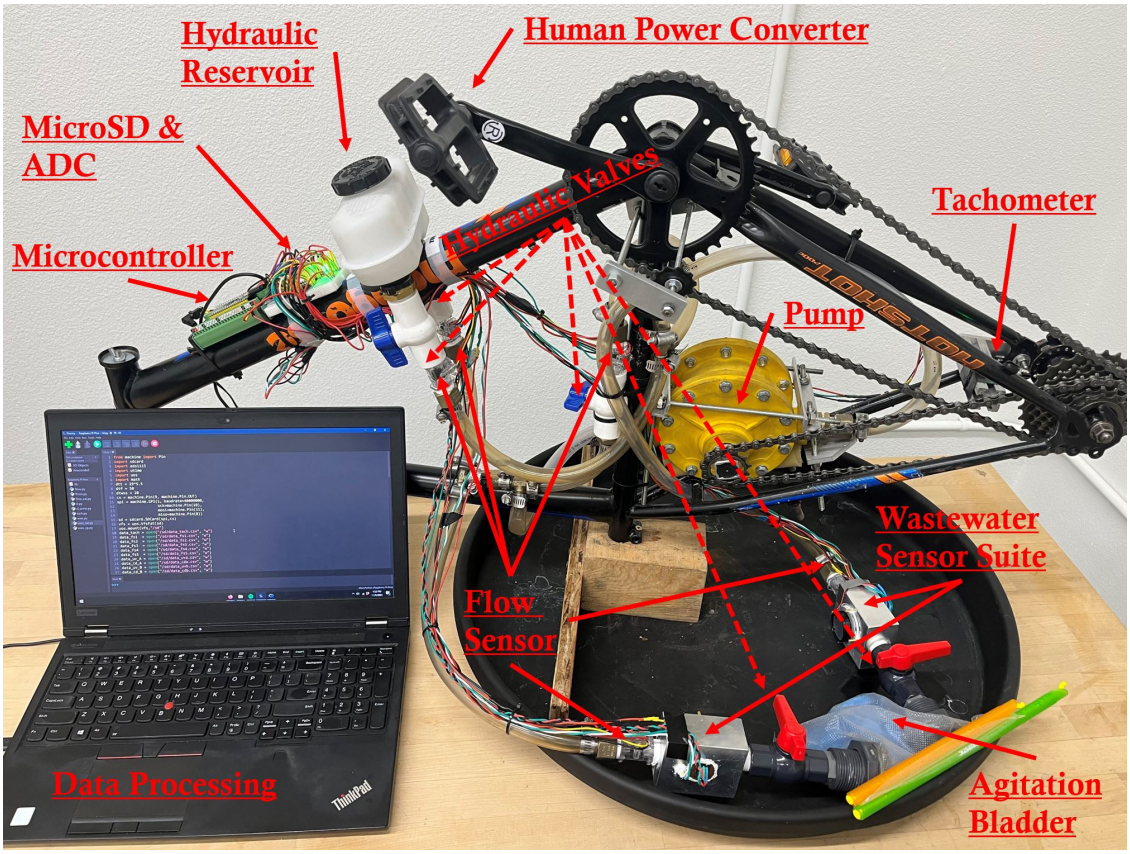

Figure 5.19: Fully assembled standalone astronaut-powered laundry machine prototype.

The main structure of the machine prototype is a bicycle frame (Figure 5.19)with pedals, a chainring, and a rear 7-level freewheel sprocket attached (originally used for changing gear ratios). There is a chain linking the chainring (with pedals attached) and freewheel to convert human-power into rotary-power. Another chain extends from the freewheel and supplies power to a corrosion-resistant reversible hand pump mounted to the bicycle frame to create a hydraulic-power source. A water reservoir is attached to the frame, feeding the hydraulic system with a bladder and valve. The conceptual schematic is shown in Figure 4.4. Half-inch vinyl tubing connected all hydraulic components and was mounted to the main structure with zip-ties, nuts, and bolts depending on the shape and flexibility of the tubing. The flow meters are attached to each valve in the hydraulic system. All sensors are connected to a power supply and terminal block with the microcontroller (per Figure 4.7), and the electrical system is covered in plastic for water protection. No electrical generator, or other

power converting source, is linked to the rotary-power supply, so a power and communication cable between a Windows 10 machine and the microcontroller was used. The Windows 10 machine runs "Thonny," a micropython-integrated development environment, to store and manage microcontroller Micropython files. The code sets up libraries for breakout boards, establishes data collection rates, and generates comma-separated value files from sensor measurements. Once everything had been assembled and integrated into the main structure, tests were run to ensure all sensors were properly communicating and recording data during operation. Figure 5.19 shows the fully assembled machine prototype ready for data collection and BG model modifications.

5.6 Machine Testing

With a prototype developed based on the astronaut-powered laundry machine concept and a data processing pipeline established, the prototype can be tested to ensure nominal operation to gather data for the Bond Graph modification and validation. Figure 5.19 shows the completed machine prototype under the reduced scope: no electrical generator, tilt plate agitator, or water filters.

To operate the completed prototype, the user must first insert a microSD card into the reader, then set the valves to a laundry-loading configuration (i.e., all agitation bladder values closed to prevent water from exiting the hydraulic system) before filling the agitation bladder with contaminated textiles and distilled water; then, power is connected to the Raspberry Pi Pico, and finally the user begins to power the system by pedaling and adjusting the valves as needed - a complete procedure is in Appendix E. The machine configuration can change throughout the laundering process to mimic an Earth-laundry cycle: fill to wet, rinse, empty, fill, agitate, empty, rinse, and wring. For testing, all the valve configurations were tested without consideration of the laundering process.

Figure 5.20 shows the initial bond graph results. Figure 5.21 and 5.22 compare the bond graph results to the data collected from machine testing. The large deviations between the simulated and filtered data in the initial results reveal that modifications to the bond graph model are needed. The next chapter covers the reduced model and modifications in detail.

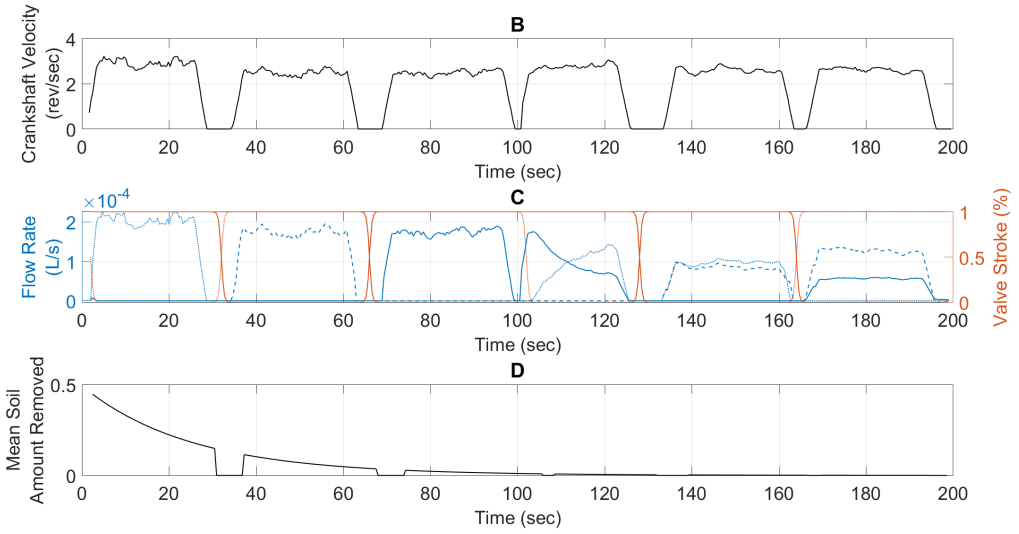

Figure 5.20: Reduced model bond graph results of a standalone astronaut-powered laundry machine.

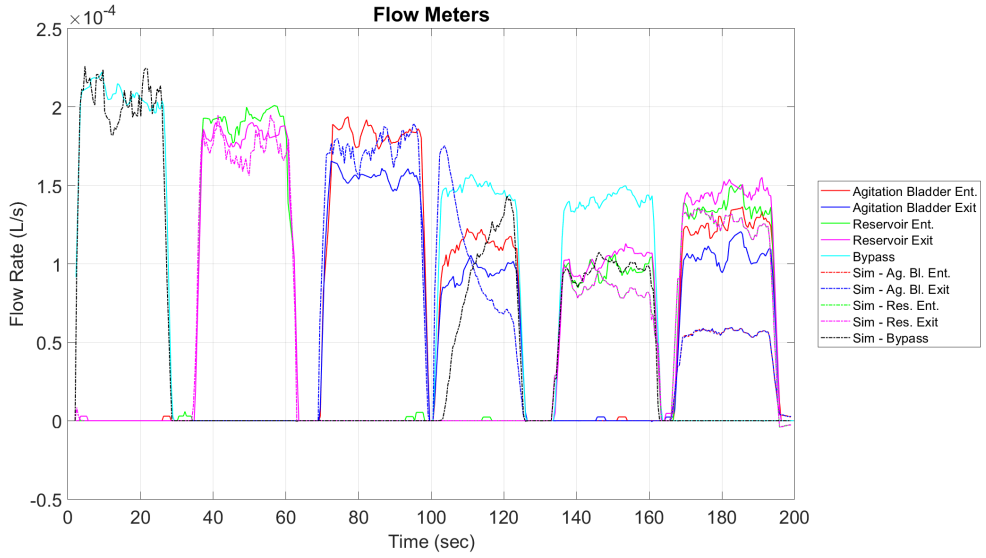

Figure 5.21: Standalone astronaut-powered laundry machine prototype experiment flow rate results with filtered data and BG model results

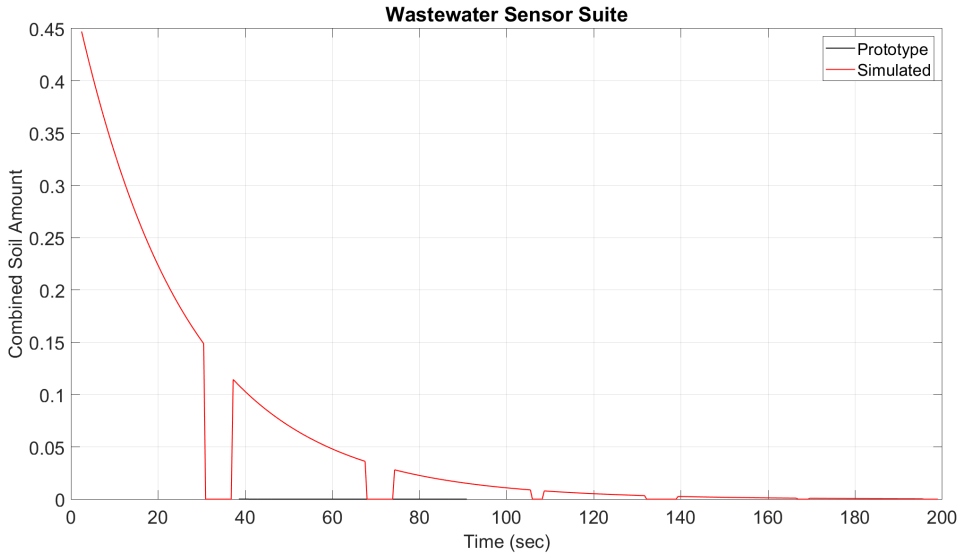

Figure 5.22: Standalone astronaut-powered laundry machine prototype experiment wastewater results with filtered data and BG model results. Prototype data is near zero between 40 and 90 seconds.

Chapter 6

Model Verification

6.1 Bond Graph Modifications

The initial model comparison to experimental data is poor, so the bond graph model needs to be modified. A torque signal actuates the whole machine model; however, the torque generated by a human to operate the machine is unknown, which means a measured variable is needed to actuate the model. The crankshaft speed was initially used because it is a state variable within the model dependent on the torque input. The tachometer data is passed through a bond graph transformer to generate a hydraulic flow rate into one side of the hydraulic system - this is inaccurate because the pressure differentials from the valve configuration also affect the flow rate generated. A more accurate model would include a modulated transformer for the hydraulic pump. Still, another data set is needed to accurately actuate the bond graph model without pressure transducers and detailed testing. Using the law of conservation, all the flow rates from a side of the hydraulic system can be added together to produce the prototype pump's flow generation from one side to the other over time. The total flow rate of the pump was then used as a flow source to actuate each respective side of the bond graph model. Only six signals can be verified: each flow rate sensor and the cleanliness equation under the reduced model and prototype.

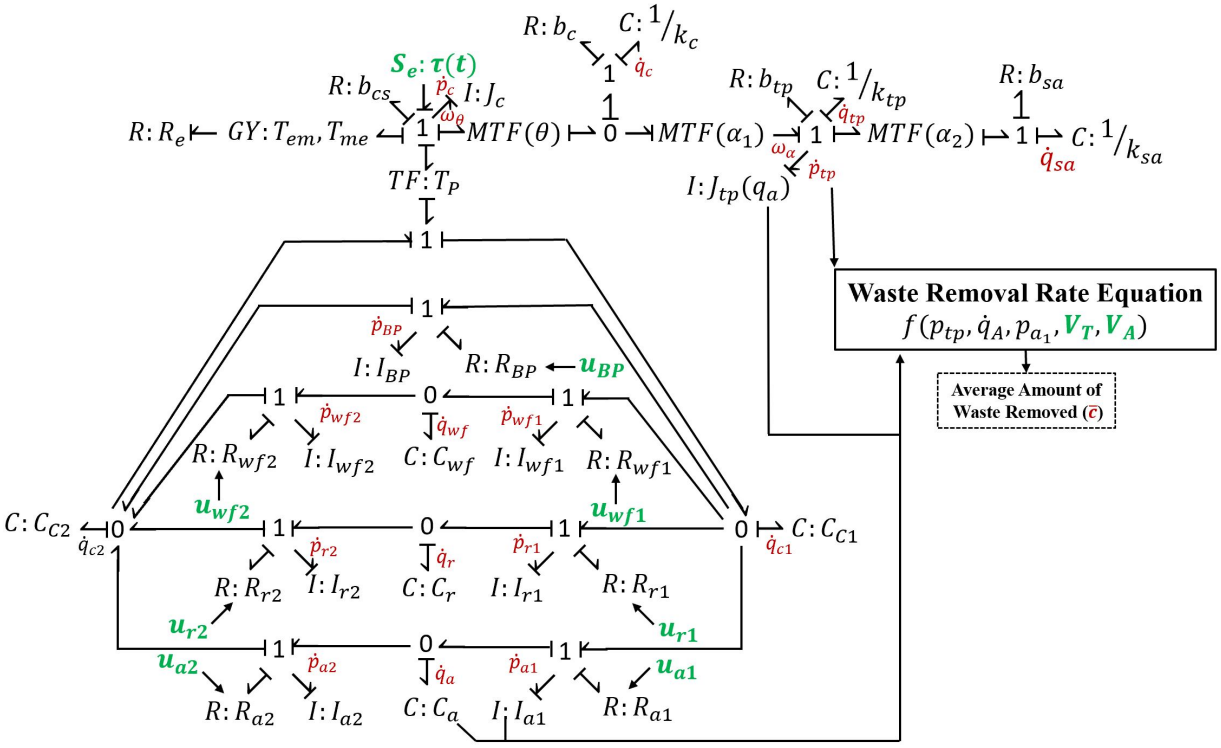

Figure 6.1: Bond Graph of an astronaut-powered laundry machine concept with inputs in green and outputs in red.

In addition to a flow source replacing the pump transformer, other modifications to the bond graph are needed to accurately account for each flow path's impact on the system. The two sides of the water flow path (P1 and P2 from Figure 4.4) are split into capacitance and inertia terms for each flow path (i.e., each tube leading to the hydraulic components needs to be considered individually in the bond graph model). Resistances are introduced into the flow for long pipes, orifice changes, gravity, and capacitor restrictions. Resistance terms are added before the valves because the pipes generate a pressure drop due to the length of each pipe being over ten times the length of the diameter (the *Pipe* subscript of Equation 6.1 shows the constitutive relation used for a laminar assumption justified by preliminary results) and the pipe's change in elevation (the G subscript of Equation 6.1 is a constant). A resistance term is added to each manifold capacitor ($C : C1$ and $C : C2$ of Figure:6.1) to account for the changing orifice sizes and to reduce simulation solution time. Resistors were also added to the reservoir and bladder capacitors ($C : C_r$ and $C : C_a$ of Figure:6.1) because of office changes, pipe layout (e.g., the in and out vectors of the reservoir are one-hundred and eighty degrees apart, so the water's momentum is impacted), and the resistance

generated by textiles within the bladder. These resistances were manually modified to match the recorded data. The capacitance of each pipe was also added to set the pressure before the valve (Equation 6.2 shows the constitutive relation used for this element where B is the Bulk Modulus of water). Figure 6.2 reflects all the bond graph modifications discussed.

$$R_{tot} = R_{\text{Pipe}} + R_{\text{G}} + R_{\text{Tune}} = \frac{128 \cdot \mu \cdot l}{\pi \cdot d^4} + \rho \cdot \text{g} \cdot \text{h} + R_{\text{Tune}} \tag{6.1}$$

$$C = \frac{\pi \cdot r_{\text{Pipe}}^2 \cdot l}{B} \tag{6.2}$$

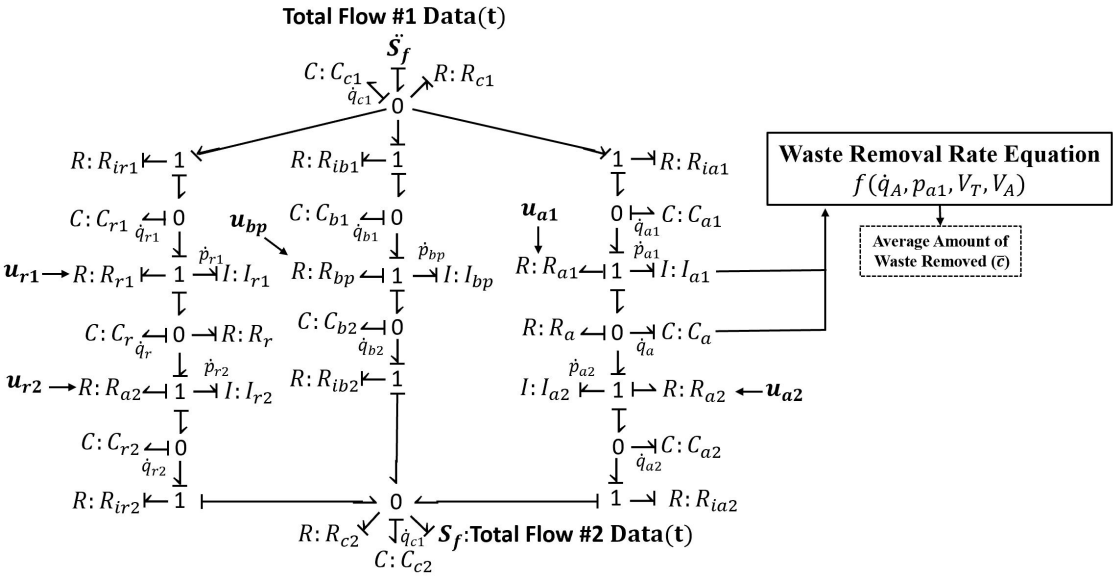

Figure 6.2: Modified reduced model bond graph of a standalone astronaut-powered laundry machine. Bold elements are user inputs to the model.

6.2 Cleanliness Equation Modifications

Modifications were made to the cleanliness equation for data processing and bond graph simulation. The primary logarithmic cleanliness equation (2.1) is used; however, the change in waste concentration (Δc) needs to be defined, and the waste removal rate coefficient (k) is reduced from the original form (3.1) to match the reduced prototype. Equation 6.3, 6.4, and 6.6 are the equations used for the collected data where the number subscripts indicate which wastewater sensor suite data set is used for calculation. The two-hundredths of a second-time step is from the 50 Hz data collection speed. The waste removal rate coefficient equation

is the same for collected data and simulation (Equation 6.6) because the same variables are available. An unexpected uncertainty with the cleanliness equation is the change in concentration equations because the absorbance and conductivity measurements need to be combined into a single value. Absorbance is unitless. Conductivity measures the voltage drop across a bulk fluid. The conductivity measurements can be made unitless using the voltage drop in distilled water as a baseline. A simple addition of the unitless measurements can then be done for the waste measurement combination, as shown in Equation 6.5. After calculations, multiple instances of an Infinite or NaN value appear in the data set (this was expected with zero-value measurements used in logarithmic calculations) and are removed. This results in sporadic data not very well suited to creating a line to compare to simulated values; therefore, the data was regressed using the MATLAB *fit* function into the expected exponential expression ($y = Ae^{Bt} + C$).

Equation 6.7, the modeled change in concentration over time, was determined from a guessed regression curve and the experimental data provided in the next section. The expected exponential expression was used as an initial guess. The simulation leading constant ($\overline{c}_{data}(t_0)$) was set from the combined raw data initial value. The mean-time simulated waste removal rate value ($\overline{k}_{sim}$) was found by averaging the calculated waste removal rate for the data set due to the expected discontinuity in the rate removal equation and no chemical aids (catalysts). The sign of the decay rate was established from the data regression for each trial (i.e., is the initial condition of the water favorable for waste removal). The decay rate (τ) is the only parameter to modify manually. A simulated time constant of fifteen minutes was used across all trials for the experimental laundering environment. Recalling that the rate of waste removal is heavily dependent on the contaminant-textile combination, the unaltered time constant can be attributed to the solubility of preparation and the wetting properties of cotton.[41]. The rates are plugged into the primary logarithmic cleanliness equation (2.1) with a kinetic order (n) value of 0.85, 1, and 1.24. The three resulting equations for the data and simulation are then averaged together and used as the simulated signal for analysis.

$$\frac{\Delta uv}{\Delta t} = \frac{(uv_2(t_{i+1}) - uv_1(t_{i+1})) - (uv_2(t_i) - uv_1(t_i))}{0.02} \tag{6.3}$$

$$\frac{\Delta cond}{\Delta t} = \frac{(cond_2(t_{i+1}) - cond_1(t_{i+1})) - (cond_2(t_i) - cond_1(t_i))}{0.02} \tag{6.4}$$

$$\frac{\Delta c_{data}}{\Delta t} = \frac{\Delta uv}{\Delta t} + \frac{\Delta cond}{\Delta t} = \frac{(\Delta uv + \Delta cond)}{0.02} \tag{6.5}$$

$$k_{data} = \left(\frac{\text{Textile Volume} \cdot \text{L/s into Bladder}}{(\text{Bladder Volume})^2 \cdot \text{Momentum into Bladder}} \right)^{0.001} = k_{sim} \tag{6.6}$$

$$\frac{\Delta c_{sim}}{\Delta t} = \overline{c}_{data}(t_0) \cdot \overline{k}_{sim} \cdot \left(1 - \frac{1}{\tau} \cdot e^{\frac{-t}{\tau}} \right), \tau = 900s \tag{6.7}$$

6.3 Verification Trials

After modifying the bond graph and cleanliness equation to match the prototype data sets, testing with four 100% cotton three-inch swatches (Figure 6.3) contaminated with different amounts of synthetic perspiration was done to verify the model further. The root-mean-square (RMS) error between the simulated and filtered data sets determines how well the model fits the prototype's performance. The RMS error is calculated with the MATLAB *rmse* function that takes the square root of the square difference between the filtered data and simulation results divided by the total number of data points. The RMS error is normalized to the magnitude of the signals (i.e., typical flow rates have a magnitude of 1e-4 L/s, so the errors are divided by 1e-4). The RMS error is a single indicator for evaluating the bond graph model. The 95% confidence interval produced by the R code is also considered in evaluating the bond graph model. Thirteen trials were done; the overall lowest RMS error and highest flow rate RMS error trials are reported below, and the rest are in Appendix C.

Figure 6.3: 100% cotton swatches and synthetic perspiration used in verification trials.

For each trial, the contamination conditions and RMS errors are shown in a table, followed by two plots: a comparison between the collected and simulated flow rates with uncertainty bars and the computed and simulated cleanliness equation. All the trials followed the same basic procedure for contaminating the textiles and preparing the machine (Appendix D and E, respectively, have the procedures). The only differences between the trials were the amount of time pedaling, the valve configurations, and the initial state of the water. By having different power inputs in different machine configurations, the robustness of the model can be explored because it will have to conform to all the other conditions without changing any simulation constants, which is expected in a typical use case of the machine. Table 6.1 reports the average RMS error calculated from the raw, outlier-removed, and filtered validation trial data sets. The red lines of the wastewater plots are the simulated logarithmic cleanliness equation resulting from Equation 6.7.

Data Type	**Bld. Ent.**	**Bld. Exit**	**Res. Ent.**	**Res. Exit**	**Bypass**	**Clean Eq.**
Raw	0.32817	0.29533	0.45161	0.31856	0.38819	0.24330
Outliers Removed	0.51438	0.48476	0.51232	0.39633	0.44284	0.35146
Filtered	0.57637	0.54772	0.49543	0.48980	0.36410	0.27285

Table 6.1: Average root-mean-squared error results with flows normalized by 1e-4 for a standalone astronaut-powered laundry machine. Bld. = Bladder, Res. = Reservoir, Ent. = Entrance, and Ext. = Exit.

Contamination Information	**Value**
Quantity of Synthetic Perspiration	4 ml
Regression Constant	4.673
Regression Rate	2.6479e-05 1/s
Signal	**RMS Error**
Bladder Entrance	0.49327
Bladder Exit	0.43377
Reservoir Entrance	0.17651
Reservoir Exit	0.20486
Bypass	0.28558
Cleanliness Equation	0.34549

Table 6.2: Contamination conditions and Root-Mean-Squared error results of a standalone astronaut-powered laundry machine for the lowest RMS error trial, #5.

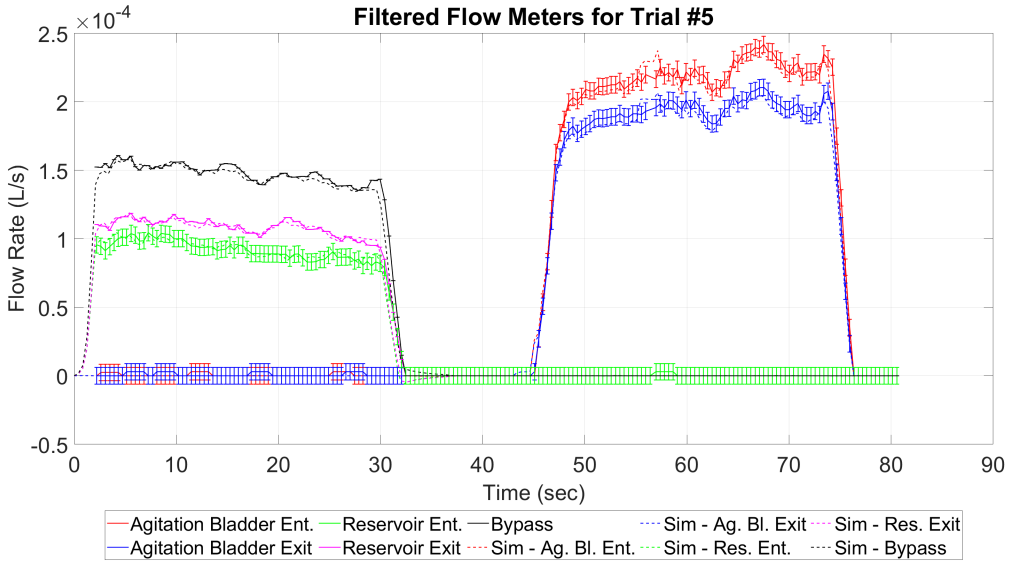

Figure 6.4: Standalone astronaut-powered laundry machine prototype experiment flow rate results with filtered and simulated data for the lowest RMS error trial.

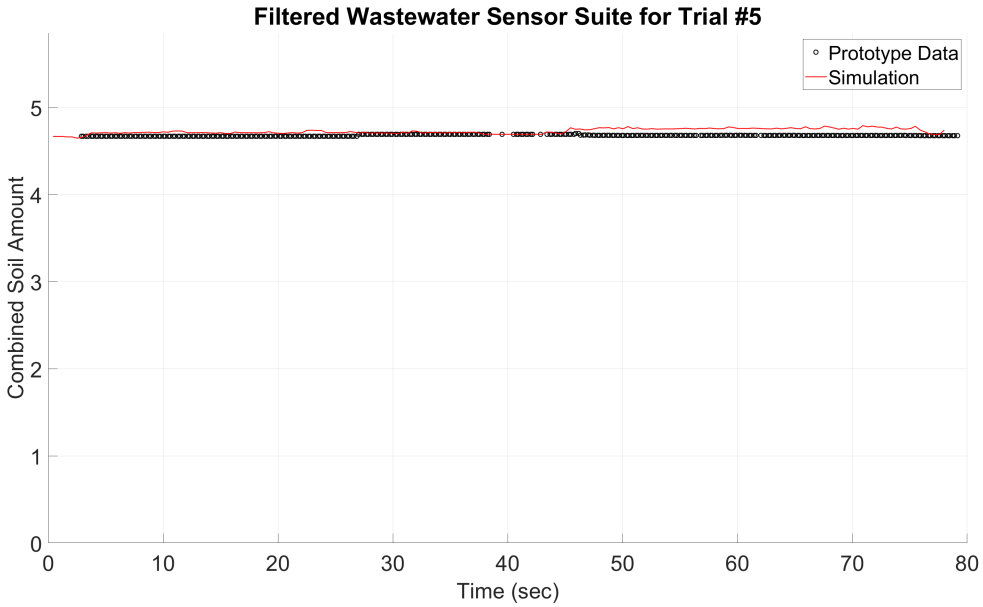

Figure 6.5: Standalone astronaut-powered laundry machine prototype experiment wastewater results with filtered and simulated data for the lowest RMS error trial at scale.

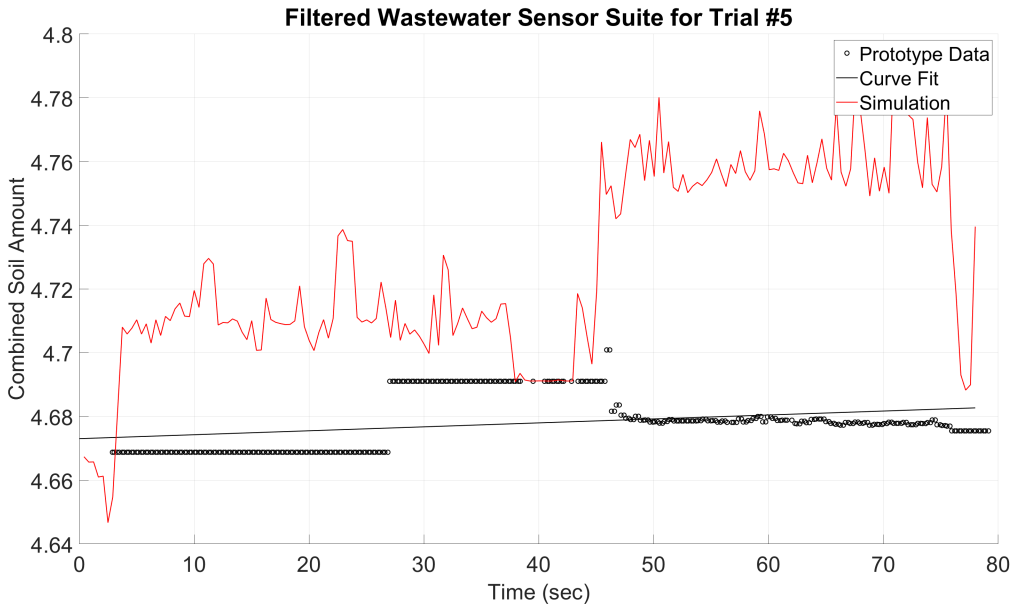

Figure 6.6: Standalone astronaut-powered laundry machine prototype experiment wastewater zoomed-in results with filtered and simulated data for the lowest RMS error trial.

Contamination Information	**Value**
Quantity of Synthetic Perspiration	4 ml
Regression Constant	3.6721
Regression Rate	-8.6278e-06 1/s
Signal	**RMS Error**
Bladder Entrance	0.11516
Bladder Exit	1.2528
Reservoir Entrance	1.991
Reservoir Exit	2.0425
Bypass	0.26965
Cleanliness Equation	0.34525

Table 6.3: Contamination conditions and Root-Mean-Squared error results of a standalone astronaut-powered laundry machine for the highest flow rate RMS error trial, #4.

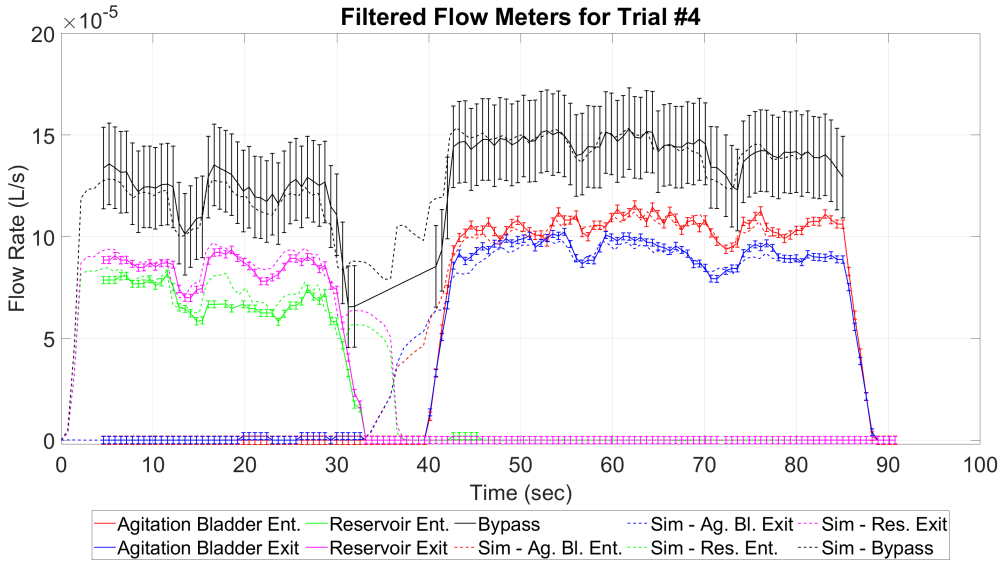

Figure 6.7: Standalone astronaut-powered laundry machine prototype experiment flow rate results with filtered and simulated data for the highest flow rate RMS error trial.

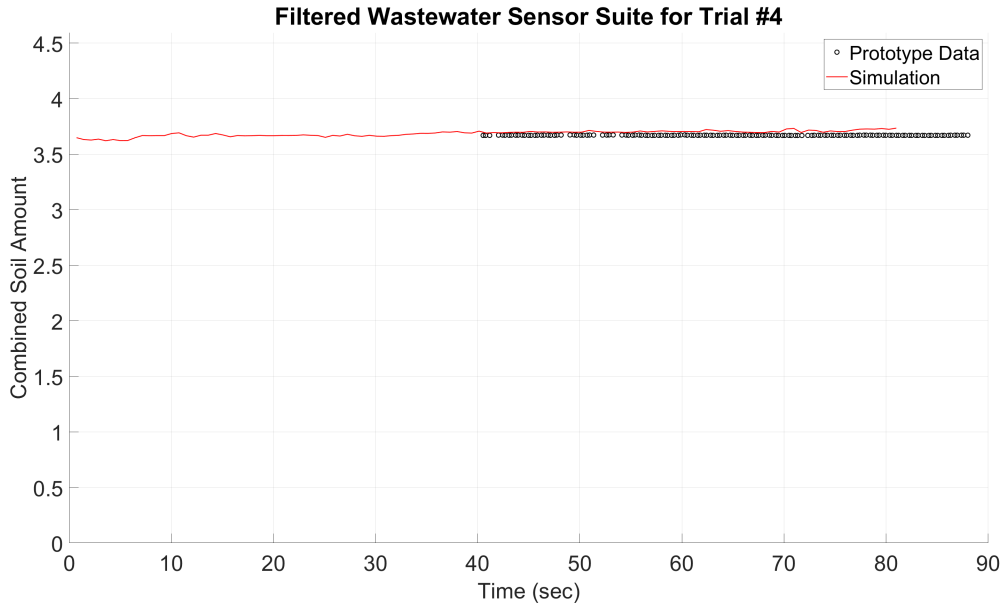

Figure 6.8: Standalone astronaut-powered laundry machine prototype experiment wastewater results with filtered and simulated data for the highest flow rate RMS error trial at scale.

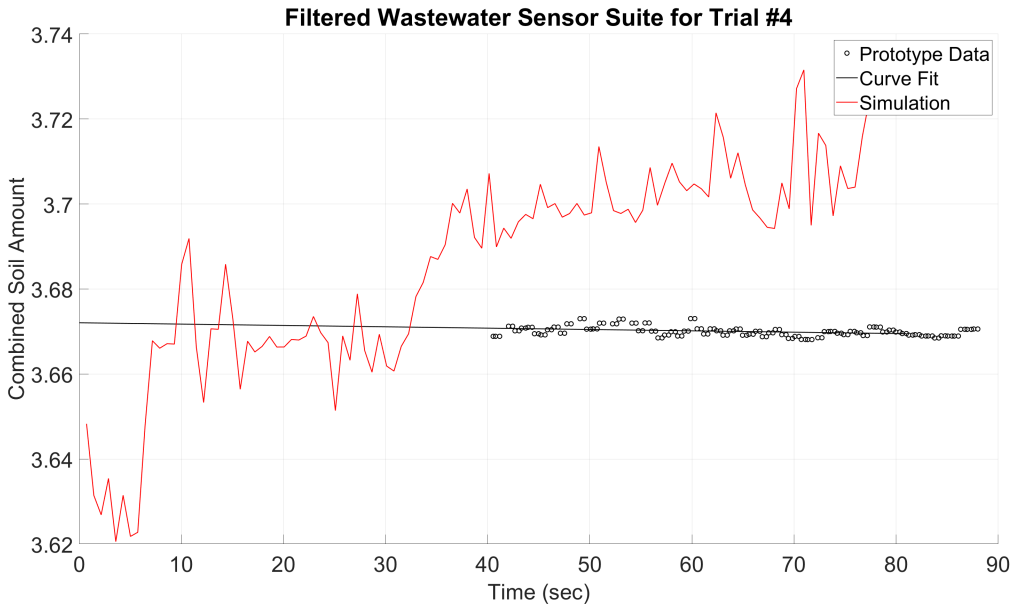

Figure 6.9: Fully assembled standalone astronaut-powered laundry machine prototype experiment wastewater zoomed-in results with filtered and simulated data for the highest flow rate RMS error trial.

The model needs higher-resolution sensors to better predict the dynamics of laundry. Such capabilities would improve insight into exercise loading and laundering efficiency per user. To predict the general laundering capabilities of this design, the tuned model is well within the uncertainty of the measurements made with COTS hardware. The simulated signals are within the calculated uncertainty even for the highest RMS error trial. The data processing also impacts the resulting 95% Confidence Interval. Evaluating all the data sets with relative uncertainty instills confidence that the simulated values represent the prototype machine. The RMS errors of the flow rates in Table 6.1 vary between the raw, outlier removed, and filtered data sets due to the reduction of data resolution. The noise of the measurements and the overall unsteady nature of flow are always present in the data, and a reduced resolution for cleaner data is an acceptable trade-off in this general context. Reevaluating the need for outlier removal, the RMS error for the raw and outlier removed flow rates are similar and further justifies the conclusion that eliminating outliers with the Thompson Tau Method does not produce misleading results. The resulting simulated cleanliness data matches the expected equation and behavior derived from Kissa's experimental results from 1975-1979.[6–8] Further testing in different laundering environments (especially ones with

other contaminates, agitation, and detergents present) is needed to verify the simulated and post-processed cleanliness equations thoroughly. There is a marginal difference in RMS error when exploring the model with gravitational effects. The difference is somewhat expected when approximately half a pound per square inch of hydraulic head is generated by gravity between the highest (reservoir) and lowest (bladder) points in the system.

An interesting phenomenon was observed during the experiments. In two cases, the measured and simulated values were different during rinsing (flow through the agitation chamber). It was found that a swatch had been sucked into the bladder exit flow path, occluding the UV LED in one trial and clogging a flow meter in the other. A machine model and algorithms could be used on the microcontroller to report possible obstructions in flow paths to a display (e.g., a message to agitate the bladder to remove the obstruction could be displayed). Custom porous caps were manufactured and integrated into the bladder to prevent textiles from unintentionally exiting the bladder. This additional hydraulic resistance significantly affected the flow rates, so the data analysis algorithms must compensate for the increased resistance. Remodeling the system consisted of adding a constant resistance (R_{plug}) to Equation 6.1 for the agitation path only. This rapid model adjustment was another proof of the amenability of using bond graphs for system modeling.

Moreover, on observations during the trials, the operation of the machine for more than a couple of minutes resulted in elevated heart rates and fatigue in the arms of the user. Changes in cardiac states support the goal of using the machine for exercise. No data was collected to quantify the cardiac changes. The last observation was the amount of hardware that failed during the manufacturing and testing. A total of one valve, one 7-speed freewheel, and two hand pumps failed throughout the prototype development. After the replacement hardware acquisition, the total repair time was about an hour. Although not suited for spaceflight, the repairs speak to the simplicity of the maintenance design.

Chapter 7

Conclusion and Future Work

Machine Weight	35 lbs
Machine Dimensions	40” x 16” x 30”
Machine Power Consumption	1.919 W
Average Modeling RMS Error	0.4152

Table 7.1: Key characteristics of the developed prototype.

Guiding questions were proposed to produce a machine and a model of an astronaut-powered laundering machine. A human-powered hydrodynamic rinsing machine prototype and bond graph model were created and tested (characteristics summarized in Table 7.1). A machine and model enable the prescription of exercise and laundering regimens for individual astronauts to ensure proper loading on the body and removal of bodily excretions from garments. A single machine to exercise and recycle textiles regardless of gravity or habitable environment would reduce a large portion of mass and volume allocations on spaceflight missions, thereby providing new mission capabilities. One effect not simulated is the gathering of air in the system as a function of gravity. With possible off-gassing and leaks, air pockets may form in the hydraulic system. On Earth, this was accounted for with the placement of the reservoir and specific valve configurations to cycle the water through and remove the entrapped air. This method may not be viable in microgravity. These effects of air in the system would modify the compliance elements of the bond graph model. Without a microgravity environment to test this result, no further information is available to answer

the research questions and validate the derived development method. Below are the topics discussed for each question under investigation in this thesis.

1. **What factors are required to launder textiles on Earth:**
    (a) Water, waste deformation and dispersion energy, chemical additives, and time.
2. **What are the characteristics of laundry mass dynamics:**
    (a) Soil types, fiber types, and their combinations.
    (b) Agitation mechanics with respect to the location of contaminate.
    (c) Water-fiber-soil interactions.
3. **How to measure general textile cleanliness:**
    (a) What are cleanliness metrics?
        i. Quantification of the waste-mass removal from fiber matrices.
        ii. Feel and smell of cleaned textiles (subjective).
    (b) How do we measure the metrics?
        i. Visual inspection of irradiated contaminate and or dyes.
        ii. Decomposition monitoring of specific chemical additives.
        iii. Wastewater visual inspection and sensor observation for contaminates.
4. **Machine design in the context of the spaceflight environment:**
    (a) Human power for sustainability and atrophy countermeasures.
    (b) Standalone, maintainable, and closed water cycle for ease of use across any spaceflight environment.
    (c) Periodic agitation to reduce textile damage and detergent usage.
    (d) UV spectrometer and conductivity sensors to monitor water contaminates.
    (e) Microelectronics for low power and real-time computations.
    (f) Bond graphs for user and machine performance predictions.

Besides a reevaluation of the mechanical assembly, the future work needed to improve this methodology is:

1. Validation of periodic agitation mechanisms.
2. Bladder wringing efficiency testing.
3. Water filtration of electrolytes, biofluids (primarily sebum and urea), and particulates.
4. Electricity generation from a mounted and modified hand crank DC generator.
5. Creation of an info-metric display for users.
6. Relate cardiovascular power output to machine performance via metabolic rate and energy expenditure calculations.
7. Integrate the state space into the microcontroller code to be used as a base for machine performance monitoring/diagnostics/prognostics - e.g., Displays warning for flow paths or regions that may be obstructed by lint.
8. Comparison of machine performance in a domestic Earth setting to the Association of Home Appliance Manufacturers standard HLW-1-2013.

Bibliography

[1] Michael Ewert et al. "Clothes Cleaning Research for Space Exploration". In: (July 10, 2022). URL: https://ttu-ir.tdl.org/handle/2346/89851 (visited on 06/27/2023).

[2] J.H. Brooks and J.R. McPhee. "The Effect of Machine Action on Soil Removal from Wool During Laundering". In: *Textile Research Journal* 37.5 (May 1967), pp. 371–376. ISSN: 0040-5175, 1746-7748. DOI: 10.1177/004051756703700506. URL: http://journals.sagepub.com/doi/10.1177/004051756703700506 (visited on 06/27/2023).

[3] Janet L. Bubl. "Laundering Cotton Fabric: Part I: Effects of Detergent Type and Water Temperature on Soil Removal". In: *Textile Research Journal* 40.7 (July 1970), pp. 637–643. ISSN: 0040-5175, 1746-7748. DOI: 10.1177/004051757004000709. URL: http://journals.sagepub.com/doi/10.1177/004051757004000709 (visited on 06/27/2023).

[4] Mary Ann Morris. "Laundering Cotton Fabric: Part II : Effect of Detergent Type and Water Temperature on Appearance, Hand, Strength, and Cost". In: *Textile Research Journal* 40.7 (July 1970), pp. 644–649. ISSN: 0040-5175, 1746-7748. DOI: 10.1177/004051757004000710. URL: http://journals.sagepub.com/doi/10.1177/004051757004000710 (visited on 06/27/2023).

[5] Mary Ann Huisman and Mary Ann Morris. "A Study of the Removal of Synthetic Sebum from Durable-Press Fabrics, Using a Liquid-Scintillation Technique". In: *Textile Research Journal* 41.8 (Aug. 1971), pp. 657–661. ISSN: 0040-5175, 1746-7748. DOI: 10.1177/004051757104100804. URL: http://journals.sagepub.com/doi/10.1177/004051757104100804 (visited on 06/27/2023).

[6] Erik Kissa. "Kinetics and Mechanisms of Detergency: Part I: Liquid Hydrophobic (Oily) Soils". In: *Textile Research Journal* 45.10 (Oct. 1975), pp. 736–741. ISSN: 0040-5175, 1746-7748. DOI: 10.1177/004051757504501007. URL: http://journals.sagepub.com/doi/10.1177/004051757504501007 (visited on 06/27/2023).

[7] Erik Kissa. "Kinetics and Mechanisms of Detergency: Part II: Particulate Soil". In: *Textile Research Journal* 48.7 (July 1978), pp. 395–399. ISSN: 0040-5175, 1746-7748. DOI: 10.1177/004051757804800705. URL: http://journals.sagepub.com/doi/10.1177/004051757804800705 (visited on 06/27/2023).

[8] Erik Kissa. "Kinetics and Mechanisms of Detergency: Part III : Effect of Soiling Conditions on Particulate Soil Detergency". In: *Textile Research Journal* 49.7 (July 1979), pp. 384–389. ISSN: 0040-5175, 1746-7748. DOI: 10.1177/004051757904900703. URL: http://journals.sagepub.com/doi/10.1177/004051757904900703 (visited on 06/27/2023).

[9] K.L. Ganguli and J. Van Eendenburg. "Mass Transfer in a Laboratory Washing Machine". In: *Textile Research Journal* 50.7 (July 1980), pp. 428–432. ISSN: 0040-5175, 1746-7748. DOI: 10.1177/004051758005000707. URL: http://journals.sagepub.com/doi/10.1177/004051758005000707 (visited on 07/03/2023).

[10] Sangwoo Shin, Patrick B. Warren, and Howard A. Stone. "Cleaning by Surfactant Gradients: Particulate Removal from Porous Materials and the Significance of Rinsing in Laundry Detergency". In: *Physical Review Applied* 9.3 (Mar. 16, 2018), p. 034012. ISSN: 2331-7019. DOI: 10.1103/PhysRevApplied.9.034012. URL: https://link.aps.org/doi/10.1103/PhysRevApplied.9.034012 (visited on 06/27/2023).

[11] S. Toumodge. "METAMODELLING: Bond Graphs and Dynamic Systems [BOOKSHELF]". In: *IEEE Control Systems* 16.6 (Dec. 1996), p. 97. ISSN: 1066-033X. DOI: 10.1109/MCS.1996.546273. URL: http://ieeexplore.ieee.org/document/546273/ (visited on 06/27/2023).

[12] Snyder Ploutz. "Prevention of Muscle Atrophy With Exercise Countermeasures: Where We are and Where We are Going". In: (Jan. 29, 2009). URL: https://ntrs.nasa.gov/citations/20090007465 (visited on 06/27/2023).

[13] Nahom Beyene. "The Art of Space Flight Exercise Hardware: Design and Implementation". In: *Space 2004 Conference and Exhibit*. Space 2004 Conference and Exhibit. San Diego, California: American Institute of Aeronautics and Astronautics, Sept. 28, 2004. ISBN: 9781624100840. DOI: 10.2514/6.2004-5837. URL: https://arc.aiaa.org/doi/10.2514/6.2004-5837 (visited on 06/27/2023).

[14] Kerrie K. Rafalik. "Crew Exercise". In: (Dec. 5, 2017). URL: https://ntrs.nasa.gov/citations/20170011663 (visited on 06/27/2023).

[15] Gail Perusek et al. "Human Research Program Advanced Exercise Concepts (AEC) Overview". In: NASA Human Research Program Investigators" Workshop. Feb. 10, 2015. URL: https://ntrs.nasa.gov/citations/20160012339 (visited on 06/27/2023).

[16] Carly Toder et al. "Countermeasures (iRED, ARED CEVIS, MEC, TVIS, T2, Periodic Fitness Evaluation, BP-ECG, HRM). Critical Readiness Review Increment 23 and 24". In: (Feb. 4, 2010). URL: https://ntrs.nasa.gov/citations/20100008451 (visited on 06/27/2023).

[17] Ruben Mercadé-Prieto and Serafim Bakalis. "Methodological study on the removal of solid oil and fat stains from cotton fabrics using abrasion". In: *Textile Research Journal* 84.1 (Jan. 2014), pp. 52–65. ISSN: 0040-5175, 1746-7748. DOI: 10.1177/0040517513490059. URL: http://journals.sagepub.com/doi/10.1177/0040517513490059 (visited on 06/27/2023).

[18] Ahjin Lee et al. "The effects of mechanical actions on washing efficiency". In: *Fibers and Polymers* 9.1 (Feb. 1, 2008), pp. 101–106. ISSN: 1875-0052. DOI: 10.1007/s12221-008-0017-1. URL: https://doi.org/10.1007/s12221-008-0017-1 (visited on 06/27/2023).

[19] M. M. C. G Warmoeskerken et al. "Laundry process intensification by ultrasound". In: *Colloids and Surfaces A: Physicochemical and Engineering Aspects* 210.2 (Nov. 1, 2002), pp. 277–285. ISSN: 0927-7757. DOI: 10.1016/S0927-7757(02)00372-2. URL: https://www.sciencedirect.com/science/article/pii/S0927775702003722 (visited on 06/27/2023).

[20] Mingbo Ma et al. "Effects of ultrasonic laundering on the properties of silk fabrics". In: *Textile Research Journal* 84.20 (Dec. 2014), pp. 2166–2174. ISSN: 0040-5175, 1746-7748. DOI: 10.1177/0040517514537370. URL: http://journals.sagepub.com/doi/10.1177/0040517514537370 (visited on 06/27/2023).

[21] H.H. Prato and M.A. Morris. "Soil Remaining on Fabrics after Laundering as Evaluated by Response Surface Methodology". In: *Textile Research Journal* 54.10 (Oct. 1984), pp. 637–644. ISSN: 0040-5175, 1746-7748. DOI: 10.1177/004051758405401001. URL: http://journals.sagepub.com/doi/10.1177/004051758405401001 (visited on 06/27/2023).

[22] Subhas Ghosh, Michael D. Cannon, and R.B. Roy. "Quantitative Analysis of Durable Press Resin on Cotton Fabrics Using Near-Infrared Reflectance Spectroscopy". In: *Textile Research Journal* 60.3 (Mar. 1990), pp. 167–172. ISSN: 0040-5175, 1746-7748. DOI: 10.1177/004051759006000308. URL: http://journals.sagepub.com/doi/10.1177/004051759006000308 (visited on 06/27/2023).

[23] Soo Chang Kim et al. "Image Analysis for Quantifying Marquisette Damage in Home Laundering". In: *Textile Research Journal* 75.6 (June 2005), pp. 474–479. ISSN: 0040-5175, 1746-7748. DOI: 10.1177/0040517505053868. URL: http://journals.sagepub.com/doi/10.1177/0040517505053868 (visited on 06/27/2023).

[24] Arunkumar Gururajan, Eric F. Hequet, and Hamed Sari-Sarraf. "Objective Evaluation of Soil Release in Fabrics". In: *Textile Research Journal* 78.9 (Sept. 2008), pp. 782–795. ISSN: 0040-5175, 1746-7748. DOI: 10.1177/0040517507090786. URL: http://journals.sagepub.com/doi/10.1177/0040517507090786 (visited on 06/27/2023).

[25] Keiko Sugita and Masaru Oya. "Improvement of the image analysis method for quantifying low-polarity oily stains on fabric". In: *Textile Research Journal* 92.5 (Mar. 2022), pp. 649–659. ISSN: 0040-5175, 1746-7748. DOI: 10.1177/00405175211041719. URL: http://journals.sagepub.com/doi/10.1177/00405175211041719 (visited on 06/27/2023).

[26] Mourad Krifa, Shamini Rajaganesh, and William Fahy. "Perspectives on textile cleanliness – detecting human sebum residues on worn clothing". In: *Textile Research Journal* 89.23 (Dec. 2019), pp. 5226–5237. ISSN: 0040-5175, 1746-7748. DOI: 10.1177/0040517519855323. URL: http://journals.sagepub.com/doi/10.1177/0040517519855323 (visited on 06/27/2023).

[27] Prajokta Ray and Andrew J. Steckl. "Label-Free Optical Detection of Multiple Biomarkers in Sweat, Plasma, Urine, and Saliva". In: *ACS Sensors* 4.5 (May 24, 2019), pp. 1346–1357. ISSN: 2379-3694, 2379-3694. DOI: 10.1021/acssensors.9b00301. URL: https://pubs.acs.org/doi/10.1021/acssensors.9b00301 (visited on 06/27/2023).

[28] Craig Maynard et al. "Miniature Exercise Device-2 (MED-2): Preliminary ISS Evaluation Results for a Compact Motorized Resistive and Aerobic Rowing Exercise Device". In: International Space Station Research & Development Conference (ISSR&D 2018). July 23, 2018. URL: https://ntrs.nasa.gov/citations/20180006490 (visited on 06/27/2023).

[29] SAE Media Group. *Advanced Resistive Exercise Device*. Oct. 1, 2007. URL: https://www.techbriefs.com/component/content/article/tb/pub/briefs/bio-medical/2311 (visited on 06/27/2023).

[30] Meghan E. Downs. "Novel Musculoskeletal Loading and Assessment System". In: 2017 NASA Human Research Program Investigators" Workshop (HRP IWS 2017). Jan. 23, 2017. URL: https://ntrs.nasa.gov/citations/20170000271 (visited on 06/27/2023).

[31] Dean Karnopp, Donald L. Margolis, and Ronald C. Rosenberg. *System dynamics: modeling, simulation, and control of mechatronic systems*. 5. ed. Hoboken, NJ: Wiley, 2012. 636 pp. ISBN: 9781118160077 9780470889084.

[32] Jose Granda and Raymond Montgomery. "Automated Modeling and Simulation Using the Bond Graph Method for the Aerospace Industry". In: *AIAA Modeling and Simulation Technologies Conference and Exhibit*. AIAA Modeling and Simulation Technologies Conference and Exhibit. Austin, Texas: American Institute of Aeronautics and Astronautics, Aug. 11, 2003. ISBN: 9781624100918. DOI: 10.2514/6.2003-5527. URL: https://arc.aiaa.org/doi/10.2514/6.2003-5527 (visited on 06/27/2023).

[33] W. Borutzky. "Bond graph modelling and simulation of multidisciplinary systems – An introduction". In: *Simulation Modelling Practice and Theory* 17.1 (Jan. 2009), pp. 3–21. ISSN: 1569190X. DOI: 10.1016/j.simpat.2007.08.008. URL: https://linkinghub.elsevier.com/retrieve/pii/S1569190X07001074 (visited on 06/27/2023).

[34] Wolfgang Borutzky, ed. *Bond Graphs for Modelling, Control and Fault Diagnosis of Engineering Systems*. Cham: Springer International Publishing, 2017. ISBN: 9783319474335 9783319474342. DOI: 10.1007/978-3-319-47434-2. URL: http://link.springer.com/10.1007/978-3-319-47434-2 (visited on 06/27/2023).

[35] George F. Oster, Alan S. Perelson, and Aharon Katchalsky. "Network thermodynamics: dynamic modelling of biophysical systems". In: *Quarterly Reviews of Biophysics* 6.1 (Feb. 1973), pp. 1–134. ISSN: 1469-8994, 0033-5835. DOI: 10.1017/S0033583500000081. URL: https://www.cambridge.org/core/journals/quarterly-reviews-of-biophysics/article/abs/network-thermodynamics-dynamic-modelling-of-biophysical-systems/77B431E57497AFE757A8597FA690AD4E (visited on 06/27/2023).

[36] J. Broenink. "Introduction to Physical Systems Modelling with Bond Graphs". In: 2000. URL: https://www.semanticscholar.org/paper/Introduction-to-Physical-Systems-Modelling-with-Broenink/edbe4223c787adebd6e4674317a197312ecef87d (visited on 06/27/2023).

[37] Dean Karnopp. "Bond graph models for electrochemical energy storage : electrical, chemical and thermal effects". In: *Journal of the Franklin Institute* 327.6 (Jan. 1990), pp. 983–992. ISSN: 00160032. DOI: 10.1016/0016-0032(90)90073-R. URL: https://linkinghub.elsevier.com/retrieve/pii/001600329090073R (visited on 06/27/2023).

[38] Dan Selişteanu, Monica Roman, and Dorin Şendrescu. "Pseudo Bond Graph modelling and on-line estimation of unknown kinetics for a wastewater biodegradation process". In: *Simulation Modelling Practice and Theory* 18.9 (Oct. 2010), pp. 1297–1313. ISSN: 1569190X. DOI: 10.1016/j.simpat.2010.05.004. URL: https://linkinghub.elsevier.com/retrieve/pii/S1569190X10000845 (visited on 06/27/2023).

[39] William J Krotiuk. "Calculation of Pressure Drop Across a Porous Media Debris BedAcross a Porous Media Debris Bed on a PWR Sump Screenon a PWR Sump Scree". ANS 2006 Winter Meeting, Nov. 12, 2006. URL: https://www.nrc.gov/docs/ML0632/ML063210166.pdf.

[40] Benjamin D. Shaw. *Uncertainty Analysis of Experimental Data with R*. 1st ed. Boca Raton : CRC Press, 2017.: Chapman and Hall/CRC, July 6, 2017. ISBN: 9781315366715. DOI: 10.1201/9781315366715. URL: https://www.taylorfrancis.com/books/9781498797337 (visited on 03/07/2024).

[41] Kathryn L. Hatch. *Textile science*. Minneapolis/Saint Paul: West Pub, 1993. 472 pp. ISBN: 9780314904713.

Appendices

Appendix A

Astronaut-Powered Laundry Machine Bond Graph Information

A.1 State Variables

Variable	Units	Representation
Mechanical Domain		
$\dot{q}_c$	$\frac{m}{s}$	**Translational velocity difference across crank arm shock absorber.**
$\dot{q}_{tp}$	$\frac{rad}{s}$	**Rotational velocity of tilt plate.**
$\dot{q}_{sa}$	$\frac{m}{s}$	**Translational velocity experienced by shock absorber.**
$\dot{p}_c$	$N \cdot m$	**Net torque acting on crank shaft.**
$\dot{p}_{tp}$	$N \cdot m$	**Net torque acting on tilt plate.**
Hydraulic Domain		
$\dot{q}_A$	$\frac{m^3}{s}$	**Net volumetric flow rate through agitation chamber.**
$\dot{q}_{c1}$	$\frac{m^3}{s}$	**Net volumetric flow rate through side #1 of hydraulic system.**
$\dot{q}_{c2}$	$\frac{m^3}{s}$	**Net volumetric flow rate through side #2 of hydraulic system.**
$\dot{q}_R$	$\frac{m^3}{s}$	**Net volumetric flow rate through water reservoir.**
$\dot{q}_{wf}$	$\frac{m^3}{s}$	**Net volumetric flow rate through water filter(s).**

$\dot{p}_{a1}$	$\frac{N}{m^2}$	**Net pressure of agitation bladder valve #1.**
$\dot{p}_{a2}$	$\frac{N}{m^2}$	**Net pressure of agitation bladder valve #2.**
$\dot{p}_{BP}$	$\frac{N}{m^2}$	**Net pressure of bypass valve.**
$\dot{p}_{r1}$	$\frac{N}{m^2}$	**Net pressure of reservoir bladder valve #1.**
$\dot{p}_{r2}$	$\frac{N}{m^2}$	**Net pressure of reservoir bladder valve #2.**
$\dot{p}_{wf1}$	$\frac{N}{m^2}$	**Net pressure of water filter valve #1.**
$\dot{p}_{wf2}$	$\frac{N}{m^2}$	**Net pressure of water filter valve #2.**

Table A.1: Bond graph state variables.

A.2 Parameters

Term	Units	Initial Simulation Value	Definition
a_a	m	**0.15**	**Distance from crank arm mount to tilt plate rotation center.**
a_{sa}	m	**0.14**	**Distance from shock absorber to tilt plate rotation center.**
$A(u)$	m^2	–	**Valve flow area as a function of valve position.**
A_A	m^2	**0.1603**	**Cross sectional area of agitation chamber.**
A_P	m^2	**2.835e-04**	**Area of hydraulic piping between reservoir and agitation chamber.**
A_{lcp}	m^2	**2.835e-04**	**Area of lint catch porous plug .**
A_{wfp}	m^2	**2.835e-04**	**Area of water filter porous plug .**
b_c	$\frac{N \cdot s}{m}$	**19.75**	**Crank arm shock absorber damping coefficient.**
b_{cs}	$\frac{N \cdot s}{m}$	**0.4750**	**Crankshaft friction.**
b_{sa}	$\frac{N \cdot s}{m}$	**0.5585**	**Tilt plate shock absorber damping coefficient.**
B	$\frac{N}{m^2}$	**2.180e+09**	**Fluid bulk modulus.**
$\overline{c}$	$mol^{\frac{1}{n}}$	–	**Average amount of waste removed.**
Δc	mol	–	**Concentration of waste in water as measured from senor array.**
$C_d(u)$	m^2	–	**Valve discharge coefficient as a function of valve position.**
$D_{P_{lc}}$	m	–	**Particle diameter of lint catch.**
$D_{P_{wr}}$	m	–	**Particle diameter of water reservoir.**
E	$\frac{N}{m^2}$	**5000000**	**Elastic modulus of bladder rubber.**
J_c	$kg \cdot m^2$	**2.0503e-05**	**Inertia of Crank Shaft.**

$J_{tp}(q_a)$	$kg \cdot m^2$	**0.0368**	**Inertia of Tilt Plate as a function of water volume.**
k	$\frac{1}{s}$	–	**Waste removal rate coefficient.**
k_c	$\frac{N}{m}$	**1.412e+02**	**Crank arm shock absorber stiffness coefficient.**
k_s		–	**Waste removal rate exponential scaling factor.**
k_{sa}	$\frac{N}{m}$	**0.452**	**Tilt plate shock absorber stiffness coefficient.**
k_{tp}	$N \cdot m \cdot s$	**1.453**	**Tilt plate stiffness coefficient.**
L_{lc}	m	–	**Length of lint catch BG resistor.**
L_{wr}	m	–	**Length of water reservoir BG resistor.**
l	m	**0.19**	**Length of crank arm.**
l_p	m	**0.75**	**Length of hydraulic path between reservoir and agitation chamber.**
l_{tp}	m	**0.4**	**Side length of square tilt plate.**
n		–	**Kinetic order of average amount of waste removed.**
ΔQ	$\frac{m^3}{s}$	–	**Volumetric flow rate difference for BG element.**
r	m	**0.015**	**Distance from crank arm mount to crankshaft rotation center.**
r_A	m	**0.01**	**Radius of agitation bladder corners.**
r_R	m	**0.01**	**Radius of water reservoir bladder corners.**
R_e	Ω	**20**	**Electrical circuit resistance.**
R_{lc}	$\frac{N}{m^2}$	–	**Linear lint catch resistance.**
R_{wf}	$\frac{N}{m^2}$	–	**Linear water filter resistance.**
t	s	**60**	**Simulation run time.**
t_A	m	**0.003**	**Thickness of agitation bladder.**
t_R	m	**0.003**	**Thickness of water reservoir bladder.**
T_{em}	$\frac{V \cdot s}{rad}$	**1.5**	**DC generator rate #1.**
T_{me}	$\frac{N \cdot m}{A}$	**1.5**	**DC generator rate #2.**

T_P	$\frac{m^3}{rad}$	**7.50e-05**	**Hydraulic pump rate.**
u	%	–	**Hydraulic valve position as a percentage of stroke.**
V_A	m^3	**0.003785**	**Volume of agitation bladder.**
V_P	m^3	**2.126e-04**	**Volume of piping.**
V_R	m^3	**0.003785**	**Volume of water reservoir bladder.**
V_T	m^3	**0.0025**	**Volume of textiles within the agitation bladder.**
V_{wf}	m^3	–	**Volume of water filter.**
α	rad	–	**Position of tilt plate rotation.**
ϵ_{lc}		–	**Porosity of lint catch .**
ϵ_{wr}		–	**Porosity of water reservoir .**
ρ	$\frac{kg}{m^3}$	**998**	**Density of washing fluid .**
θ	rad	–	**Position of crankshaft rotation.**
$\tau(t)$	$N \cdot m$	–	**Human Generated torque over time.**
μ	$\frac{N \cdot s}{m^2}$	**1.0e-03**	**Dynamic viscosity of washing fluid.**

Table A.2: Bond graph model parameters. "–" values are for calculated, time dependent, or non-simulated variables

Variable	**Units**	**Value**	**Description**
Mechanical Domain			
q_c	m	**0**	**Displacement across crank arm shock absorber.**
q_{tp}	rad	**0**	**Angular displacement of tilt plate.**
q_{sa}	m	**0**	**Displacement across shock absorber.**
p_c	$N \cdot m \cdot s$	**0**	**Momentum of crank shaft.**
p_{tp}	$N \cdot m \cdot s$	**0**	**Momentum of tilt plate.**
Hydraulic Domain			
q_A	m^3	**-0.0013**	**Volume of agitation chamber.**

q_{c1}	m^3	**0**	**Volume of washing fluid inside #1 of hydraulic system.**
q_{c2}	m^3	**0**	**Volume of washing fluid in side #2 of hydraulic system.**
q_R	m^3	**0.0013**	**Volume of washing fluid in reservoir.**
q_{wf}	m^3	**0**	**Volume of washing fluid in water filter(s).**
p_{a1}	$\frac{N \cdot s}{m^2}$	**0**	**Momentum of washing fluid in agitation bladder valve #1.**
p_{a2}	$\frac{N \cdot s}{m^2}$	**0**	**Momentum of washing fluid in agitation bladder valve #2.**
p_{a2}	$\frac{N \cdot s}{m^2}$	**0**	**Momentum of washing fluid in agitation bladder valve #2.**
p_{BP}	$\frac{N \cdot s}{m^2}$	**0**	**Momentum of washing fluid in bypass valve #2.**
p_{r1}	$\frac{N \cdot s}{m^2}$	**0**	**Momentum of washing fluid in reservoir bladder valve #1.**
p_{r2}	$\frac{N \cdot s}{m^2}$	**0**	**Momentum of washing fluid in reservoir bladder valve #2.**
p_{wf1}	$\frac{N \cdot s}{m^2}$	**0**	**Momentum of washing fluid in water filter valve #1.**
p_{wf2}	$\frac{N \cdot s}{m^2}$	**0**	**Momentum of washing fluid in water filter valve #2.**

Table A.3: Bond graph initial value of variables.

A.3 Constitutive Equations

Physical Element	Bond Graph Element	Constitutive Relation
Applied Torque	**Effort Source**	$S_{e_1} = \tau(t)$
Crankshaft	**Inertia**	$\Phi_{I_1} = J_C$
Crankshaft Friction	**Resistor**	$\Phi_{R_1} = b_{cs}$
Shock Abs. #	**Resistor**	$\Phi_{R_2} = b_C$
Shock Abs.	**Capacitor**	$\Phi_{C_1} = \frac{1}{k_C}$
Hinge	**Resistor**	$\Phi_{R_3} = b_{tp}$
Hinge	**Capacitor**	$\Phi_{C_2} = \frac{1}{k_{tp}}$
Tilt Plate	**Inertia**	$\Phi_{I_2} = J_{tp} + \frac{\rho \cdot q_a \cdot l_{tp}}{12}$
Shock Abs. #2	**Resistor**	$\Phi_{R_4} = b_{sa1}$
Shock Abs. #2	**Capacitor**	$\Phi_{C_3} = \frac{1}{k_{sa1}}$
Crank-Follower	**Modulated Transformer**	$m(\theta) = r \cdot sin(\theta) + (\frac{l \cdot \frac{r}{l}^2) \cdot cos(\theta) \cdot sin(\theta)}{\sqrt{1 - \frac{r}{l}^2 \cdot sin^2(\theta)}}$
Shock Abs. #1 Mount	**Modulated Transformer**	$m_2(\alpha_1) = a_1 \cdot cos(\alpha)$
Shock Abs. #2 Mount	**Modulated Transformer**	$m_3(\alpha_2) = a_2 \cdot cos(\alpha)$
DC Generator	**Gyrator**	$r_1 = T_{em}$
DC Generator	**Gyrator**	$r_2 = T_{me}$
Resistor	**Resistor**	$\Phi_{R_5}^{-1} = R_e$

Hydraulic Pump	**Transformer**	$m_4 = T_P$
Path Inertia	**Inertia**	$\Phi_{I_{3_i}} = \frac{\rho \cdot l_i}{4 \cdot A_i}$
Hydraulic Valve	**Resistor**	$\Phi_{R_6} = \frac{\rho \cdot \Delta Q_i \lvert \Delta Q_i \rvert}{2 \cdot C_d^2 \cdot (u_i) \cdot A^2 \cdot (u_i)}$
Lint Catch	**Nonlinear Resistor**	$\Phi_{R_7} = \frac{9.375 \cdot \Delta Q \cdot \mu \cdot L \cdot (\frac{4}{D_p}^2) \cdot (1-\epsilon)^2}{A_{lcp} \cdot \epsilon^3} + \frac{0.4375 \cdot \Delta Q^2 \cdot \rho \cdot L \cdot (\frac{4}{D_p}) \cdot (1-\epsilon)}{A_{lcp}^2 \cdot \epsilon^3}$
Water Filter	**Nonlinear Resistor**	$\Phi_{R_8} = \frac{4.167 \cdot \Delta Q \cdot \mu \cdot L \cdot (\frac{6}{D_p}^2) \cdot (1-\epsilon)^2}{A_{wrp} \cdot \epsilon^3} + \frac{0.2917 \cdot \Delta Q^2 \cdot \rho \cdot L \cdot (\frac{6}{D_p}) \cdot (1-\epsilon)}{A_{wrp}^2 \cdot \epsilon^3}$
Lint Catch	**Resistor**	$\Phi_{R_9} = R_{lc} \Delta Q$
Water Filter	**Resistor**	$\Phi_{R10} = R_{wf} \Delta Q$
Agitation Bladder	**Capacitor**	$\Phi_{C_4} = \frac{6 \cdot r_A \cdot V_A}{t_A \cdot E} + \frac{V_A}{B}$
Water Reservoir	**Capacitor**	$\Phi_{C_5} = \frac{10 \cdot r_R \cdot V_R}{t_R \cdot E} + \frac{V_R}{B}$
Water Filter	**Capacitor**	$\Phi_{C_6} = \frac{V_w f}{B}$
Pipe	**Capacitor**	$\Phi_{C_7} = \frac{V_p}{B}$

Table A.4: Bond graph model consecutive equations.

A.4 State Space Derivation

The following state space derivation is done in the context of the labeled power bonds in Figure A.1.

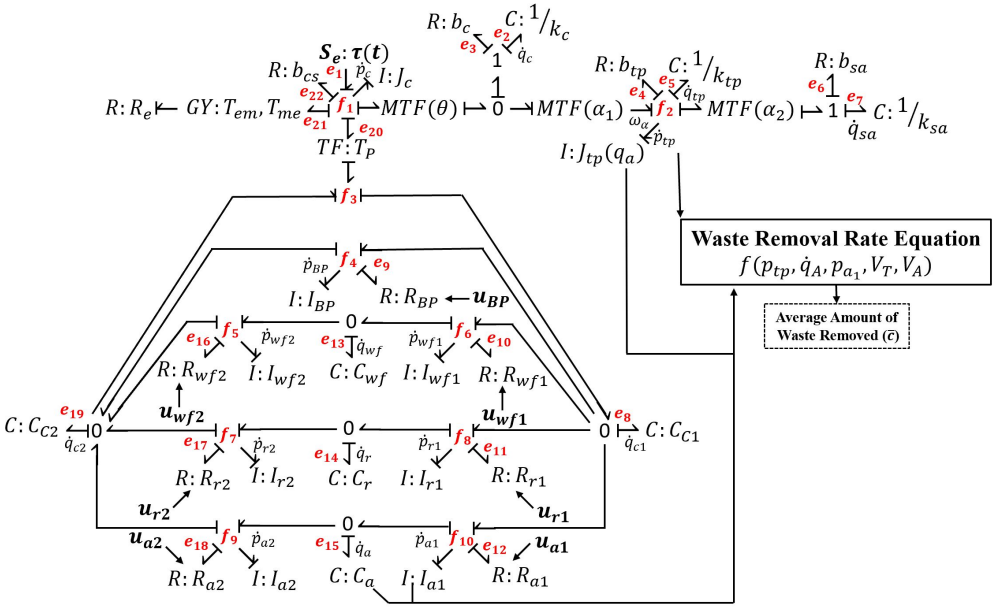

Figure A.1: Effort and Flow labeled Bond Graph of spaceflight exercise and textile laundering machine concept.

A.4.1 Derivation with Annotated Efforts and Flows

$$\dot{q}_c = MTF(\theta) \cdot f_1 - MTF(\alpha_1) \cdot f_2 \tag{A.1}$$

$$\dot{q}_t p = f_2 \tag{A.2}$$

$$\dot{q}_{sa} = MTF(\alpha_2) \cdot f_2 \tag{A.3}$$

$$\dot{p}_c = e_1 - MTF(\theta) \cdot (e_2 + e_3) - e_{20} - e_{21} - e_{22} \tag{A.4}$$

$$\dot{p}_{tp} = MTF(\alpha_1) \cdot (e_2 + e_3) - e_4 - e_5 - MTF(\alpha_2) \cdot (e_6 + e_7) \tag{A.5}$$

$$\dot{q}_{c1} = f_3 - f_4 - f_6 - f_8 - f_{10} \tag{A.6}$$

$$\dot{q}_{c2} = -f_3 + f_4 + f_5 + f_7 + f_9 \tag{A.7}$$

$$\dot{q}_A = f_{10} - f_9 \tag{A.8}$$

$$\dot{q}_R = f_8 - f_7 \tag{A.9}$$

$$\dot{q}_{wf} = f_6 - f_5 \tag{A.10}$$

$$\dot{p}_{a1} = e_8 - e_{12} - e_{15} \tag{A.11}$$

$$\dot{p}_{a2} = e_{15} - e_{18} - e_{19} \tag{A.12}$$

$$\dot{p}_{BP} = e_8 - e_{19} \tag{A.13}$$

$$\dot{p}_{r1} = e_8 - e_{11} - e_{14} \tag{A.14}$$

$$\dot{p}_{r2} = e_{14} - e_{17} - e_{19} \tag{A.15}$$

$$\dot{p}_{wf1} = e_8 - e_{10} - e_{13} \tag{A.16}$$

$$\dot{p}_{wf2} = e_{13} - e_{16} - e_{19} \tag{A.17}$$

A.4.2 Annotated Effort and Flows with Parameters

$$f_1 = \Phi_{I_1}^{-1} \cdot p_c = \frac{p_c}{J_c} \tag{A.18}$$

$$f_2 = \Phi_{I_2}^{-1} \cdot p_{tp} = \frac{p_{tp}}{J_{tp}} \tag{A.19}$$

$$f_3 = m_5 \cdot f_1 = \frac{T_p \cdot p_c}{J_c} \tag{A.20}$$

$$f_4 = \Phi_{I_3}^{-1} \cdot p_{BP} = \frac{p_{BP}}{\frac{\rho \cdot l_{BP}}{4 \cdot A_{BP}}} \tag{A.21}$$

$$f_5 = \Phi_{I_3}^{-1} \cdot p_{wf2} = \frac{p_{wf2}}{\frac{\rho \cdot l_{wf2}}{4 \cdot A_{wf2}}} \tag{A.22}$$

$$f_6 = \Phi_{I_3}^{-1} \cdot p_{wf1} = \frac{p_{wf1}}{\frac{\rho \cdot l_{wf1}}{4 \cdot A_{wf1}}} \tag{A.23}$$

$$f_7 = \Phi_{I_3}^{-1} \cdot p_{r2} = \frac{p_{r2}}{\frac{\rho \cdot l_{r2}}{4 \cdot A_{r2}}} \tag{A.24}$$

$$f_8 = \Phi_{I_3}^{-1} \cdot p_{r1} = \frac{p_{r1}}{\frac{\rho \cdot l_{r1}}{4 \cdot A_{r1}}} \tag{A.25}$$

$$f_9 = \Phi_{I_3}^{-1} \cdot p_{a2} = \frac{p_{a2}}{\frac{\rho \cdot l_{a2}}{4 \cdot A_{a2}}} \tag{A.26}$$

$$f_{10} = \Phi_{I_3}^{-1} \cdot p_{a1} = \frac{p_{a1}}{\frac{\rho \cdot l_{a1}}{4 \cdot A_{a1}}} \tag{A.27}$$

$$e_1 = S_{e1} = \tau(t) \tag{A.28}$$

$$e_2 = \Phi_{C_1}^{-1} \cdot q_c = k_c \cdot q_c \tag{A.29}$$

$$e_3 = \Phi_{R_2} \cdot (m_1 \cdot (\theta) \cdot f_1 - m_2 \cdot (\alpha_1) \cdot f_2) = b_c \left\{ \frac{p_c}{J_c} \cdot r \cdot sin(\theta) + \frac{l \cdot \frac{r}{l}^2) \cdot cos(\theta) \cdot sin(\theta)}{\sqrt{1 - \frac{r}{l}^2 \cdot sin^2(\theta)}} - \frac{p_{tp}}{J_{tp}} \cdot \alpha_1 \cdot cos(\alpha) \right\} \tag{A.30}$$

$$e_4 = \Phi_{R_3} \cdot f_2 = \frac{b_{tp} \cdot p_{tp}}{J_{tp}} \tag{A.31}$$

$$e_5 = \Phi_{C_2}^{-1} \cdot q_{tp} = k_{tp} \cdot q_{tp} \tag{A.32}$$

$$e_6 = \Phi_{R_4} \cdot m_3(\alpha_2) \cdot f_2 = b_{sa1} \cdot \frac{p_{tp}}{J_{tp}} \cdot a_2 \cdot cos(\alpha) \tag{A.33}$$

$$e_7 = \Phi_{C_3}^{-1} \cdot q_{sa1} = k_{sa1} \cdot q_{sa1} \tag{A.34}$$

$$e_8 = \Phi_{C_8}^{-1} \cdot q_{c1} = \frac{B}{V_p} \cdot q_{c1} \tag{A.35}$$

$$e_9 = \Phi_{C_7}(f_4) = \frac{\rho(f_4) \cdot |f_4|}{2 \cdot C_d^2 \cdot (u_{BP}) \cdot A^2 \cdot (u_{BP})} \tag{A.36}$$

$$\begin{aligned} e_{10} &= \Phi_{R_7}(f_6) + \Phi_{R_9}(f_6) \\ &= \frac{\rho(f_6) \cdot |f_6|}{2 \cdot C_d^2 \cdot (u_{wf1}) \cdot A^2 \cdot (u_{wf1})} + \frac{4.167 \cdot (f_6)) \cdot \mu \cdot L_{wr} \cdot (\frac{6}{D_{pwr}}^2) \cdot (1 - \epsilon_{wr})^2}{A_{wrp} \cdot \epsilon_{wr}^3} \\ &\quad + \frac{0.2917 \cdot (f_6))^2 \cdot \rho \cdot L_{wr} \cdot (\frac{6}{D_{pwr}}) \cdot (1 - \epsilon_{wr})}{A_{wrp}^2 \cdot \epsilon_{wr}^3} \end{aligned} \tag{A.37}$$

$$e_{11} = \Phi_{R_7}(f_8) = \frac{\rho(f_8) \cdot |f_8|}{2 \cdot C_d^2 \cdot (u_{r1}) \cdot A^2 \cdot (u_{r1})} \tag{A.38}$$

$$\begin{aligned} e_{12} &= \Phi_{R_7}(f_{10}) + \Phi_{R_8}(f_{10}) \\ &= \frac{\rho(f_{10}) \cdot |f_{10}|}{2 \cdot C_d^2 \cdot (u_{a1}) \cdot A^2 \cdot (u_{a1})} + \frac{9.375 \cdot (f_{10})) \cdot \mu \cdot L_{lc} \cdot (\frac{4}{D_{p_{lc}}}^2) \cdot (1 - \epsilon_{lc})^2}{A_{lcp} \cdot \epsilon_{lc}^3} \\ &\quad + \frac{0.4375 \cdot (f_{10}))^2 \cdot \rho \cdot L_{lc} \cdot (\frac{4}{D_{p_{lc}}}) \cdot (1 - \epsilon_{lc})}{A_{lcp}^2 \cdot \epsilon_{lc}^3} \end{aligned} \tag{A.39}$$

$$e_{13} = \Phi_{C_7}^{-1} \cdot q_{wf} = \frac{B}{V_{wf}} \cdot q_{wf} \tag{A.40}$$

$$e_{14} = \Phi_{C_6}^{-1} \cdot q_r = \left\{ \frac{t_R \cdot E}{10 \cdot r_R \cdot V_R} + \frac{B}{V_R} \right\} \cdot q_r \tag{A.41}$$

$$e_{15} = \Phi_{C_5}^{-1} \cdot q_a = \left\{ \frac{t_A \cdot E}{6 \cdot r_A \cdot V_A} + \frac{B}{V_A} \right\} \cdot q_a \tag{A.42}$$

$$\begin{aligned} e_{16} &= \Phi_{R_7}(f_5) + \Phi_{R_9}(f_5) \\ &= \frac{\rho(f_5) \cdot |f_5|}{2 \cdot C_d^2 \cdot (u_{wf2}) \cdot A^2 \cdot (u_{wf2})} + \frac{4.167 \cdot (f_5)) \cdot \mu \cdot L_{wr} \cdot (\frac{6}{D_{pwr}}^2) \cdot (1 - \epsilon_{wr})^2}{A_{wrp} \cdot \epsilon_{wr}^3} \\ &\quad + \frac{0.2917 \cdot (f_5))^2 \cdot \rho \cdot L_{wr} \cdot (\frac{6}{D_{pwr}}) \cdot (1 - \epsilon_{wr})}{A_{wrp}^2 \cdot \epsilon_{wr}^3} \end{aligned} \tag{A.43}$$

$$e_{17} = \Phi_{R_7}(f_7) = \frac{\rho(f_7) \cdot |f_7|}{2 \cdot C_d^2 \cdot (u_{r2}) \cdot A^2 \cdot (u_{r2})} \tag{A.44}$$

$$e_{18} = \Phi_{R_7}(f_9) = \frac{\rho(f_97) \cdot |f_9|}{2 \cdot C_d^2 \cdot (u_{a2}) \cdot A^2 \cdot (u_{a2})} \tag{A.45}$$

$$e_{19} = \Phi_{C_8}^{-1} \cdot q_{c2} = \frac{B}{V_p} \cdot q_{c2} \tag{A.46}$$

$$e_{20} = m_5 \cdot (e_{21} - e_{10}) = \frac{T_p \cdot B}{V_p} \cdot (q_{c2} - q_{c1}) \tag{A.47}$$

$$e_{21} = \Phi_{R_r} \cdot r_1 \cdot r_2 \cdot f_1 \cdot = \frac{T_{em} \cdot T_{me} \cdot p_c}{R_e \cdot J_c} \tag{A.48}$$

$$e_{22} = \Phi_{R_1} \cdot f_1 = \frac{b_{cs} \cdot p_c}{J_c} \tag{A.49}$$

Appendix B

Modified Bond Graph Information

B.1 State Variables

Variable	Units	Representation
$\dot{q}_a$	$\frac{m^3}{s}$	**Net volumetric flow rate through agitation chamber.**
$\dot{q}_{a1}$	$\frac{m^3}{s}$	**Net volumetric flow rate through agitation pipe #1.**
$\dot{q}_{a2}$	$\frac{m^3}{s}$	**Net volumetric flow rate through agitation pipe #2.**
$\dot{q}_{b1}$	$\frac{m^3}{s}$	**Net volumetric flow rate through bypass pipe #1.**
$\dot{q}_{b2}$	$\frac{m^3}{s}$	**Net volumetric flow rate through bypass pipe #2.**
$\dot{q}_{c1}$	$\frac{m^3}{s}$	**Net volumetric flow rate through manifold #1.**
$\dot{q}_{c2}$	$\frac{m^3}{s}$	**Net volumetric flow rate through manifold #2.**
$\dot{q}_r$	$\frac{m^3}{s}$	**Net volumetric flow rate through water reservoir.**
$\dot{q}_{r1}$	$\frac{m^3}{s}$	**Net volumetric flow rate through reservoir pipe #1.**
$\dot{q}_{r2}$	$\frac{m^3}{s}$	**Net volumetric flow rate through reservoir pipe #2.**
$\dot{p}_{a1}$	$\frac{m^3}{s}$	**Net pressure differential of agitation bladder valve #1.**
$\dot{p}_{a2}$	$\frac{N}{m^2}$	**Net pressure differential of agitation bladder valve #2.**
$\dot{p}_{BP}$	$\frac{N}{m^2}$	**Net pressure differential of of bypass valve.**
$\dot{p}_{r1}$	$\frac{N}{m^2}$	**Net pressure differential of reservoir bladder valve #1.**
$\dot{p}_{r2}$	$\frac{N}{m^2}$	**Net pressure differential of reservoir bladder valve #2.**

Table B.1: Bond graph state variables.

B.2 Parameters

Term	Units	Initial Value	Definition
a_{1h}	in	**-13**	**Distance reservoir head datum to agitation valve #1.**
a_{2h}	in	**-13**	**Distance reservoir head datum to agitation valve #2.**
a_{1l}	m	**0.3556**	**Agitation pipe length #1.**
a_{2l}	m	**0.5842**	**Agitation pipe length #2.**
A_A	m^2	**0.1017**	**Cross sectional area of agitation chamber.**
B	$\frac{N}{m^2}$	**2.180e+09**	**Fluid bulk modulus.**
b_{1l}	m	**0.1016**	**Bypass pipe length #1.**
b_{2l}	m	**0.2540**	**Bypass pipe length #2.**
bph	in	**-4**	**Distance reservoir head datum to bypass valve.**
c_{1l}	m	**0.0254**	**Manifold pipe length #1.**
c_{2l}	m	**0.0254**	**Manifold pipe length #2.**
C_a	$\frac{m^5}{N}$	**7.3378e+07**	**Agitation bladder capacitance.**
C_{a1}	$\frac{m^5}{N}$	**4.83947e+13**	**Agitation pipe #1 capacitance.**
C_{a2}	$\frac{m^5}{N}$	**2.94576e+13**	**Agitation pipe #2 capacitance.**
C_{b1}	$\frac{m^5}{N}$	**1.69381e+14**	**Bypass pipe #1 capacitance.**
C_{b2}	$\frac{m^5}{N}$	**6.77525e+13**	**Bypass pipe #2 capacitance.**
C_{c1}	$\frac{m^5}{N}$	**6.77525e+14**	**Manifold pipe #1 capacitance.**
C_{c2}	$\frac{m^5}{N}$	**6.77525e+14**	**Manifold pipe #2 capacitance.**
C_d		**0.64**	**Coefficient of discharge.**
C_r	$\frac{m^5}{N}$	**4.60716e+12**	**Reservoir capacitance.**
C_{r1}	$\frac{m^5}{N}$	**1.35505e+14**	**Reservoir pipe #1 capacitance.**
C_{r2}	$\frac{m^5}{N}$	**5.64604e+13**	**Reservoir pipe #2 capacitance.**
E	$\frac{N}{m^2}$	**5000000**	**Elastic modulus of bladder rubber.**

g	$\frac{m}{s^2}$	**9.81**	**Gravity**
I_{a1}	$\frac{kg}{m^4}$	**2.802e+06**	**Inertia of agitation pipe segment #1.**
I_{a2}	$\frac{kg}{m^4}$	**4.603e+06**	**Inertia of agitation pipe segment #2.**
I_{bp}	$\frac{kg}{m^4}$	**2.802e+06**	**Inertia of bypass pipe segments.**
I_{r1}	$\frac{kg}{m^4}$	**1.001e+06**	**Inertia of reservoir pipe segment #1.**
I_{r2}	$\frac{kg}{m^4}$	**2.401e+06**	**Inertia of reservoir pipe segment #2.**
k	$\frac{1}{s}$	–	**Waste removal rate coefficient.**
k_s		–	**Waste removal rate exponential scaling factor.**
n		–	**Kinetic order of average amount of waste removed.**
ΔQ	$\frac{m^3}{s}$	–	**Volumetric flow rate difference for BG element.**
r_A	m	**0.01**	**Radius of agitation bladder corners.**
r_a	$\frac{N \cdot s}{m^5}$	**1**	**Agitation bladder resistance.**
r_R	m	**0.01**	**Radius of water reservoir bladder corners.**
r_r	$\frac{N \cdot s}{m^5}$	**200000**	**Reservoir resistance.**
r_{1h}	in	**0**	**Distance reservoir head datum to reservoir valve. #1.**
r_{2h}	in	**0**	**Distance reservoir head datum to reservoir valve. #2.**
r_{1l}	m	**0.1270**	**Reservoir pipe length #1.**
r_{2l}	m	**0.3048**	**Reservoir pipe length #2.**
ri_{a1}	$\frac{N \cdot s}{m^5}$	**1.180e+06**	**Agitation pipe #1 total resistance.**
ri_{a2}	$\frac{N \cdot s}{m^5}$	**1.538e+06**	**Agitation pipe #2 total resistance.**
ri_{b1}	$\frac{N \cdot s}{m^5}$	**4.625e+05**	**Bypass pipe #1 total resistance.**
ri_{b2}	$\frac{N \cdot s}{m^5}$	**7.012e+05**	**Bypass pipe #2 total resistance.**
ri_{c1}	$\frac{N \cdot s}{m^5}$	**3.978e+07**	**Manifold pipe #1 total resistance.**
ri_{c2}	$\frac{N \cdot s}{m^5}$	**3.978e+07**	**Manifold pipe #2 total resistance.**

ri_{r1}	$\frac{N \cdot s}{m^5}$	**6.989e+05**	**Reservoir pipe #1 total resistance.**
ri_{r2}	$\frac{N \cdot s}{m^5}$	**9.774e+05**	**Reservoir pipe #2 total resistance.**
r_{pipe}	in	**0.5**	**Pipe radius.**
t_A	m	**0.003**	**Thickness of agitation bladder.**
t_R	m	**0.003**	**Thickness of water reservoir bladder.**
u	$\%$	–	**Hydraulic valve position as a percentage of stroke.**
V_A	m^3	**0.003785**	**Volume of agitation bladder.**
V_R	m^3	**0.003785**	**Volume of water reservoir bladder.**
V_T	m^3	**2.304e-06**	**Volume of textiles within the agitation bladder.**
ρ	$\frac{kg}{m^3}$	**998**	**Density of washing fluid .**
μ	$\frac{N \cdot s}{m^2}$	**1.0e-03**	**Dynamic viscosity of washing fluid.**

Table B.2: Bond graph model parameters. "–" values are for calculated, time dependent, or non-simulated variables

Term	Units	Initial Value	Definition
Hydraulic Domain			
q_a	m^3	**0.00189**	**Net volume of agitation chamber.**
q_{a1}	m^3	**4.505e-05**	**Net volume of agitation pipe #1.**
q_{a2}	m^3	**7.400e-05**	**Net volume of agitation pipe #2.**
q_{b1}	m^3	**1.287e-05**	**Net volume of bypass pipe #1.**
q_{b2}	m^3	**3.218e-05**	**Net volume of bypass pipe #2.**
q_{c1}	m^3	**3.218e-06**	**Net volume of manifold #1.**
q_{c2}	m^3	**3.218e-06**	**Net volume of manifold #2.**
q_r	m^3	**4.732e-04**	**Net volume of water reservoir.**
q_{r1}	m^3	**1.609e-05**	**Net volume of reservoir pipe #1.**
q_{r2}	m^3	**3.861e-05**	**Net volume of reservoir pipe #2.**
p_{a1}	$\frac{N \cdot s}{m^2}$	**0**	**Net momentum of agitation bladder valve #1.**
p_{a2}	$\frac{N \cdot s}{m^2}$	**0**	**Net momentum of agitation bladder valve #2.**
p_{BP}	$\frac{N \cdot s}{m^2}$	**0**	**Net momentum of of bypass valve.**
p_{r1}	$\frac{N \cdot s}{m^2}$	**0**	**Net momentum of reservoir bladder valve #1.**
p_{r2}	$\frac{N \cdot s}{m^2}$	**0**	**Net momentum of reservoir bladder valve #2.**

Table B.3: Bond graph initial value of variables.

B.3 Constitutive Equations

Physical Element	**Bond Graph Element**	**Constitutive Relation**
Applied Flow	**Flow Source**	$S_{f_1} =$ **Total Flow #1 Data(t)**
Applied Flow	**Flow Source**	$S_{f_2} =$ **Total Flow #2 Data(t)**
Pipe Inertia (ni)	**Inertia**	$\Phi_{I_{ni}} = \frac{\rho \cdot l_{ni}}{4 \cdot A_{ni}}$
Pipe Length (ni)	**Resistor**	$\Phi_{Ri_{ni}} = \frac{128 \cdot \mu \cdot l_{ni}}{\pi \cdot d_{pipe}^4} + \rho \cdot \mathbf{g} \cdot h_{ni} + R_{\mathbf{Tune}}$
Hydraulic Valve	**Resistor**	$\Phi_{R_{ni}} = \frac{\rho \cdot \Delta Q_i \lvert \Delta Q_i \rvert}{2 \cdot C_d^2 \cdot (u_{ni}) \cdot A^2 \cdot (u_i)}$
Agitation Bladder	**Capacitor**	$\Phi_{C_a} = \frac{6 \cdot r_A \cdot V_A}{t_A \cdot E} + \frac{V_A}{B}$
Water Reservoir	**Capacitor**	$\Phi_{C_r} = \frac{10 \cdot r_R \cdot V_R}{t_R \cdot E} + \frac{V_R}{B}$
Pipe	**Capacitor**	$\Phi_{C_{ni}} = \frac{\pi \cdot r_{Pipe}^2 \cdot l_{ni}}{B}$

Table B.4: Bond graph model consecutive equations. "ni" refer to the hydraulic path (where n is either a = agitation, b = bypass, c = manifold, and r = reservoir) and component number (i).

B.4 State Space Derivation

The derivation is done from the bond graph in Figure 6.2.

B.4.1 Derivation of State Derivatives

$$\dot{q}_a = \frac{p_{a1}}{I_{a1}} - \frac{p_{a2}}{I_{a2}} - \frac{q_a \cdot c_a}{r_a} \tag{B.1}$$

$$\dot{q}_{a1} = \frac{(q_{m1} \cdot c_{m1} - q_{a1} \cdot c_{a1})}{ri_{a1}} - \frac{p_{a1}}{I_{a1}} \tag{B.2}$$

$$\dot{q}_{a2} = \frac{p_{a2}}{I_{a2}} - \frac{(q_{a2} \cdot c_{a2} - q_{m2} \cdot c_{m2})}{ri_{a2}} \tag{B.3}$$

$$\dot{q}_{b1} = \frac{(q_{m1} \cdot c_{m1} - q_{b1} \cdot c_{b1})}{ri_{b1}} - \frac{p_{bp}}{I_{bp}} \tag{B.4}$$

$$\dot{q}_{b2} = \frac{p_{bp}}{I_{bp}} - \frac{(q_{b2} \cdot c_{b2} - q_{m2} \cdot c_{m2})}{ri_{b2}} \tag{B.5}$$

$$\dot{q}_{c1} = S_{f_1} - \frac{(q_{m1} \cdot c_{m1} - q_{r1} \cdot c_{r1})}{ri_{r1}} - \frac{(q_{m1} \cdot c_{m1} - q_{a1} \cdot c_{a1})}{ri_{a1}} - \frac{(q_{m1} \cdot c_{m1} - q_{b1} \cdot c_{b1})}{ri_{b1}} - \frac{q_{m1} \cdot c_{m1}}{ri_{m1}} \tag{B.6}$$

$$\dot{q}_{c2} = \frac{(q_{r2} \cdot c_{r2} - q_{m2} \cdot c_{m2})}{ri_{r2}} + \frac{(q_{a2} \cdot c_{a2} - q_{m2} \cdot c_{m2})}{ri_{a2}} + \frac{(q_{b2} \cdot c_{b2} - q_{m2} \cdot c_{m2})}{ri_{b2}} - \frac{q_{m2} \cdot c_{m2}}{ri_{m2}} - S_{f_2} \tag{B.7}$$

$$\dot{q}_r = \frac{p_{r1}}{I_{r1}} - \frac{p_{r2}}{I_{r2}} - \frac{q.c_r}{r_r} \tag{B.8}$$

$$\dot{q}_{r1} = \frac{(q_{m1} \cdot c_{m1} - q_{r1} \cdot c_{r1})}{ri_{r1}} - \frac{p_{r1}}{I_{r1}} \tag{B.9}$$

$$\dot{q}_{r2} = \frac{p_{r2}}{I_{r2}} - \frac{(q_{r2} \cdot c_{r2} - q_{m2} \cdot c_{m2})}{ri_{r2}} \tag{B.10}$$

$$\dot{p}_{a1} = q_{a1} \cdot c_{a1} - q_a \cdot c_a - r_{a1} \tag{B.11}$$

$$\dot{p}_{a2} = q_a \cdot c_a - q_{a2} \cdot c_{a2} - r_{a2} \tag{B.12}$$

$$\dot{p}_{BP} = q_{b1} \cdot c_{b1} - q_{b2} \cdot c_{b2} - r_{bp} \tag{B.13}$$

$$\dot{p}_{r1} = q_{r1} \cdot c_{r1} - q_r \cdot c_r - r_{r1} \tag{B.14}$$

$$\dot{p}_{r2} = q_r \cdot c_r - q_{r2} \cdot c_{r2} - r_{r2} \tag{B.15}$$

Appendix C

Astronaut-Powered Laundry Machine Prototype and Bond Graph Model Verification Trials

Contamination Information	**Value**
Quantity of Synthetic Perspiration	0 ml
Regression Constant	4.9819
Regression Rate	0 1/s
Signal	**RMS Error**
Bladder Entrance	0.39856
Bladder Exit	0.44157
Reservoir Entrance	0.49601
Reservoir Exit	0.32733
Bypass	0.3221
Cleanliness Equation	0.25865

Table C.1: Contamination conditions and Root-Mean-Squared error results of a standalone astronaut-powered laundry machine for trial #1.

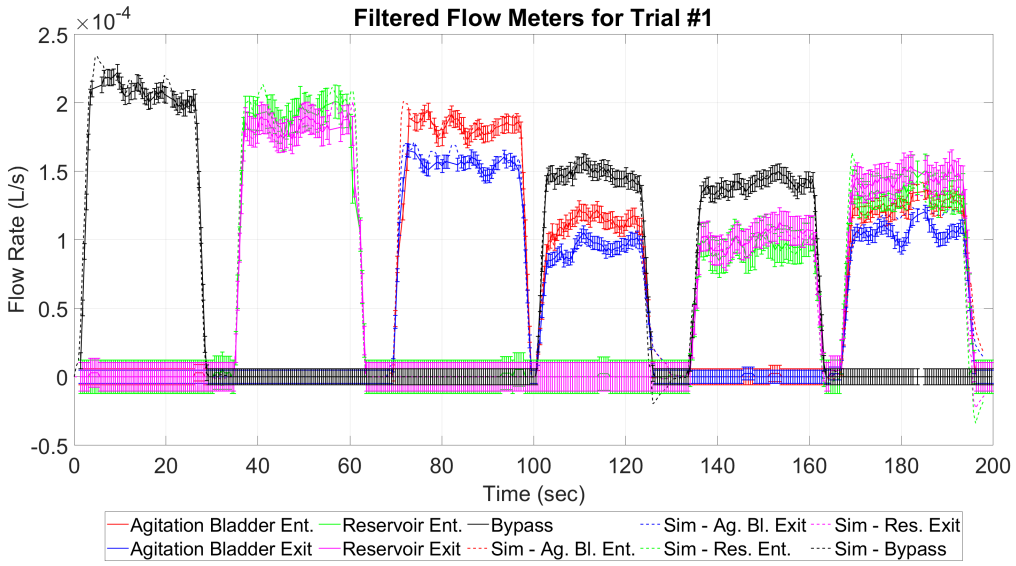

Figure C.1: Standalone astronaut-powered laundry machine prototype experiment flow rate results with filtered and simulated data for trial #1.

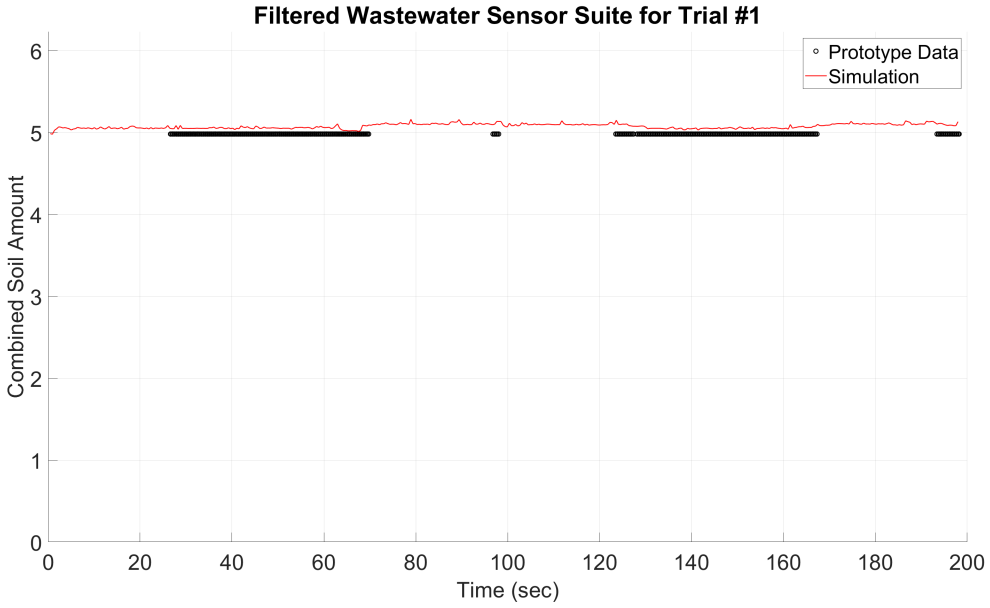

Figure C.2: Standalone astronaut-powered laundry machine prototype experiment wastewater results with filtered and simulated data for trial #1 at scale.

Figure C.3: Standalone astronaut-powered laundry machine prototype experiment wastewater zoomed-in results with filtered and simulated data for trial #1.

Contamination Information	**Value**
Quantity of Synthetic Perspiration	3 ml
Regression Constant	4.966
Regression Rate	-8.2565e-06 1/s
Signal	**RMS Error**
Bladder Entrance	0.77458
Bladder Exit	0.66752
Reservoir Entrance	0.65921
Reservoir Exit	0.69439
Bypass	0.2091
Cleanliness Equation	0.23955

Table C.2: Contamination conditions and Root-Mean-Squared error results of a standalone astronaut-powered laundry machine for trial #2.

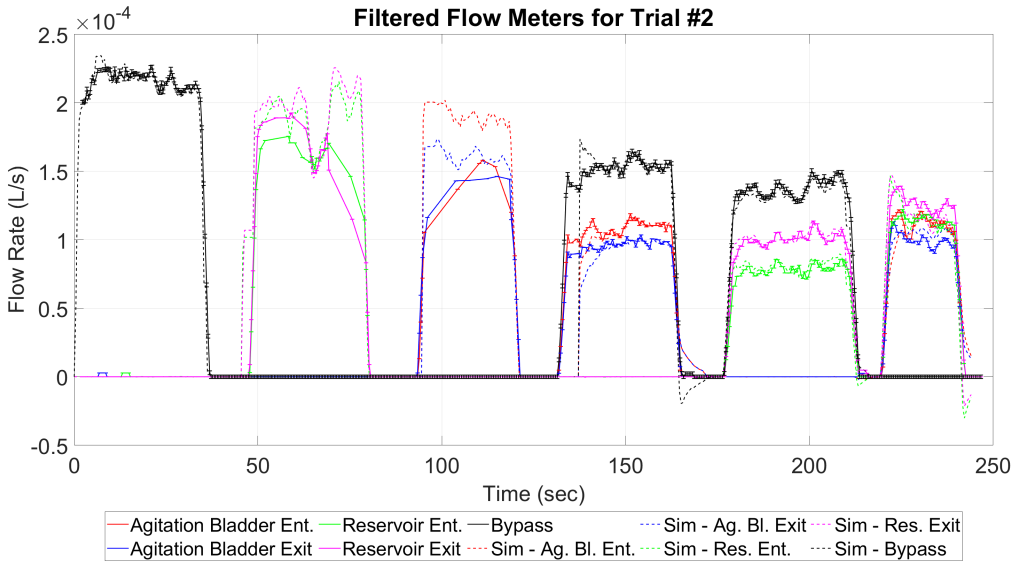

Figure C.4: Standalone astronaut-powered laundry machine prototype experiment flow rate results with filtered and simulated data for trial #2.

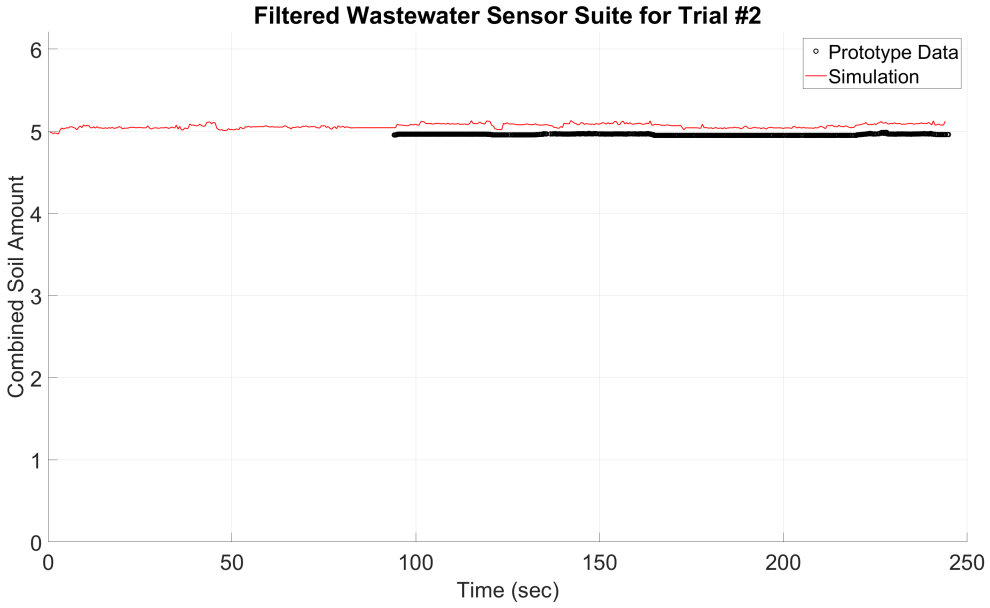

Figure C.5: Standalone astronaut-powered laundry machine prototype experiment wastewater results with filtered and simulated data for trial #2 at scale.

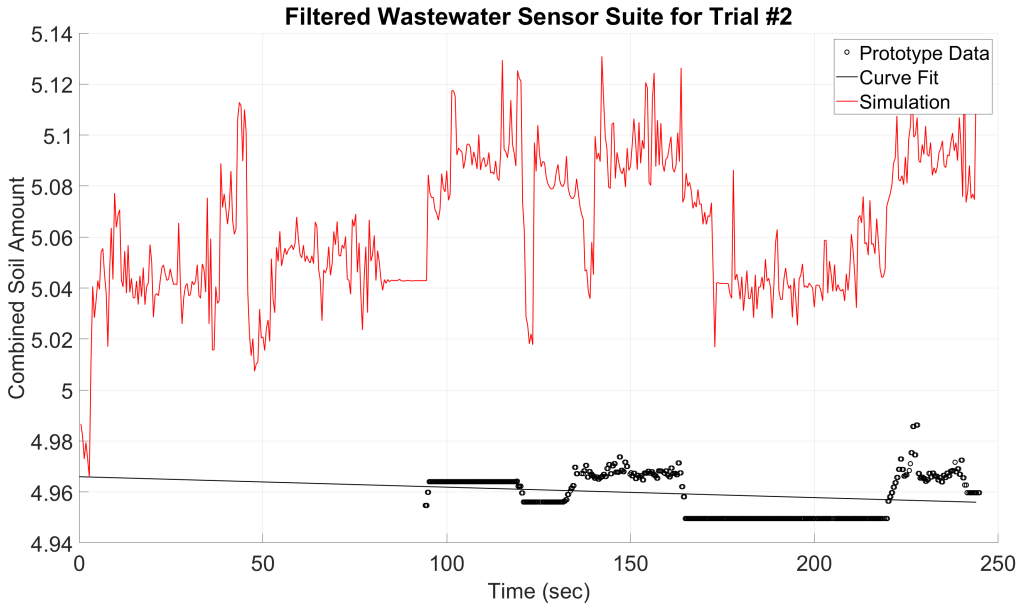

Figure C.6: Standalone astronaut-powered laundry machine prototype experiment wastewater zoomed-in results with filtered and simulated data for trial #2.

Contamination Information	**Value**
Quantity of Synthetic Perspiration	4 ml
Regression Constant	5.0596
Regression Rate	-1.4336e-05 1/s
Signal	**RMS Error**
Bladder Entrance	1.4092
Bladder Exit	0.13922
Reservoir Entrance	0.15912
Reservoir Exit	0.15384
Bypass	0.12775
Cleanliness Equation	0.30816

Table C.3: Contamination conditions and Root-Mean-Squared error results of a standalone astronaut-powered laundry machine for trial #3.

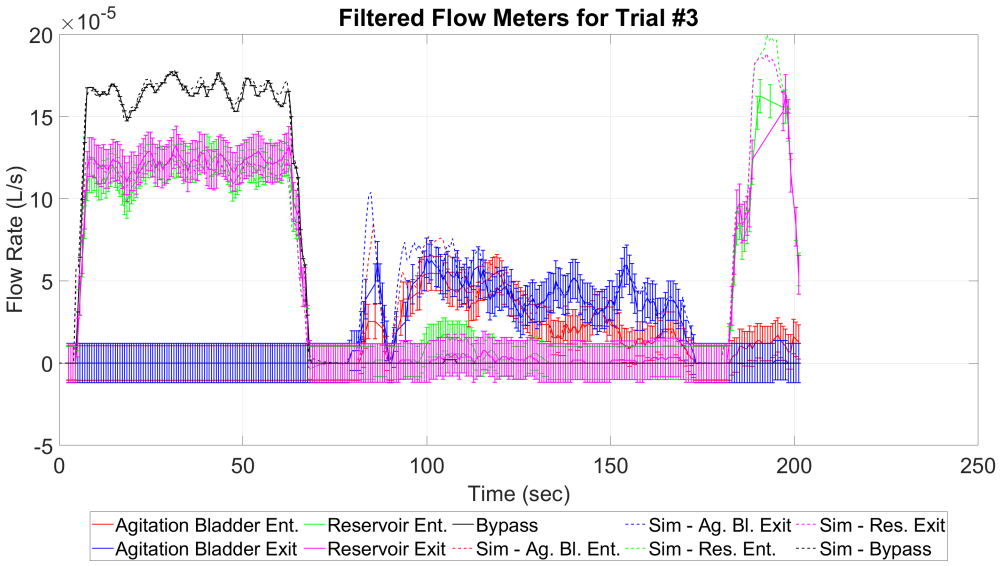

Figure C.7: Standalone astronaut-powered laundry machine prototype experiment flow rate results with filtered and simulated data for trial #3.

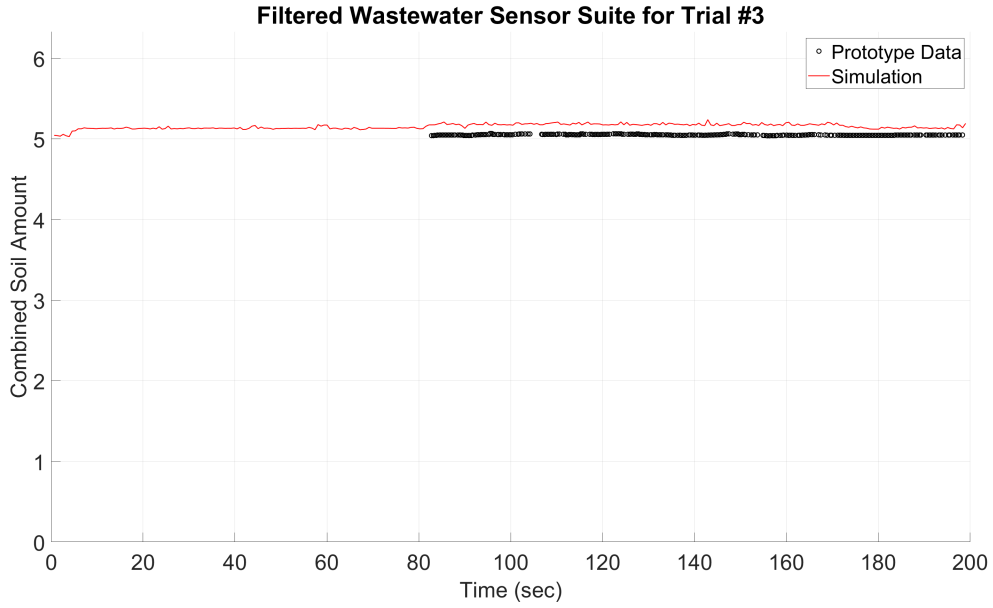

Figure C.8: Standalone astronaut-powered laundry machine prototype experiment wastewater results with filtered and simulated data for trial #3 at scale.

Figure C.9: Standalone astronaut-powered laundry machine prototype experiment wastewater zoomed-in results with filtered and simulated data for trial #3.

Contamination Information	**Value**
Quantity of Synthetic Perspiration	4 ml
Regression Constant	3.6721
Regression Rate	-8.6278e-06 1/s
Signal	**RMS Error**
Bladder Entrance	0.11516
Bladder Exit	1.2528
Reservoir Entrance	1.991
Reservoir Exit	2.0425
Bypass	0.26965
Cleanliness Equation	0.34525

Table C.4: Contamination conditions and Root-Mean-Squared error results of a standalone astronaut-powered laundry machine for trial #4.

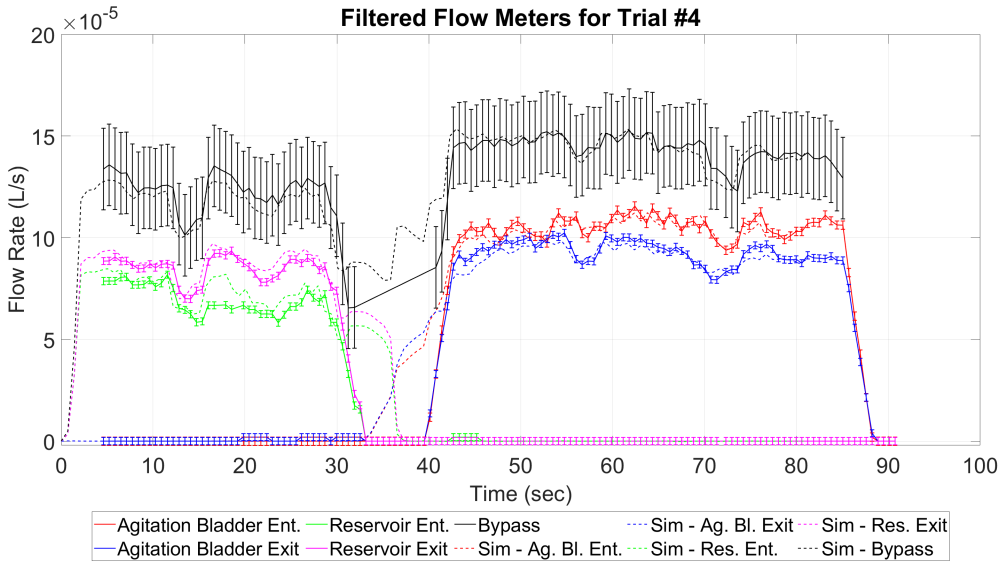

Figure C.10: Standalone astronaut-powered laundry machine prototype experiment flow rate results with filtered and simulated data for trial #4.

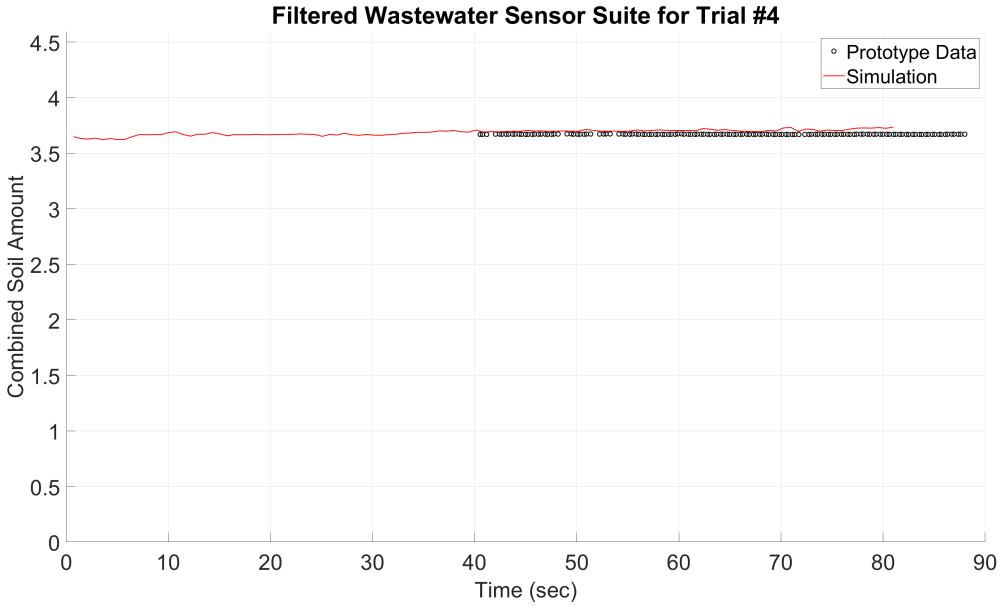

Figure C.11: Standalone astronaut-powered laundry machine prototype experiment wastewater results with filtered and simulated data for trial #4 at scale.

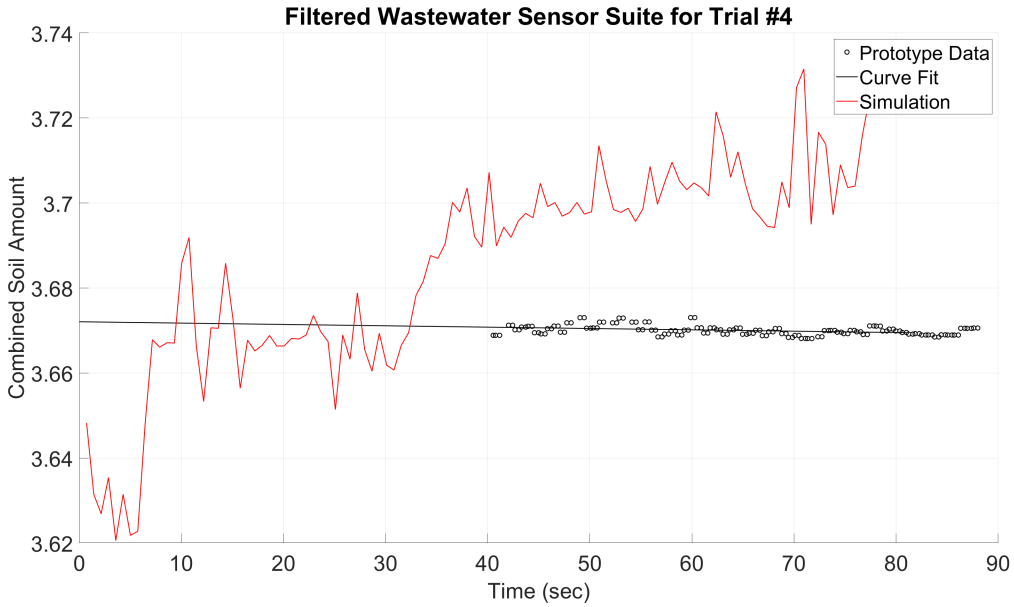

Figure C.12: Standalone astronaut-powered laundry machine prototype experiment wastewater zoomed-in results with filtered and simulated data for trial #4.

Contamination Information	**Value**
Quantity of Synthetic Perspiration	4 ml
Regression Constant	4.673
Regression Rate	2.6479e-05 1/s
Signal	**RMS Error**
Bladder Entrance	0.49327
Bladder Exit	0.43377
Reservoir Entrance	0.17651
Reservoir Exit	0.20486
Bypass	0.28558
Cleanliness Equation	0.34549

Table C.5: Contamination conditions and Root-Mean-Squared error results of a standalone astronaut-powered laundry machine for trial #5.

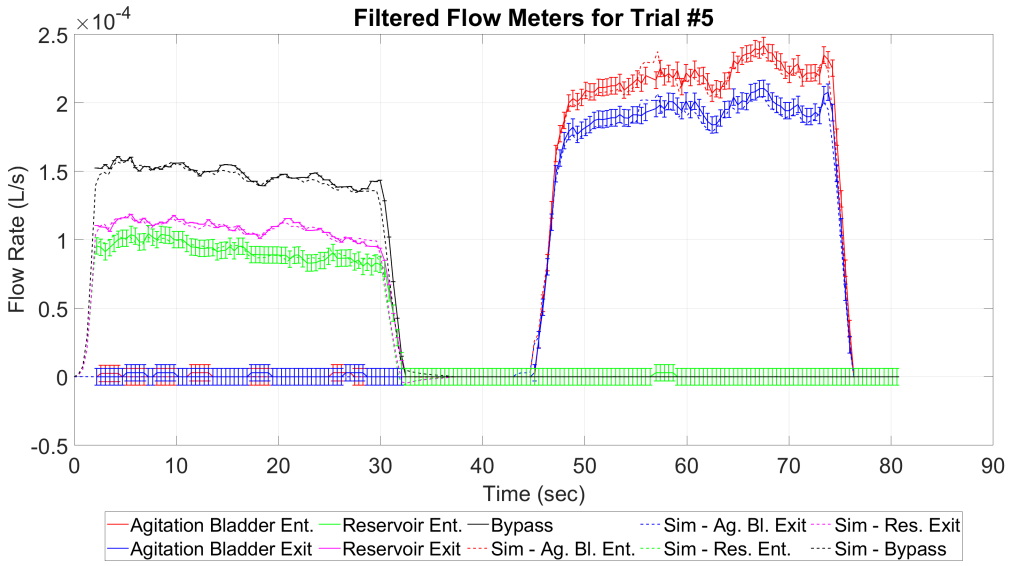

Figure C.13: Standalone astronaut-powered laundry machine prototype experiment flow rate results with filtered and simulated data for trial #5.

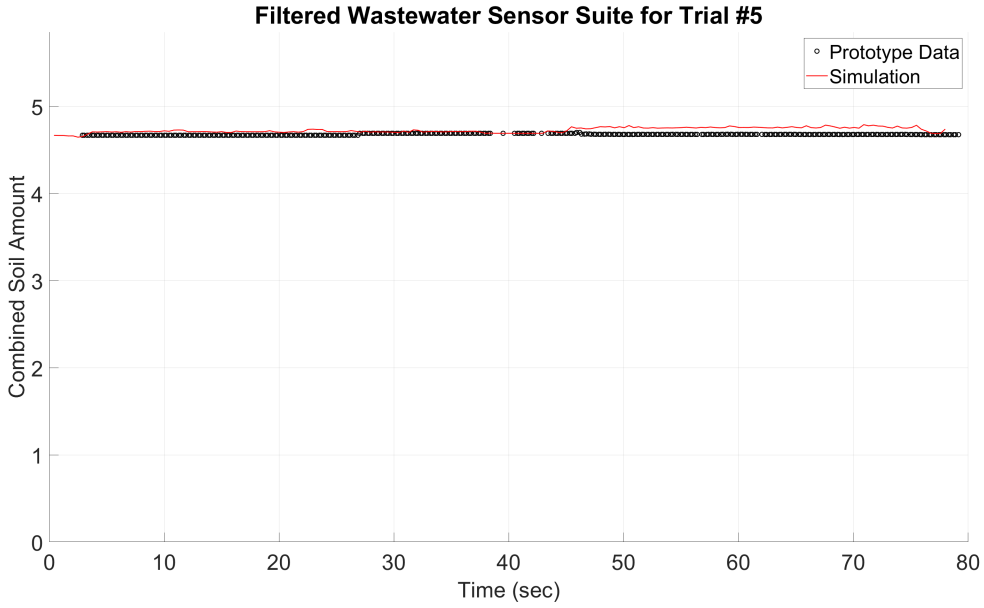

Figure C.14: Standalone astronaut-powered laundry machine prototype experiment wastewater results with filtered and simulated data for trial #5 at scale.

Figure C.15: Standalone astronaut-powered laundry machine prototype experiment wastewater zoomed-in results with filtered and simulated data for trial #5.

Contamination Information	**Value**
Quantity of Synthetic Perspiration	5 ml
Regression Constant	7.5107
Regression Rate	8.7631e-06 1/s
Signal	**RMS Error**
Bladder Entrance	0.70433
Bladder Exit	0.55197
Reservoir Entrance	0.6177
Reservoir Exit	0.50829
Bypass	0.60114
Cleanliness Equation	0.43063

Table C.6: Contamination conditions and Root-Mean-Squared error results of a standalone astronaut-powered laundry machine for trial #6.

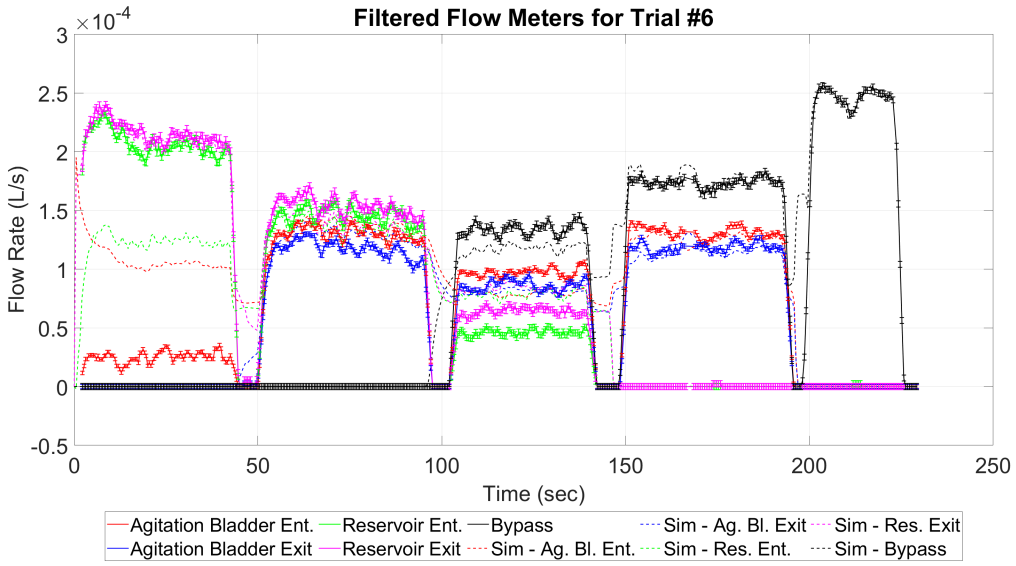

Figure C.16: Standalone astronaut-powered laundry machine prototype experiment flow rate results with filtered and simulated data for trial #6.

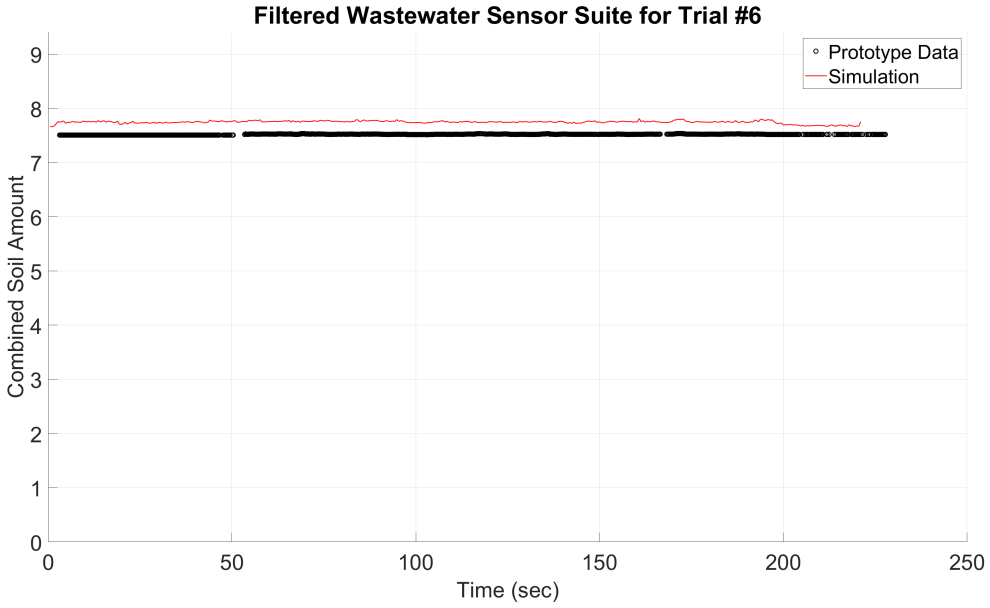

Figure C.17: Standalone astronaut-powered laundry machine prototype experiment wastewater results with filtered and simulated data for trial #6 at scale.

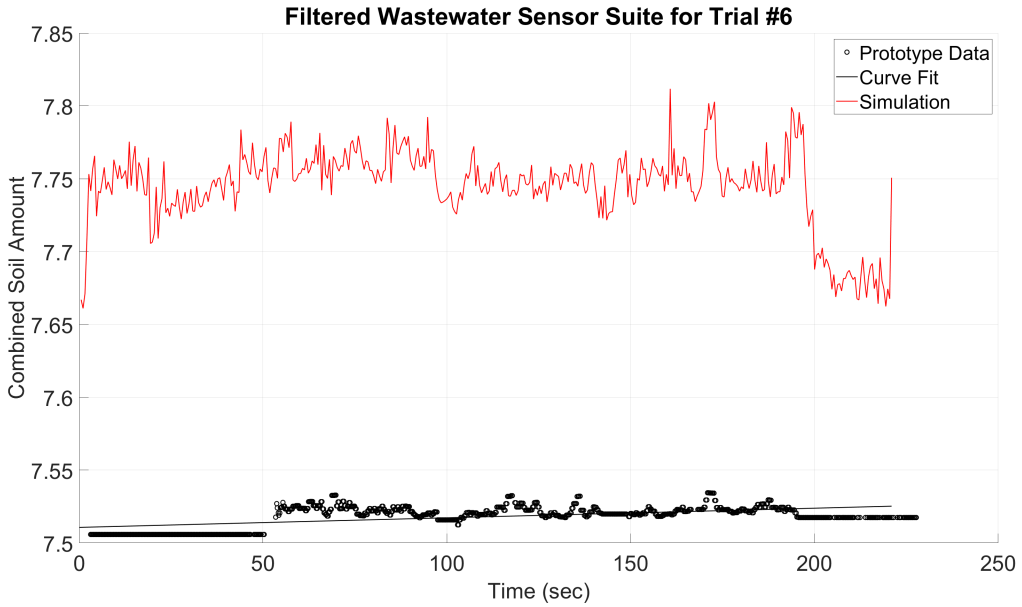

Figure C.18: Standalone astronaut-powered laundry machine prototype experiment wastewater zoomed-in results with filtered and simulated data for trial #6.

Contamination Information	**Value**
Quantity of Synthetic Perspiration	3 ml
Regression Constant	4.909
Regression Rate	-1.9694e-06 1/s
Signal	**RMS Error**
Bladder Entrance	0.33256
Bladder Exit	0.30634
Reservoir Entrance	0.31523
Reservoir Exit	0.31788
Bypass	0.27691
Cleanliness Equation	0.27782

Table C.7: Contamination conditions and Root-Mean-Squared error results of a standalone astronaut-powered laundry machine for trial #7.

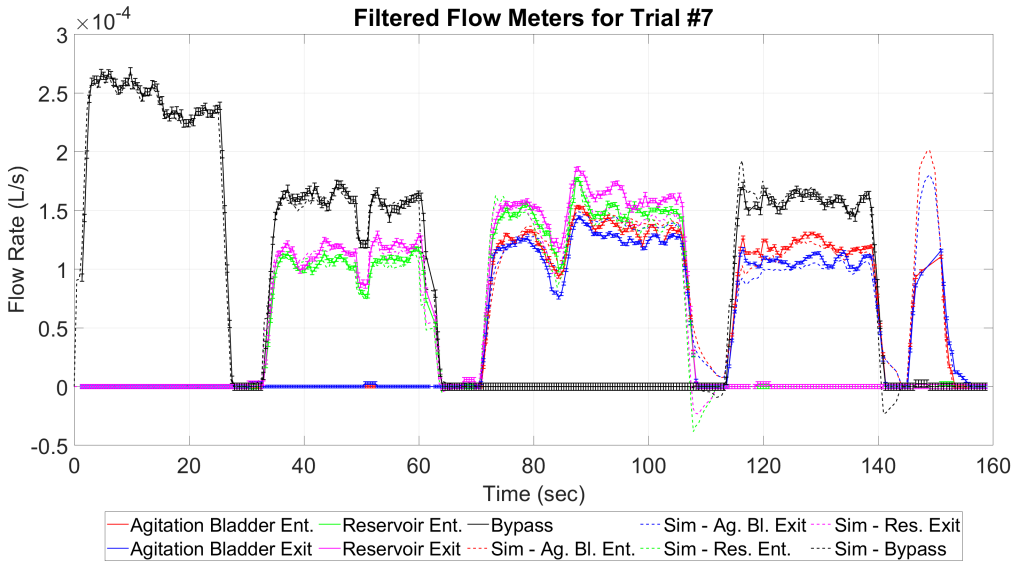

Figure C.19: Standalone astronaut-powered laundry machine prototype experiment flow rate results with filtered and simulated data for trial #7.

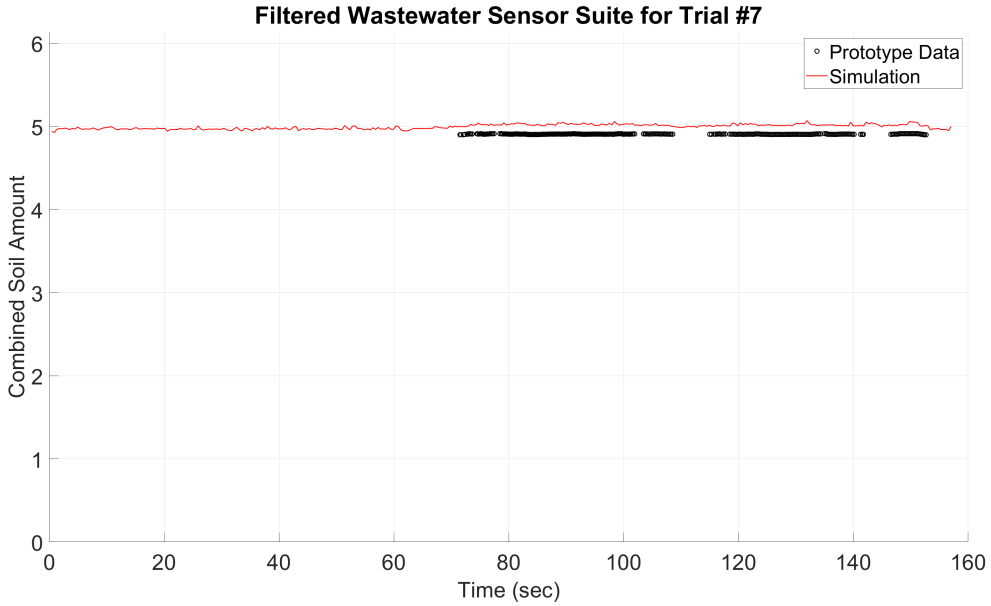

Figure C.20: Standalone astronaut-powered laundry machine prototype experiment wastewater results with filtered and simulated data for trial #7 at scale.

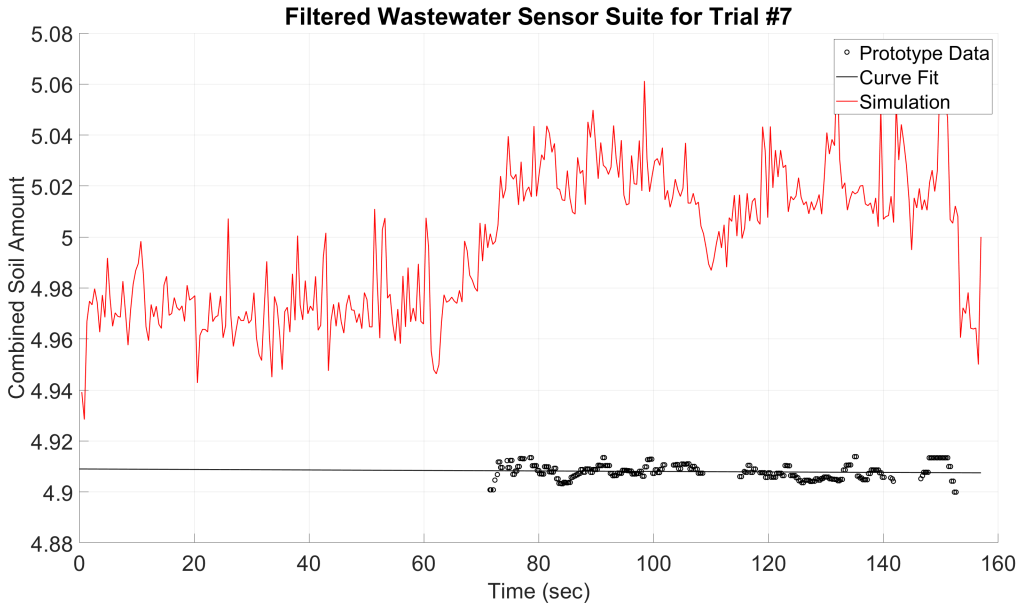

Figure C.21: Standalone astronaut-powered laundry machine prototype experiment wastewater zoomed-in results with filtered and simulated data for trial #7.

Contamination Information	**Value**
Quantity of Synthetic Perspiration	3 ml
Regression Constant	8.9558
Regression Rate	0 1/s
Signal	**RMS Error**
Bladder Entrance	0.36621
Bladder Exit	0.428
Reservoir Entrance	0.39786
Reservoir Exit	0.40793
Bypass	0.52489
Cleanliness Equation	0.68752

Table C.8: Contamination conditions and Root-Mean-Squared error results of a standalone astronaut-powered laundry machine for trial #8.

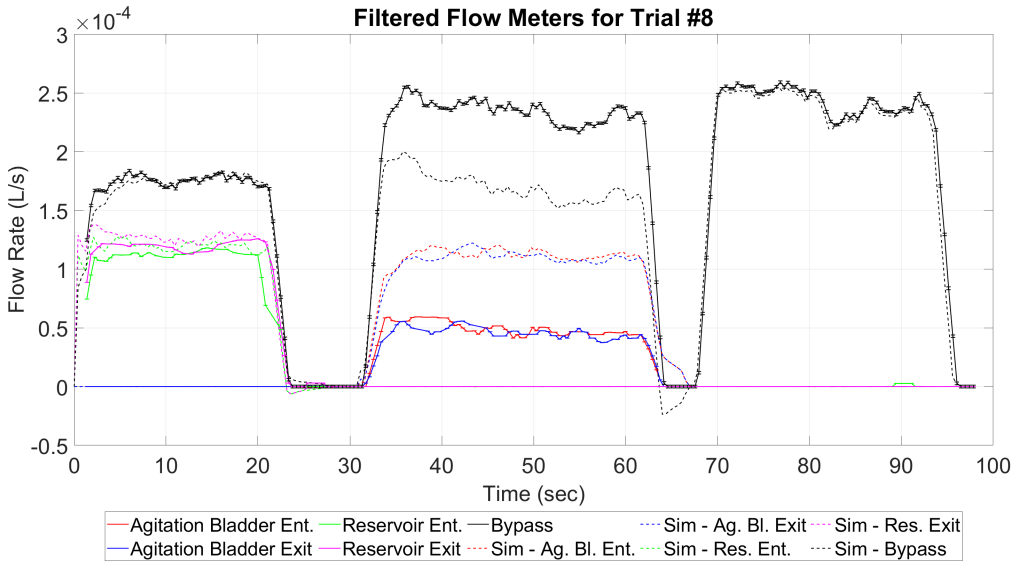

Figure C.22: Standalone astronaut-powered laundry machine prototype experiment flow rate results with filtered and simulated data for trial #8.

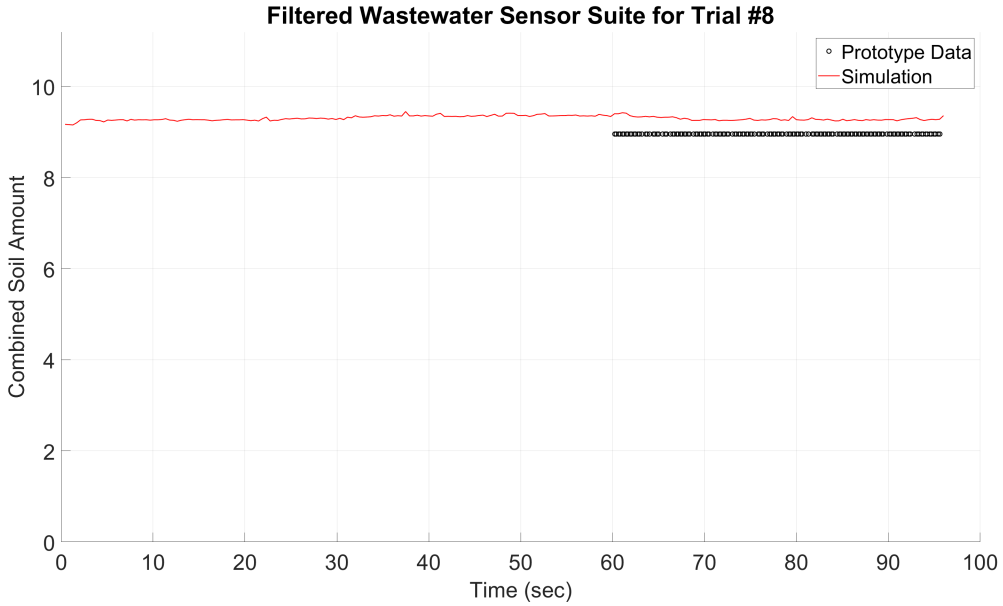

Figure C.23: Standalone astronaut-powered laundry machine prototype experiment wastewater results with filtered and simulated data for trial #8 at scale.

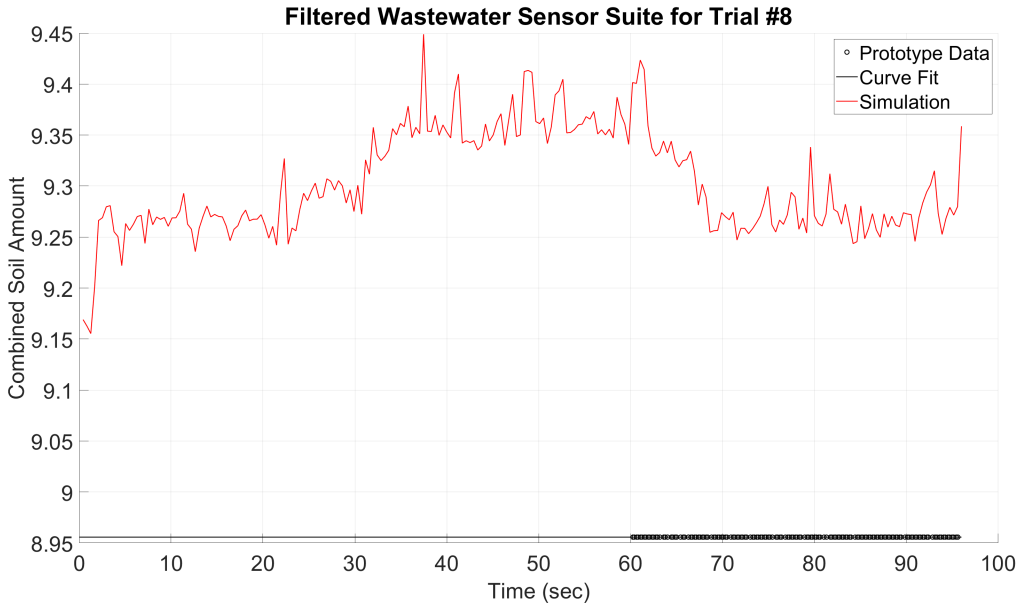

Figure C.24: Standalone astronaut-powered laundry machine prototype experiment wastewater zoomed-in results with filtered and simulated data for trial #8.

Contamination Information	**Value**
Quantity of Synthetic Perspiration	5 ml
Regression Constant	1.1564
Regression Rate	-1.505e-05 1/s
Signal	**RMS Error**
Bladder Entrance	0.32694
Bladder Exit	0.31803
Reservoir Entrance	0.48164
Reservoir Exit	0.50013
Bypass	0.42504
Cleanliness Equation	0.087357

Table C.9: Contamination conditions and Root-Mean-Squared error results of a standalone astronaut-powered laundry machine for trial #9.

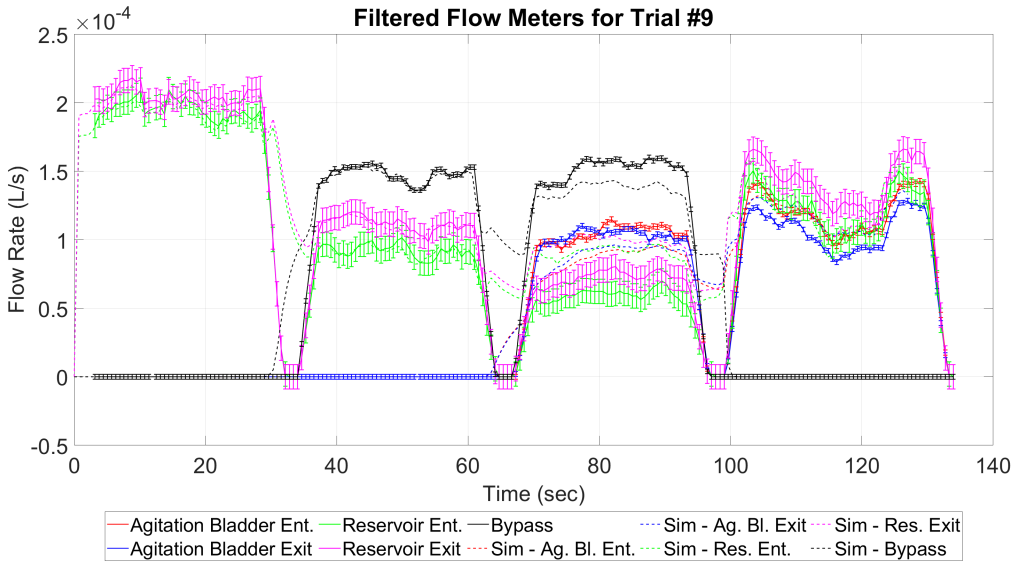

Figure C.25: Standalone astronaut-powered laundry machine prototype experiment flow rate results with filtered and simulated data for trial #9.

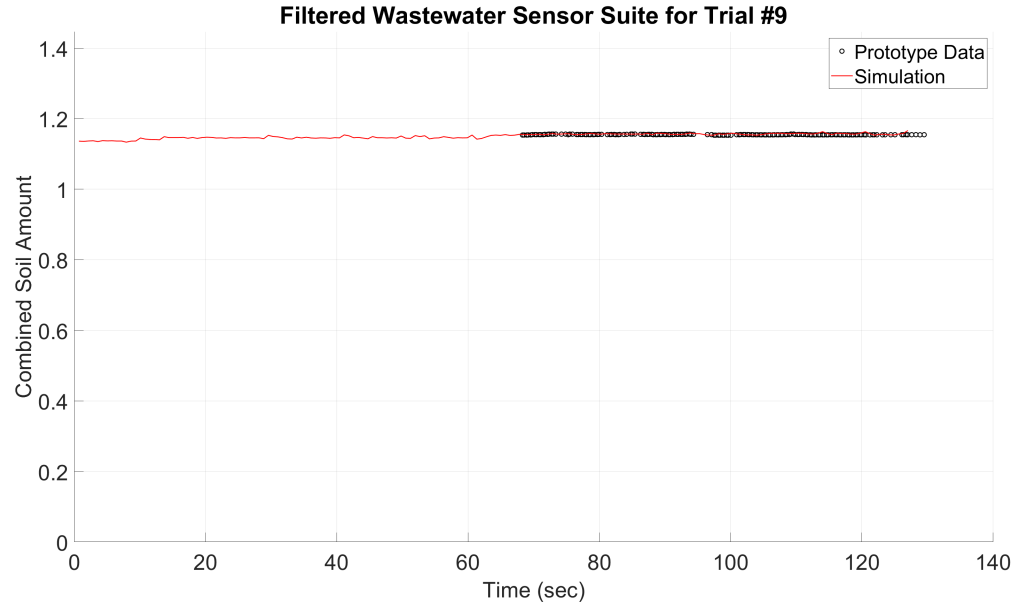

Figure C.26: Standalone astronaut-powered laundry machine prototype experiment wastewater results with filtered and simulated data for trial #9 at scale.

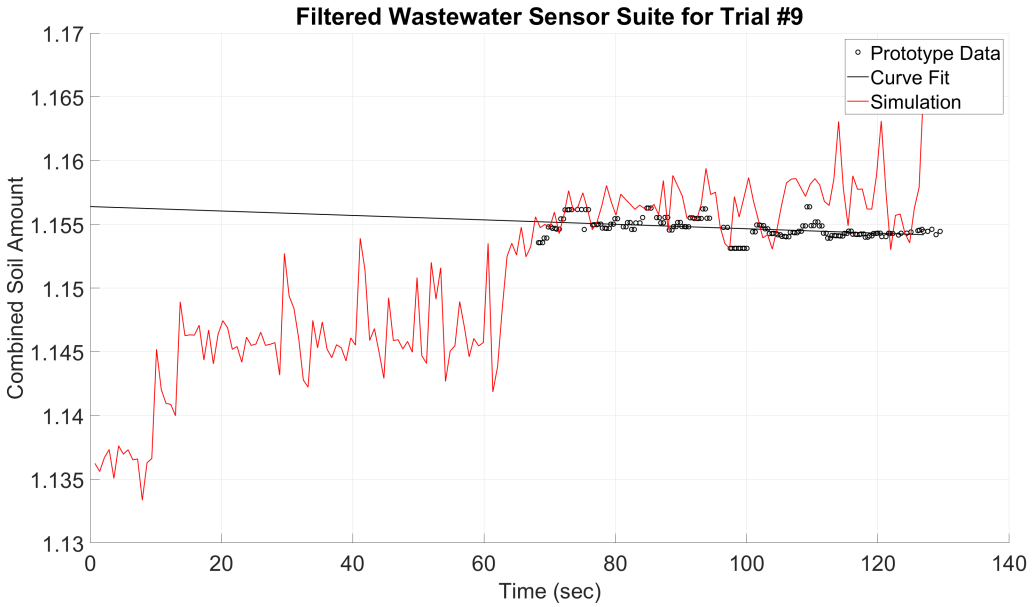

Figure C.27: Standalone astronaut-powered laundry machine prototype experiment wastewater zoomed-in results with filtered and simulated data for trial #9.

Contamination Information	**Value**
Quantity of Synthetic Perspiration	4 ml
Regression Constant	1.8462
Regression Rate	-8.3659e-06 1/s
Signal	**RMS Error**
Bladder Entrance	0.49396
Bladder Exit	0.48529
Reservoir Entrance	0.22209
Reservoir Exit	0.24024
Bypass	0.55595
Cleanliness Equation	0.12418

Table C.10: Contamination conditions and Root-Mean-Squared error results of a standalone astronaut-powered laundry machine for trial #10.

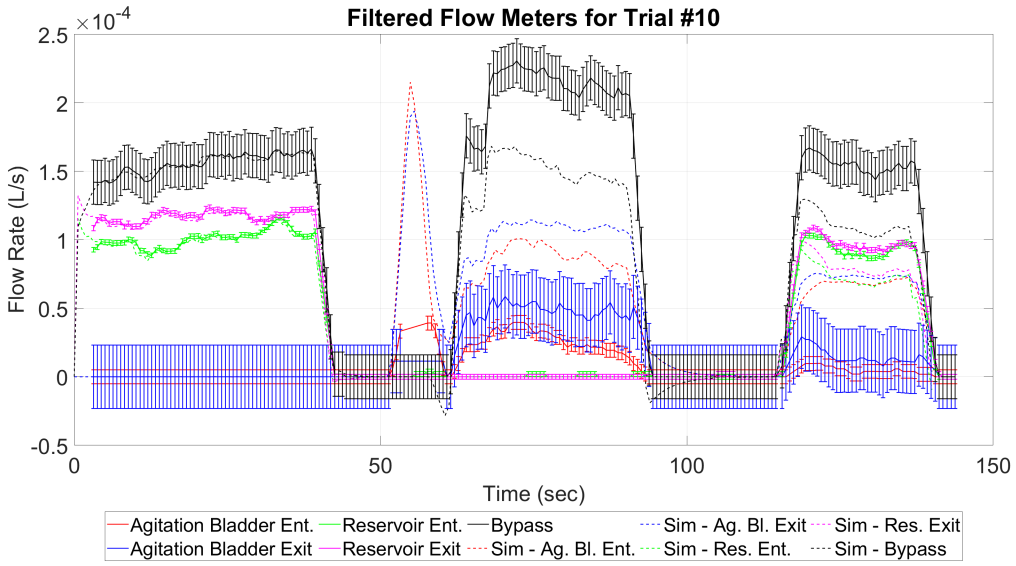

Figure C.28: Standalone astronaut-powered laundry machine prototype experiment flow rate results with filtered and simulated data for trial #10.

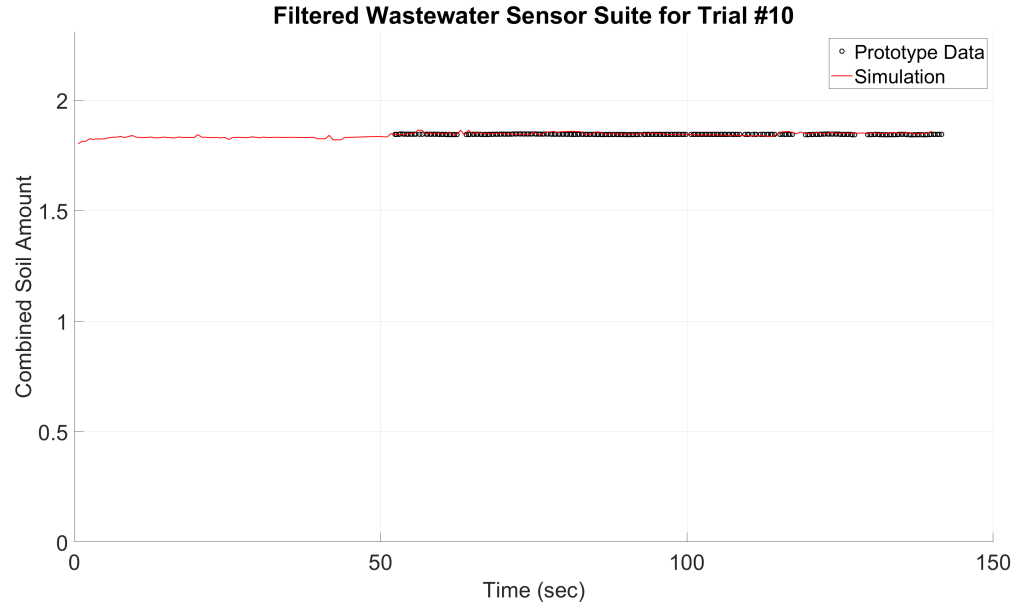

Figure C.29: Standalone astronaut-powered laundry machine prototype experiment wastewater results with filtered and simulated data for trial #10 at scale.

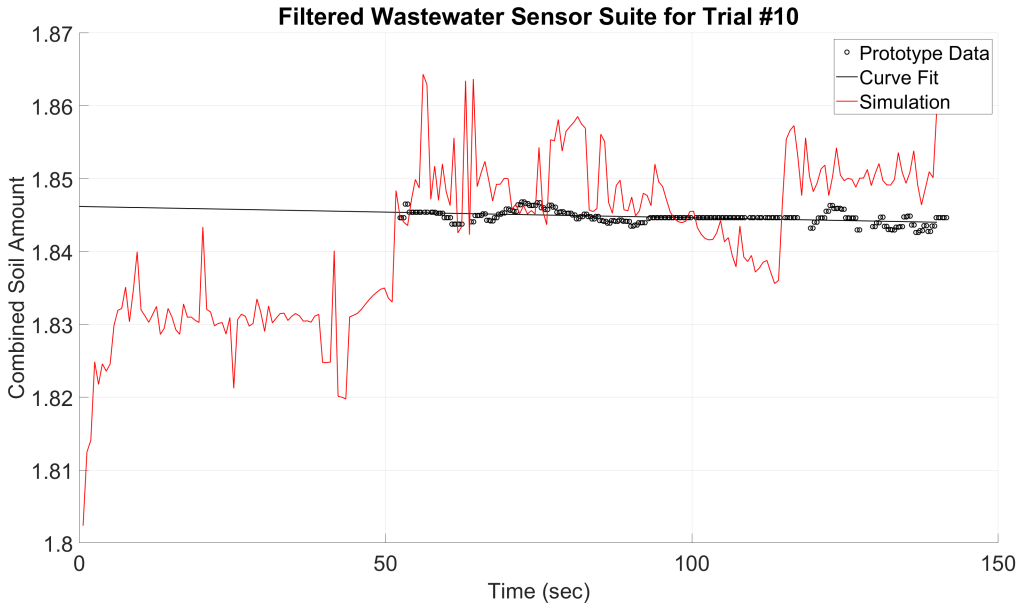

Figure C.30: Standalone astronaut-powered laundry machine prototype experiment wastewater zoomed-in results with filtered and simulated data for trial #10.

Contamination Information	**Value**
Quantity of Synthetic Perspiration	4 ml
Regression Constant	2.8497
Regression Rate	3.8667e-05 1/s
Signal	**RMS Error**
Bladder Entrance	1.4264
Bladder Exit	1.503
Reservoir Entrance	0.11253
Reservoir Exit	0.12298
Bypass	0.40666
Cleanliness Equation	0.24146

Table C.11: Contamination conditions and Root-Mean-Squared error results of a standalone astronaut-powered laundry machine for trial #11.

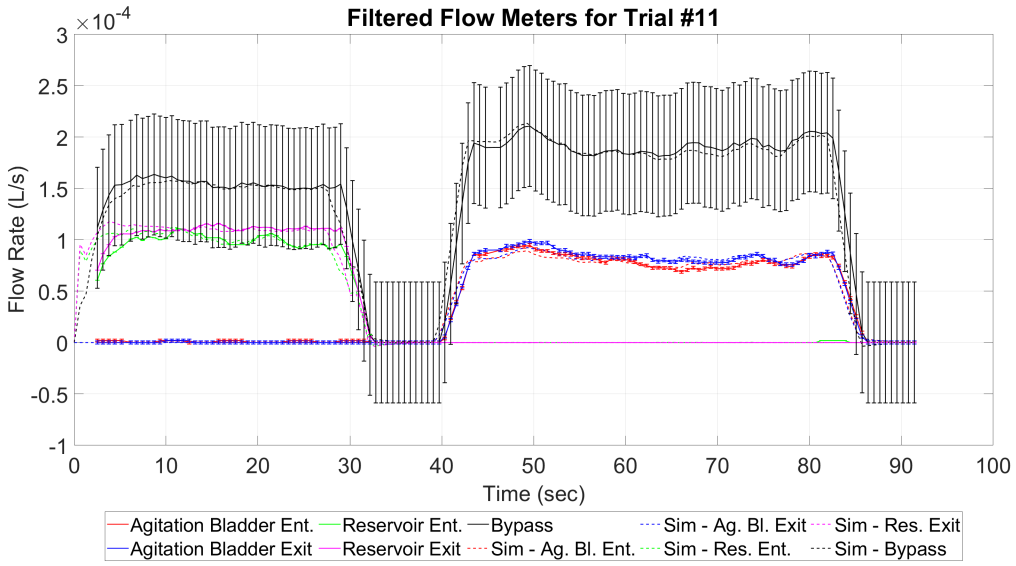

Figure C.31: Standalone astronaut-powered laundry machine prototype experiment flow rate results with filtered and simulated data for trial #11.

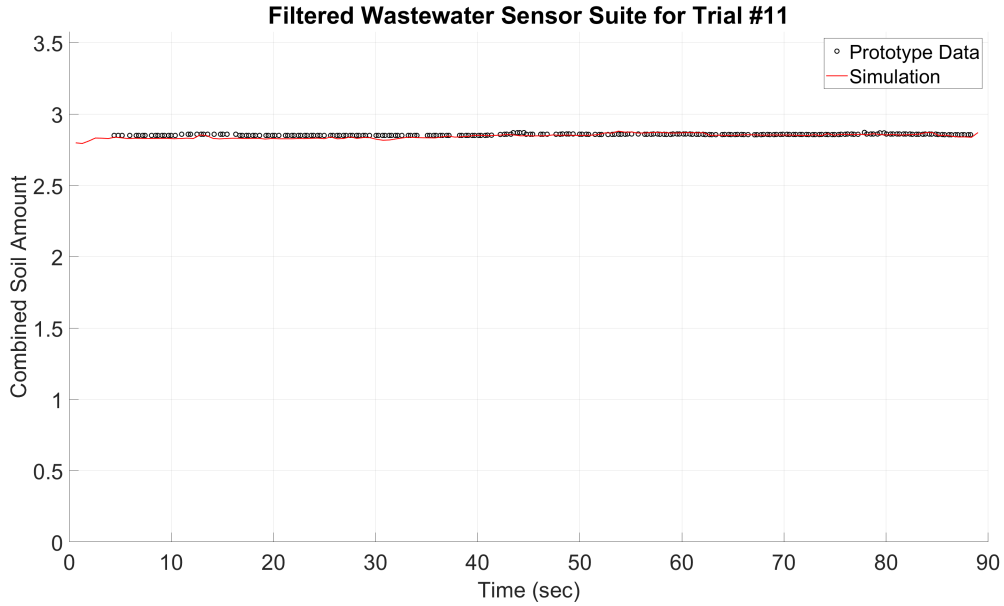

Figure C.32: Standalone astronaut-powered laundry machine prototype experiment wastewater results with filtered and simulated data for trial #11 at scale.

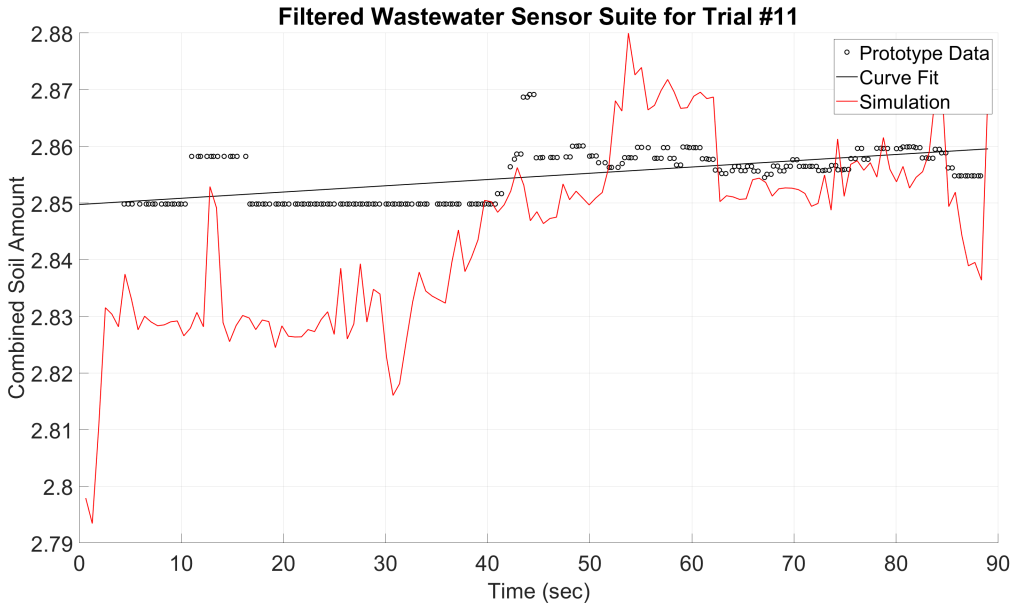

Figure C.33: Standalone astronaut-powered laundry machine prototype experiment wastewater zoomed-in results with filtered and simulated data for trial #11.

Contamination Information	**Value**
Quantity of Synthetic Perspiration	5 ml
Regression Constant	1.6079
Regression Rate	-1.0174e-05 1/s
Signal	**RMS Error**
Bladder Entrance	0.50072
Bladder Exit	0.44735
Reservoir Entrance	0.51635
Reservoir Exit	0.54429
Bypass	0.55204
Cleanliness Equation	0.097014

Table C.12: Contamination conditions and Root-Mean-Squared error results of a standalone astronaut-powered laundry machine for trial #12.

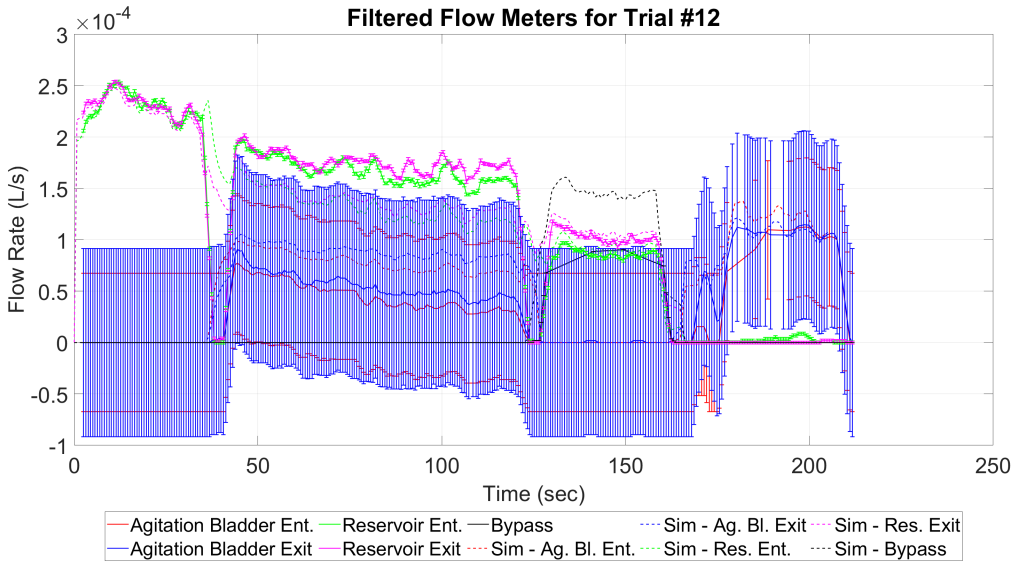

Figure C.34: Standalone astronaut-powered laundry machine prototype experiment flow rate results with filtered and simulated data for trial #12.

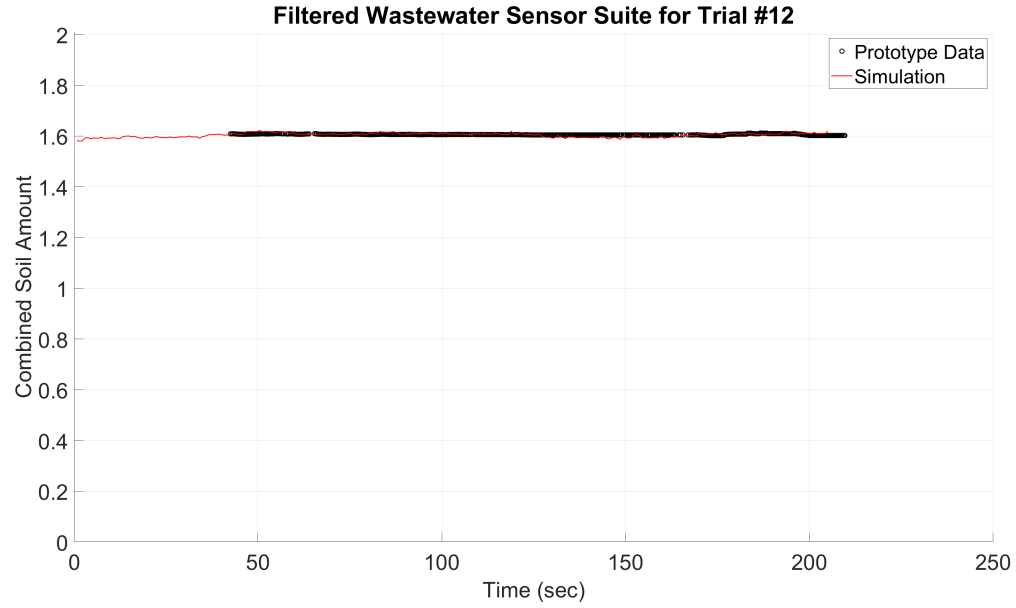

Figure C.35: Standalone astronaut-powered laundry machine prototype experiment wastewater results with filtered and simulated data for trial #12 at scale.

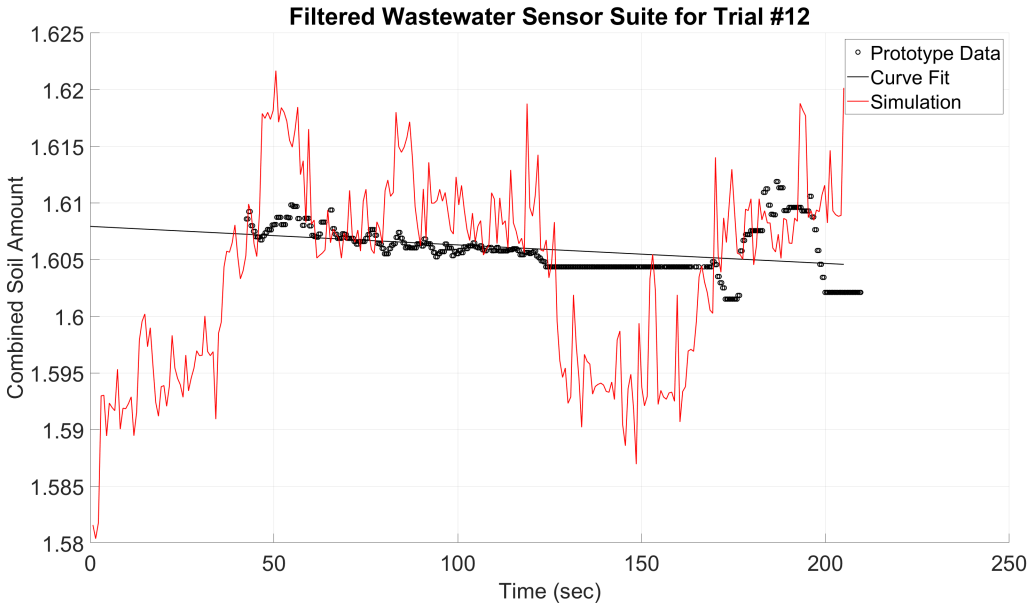

Figure C.36: Standalone astronaut-powered laundry machine prototype experiment wastewater zoomed-in results with filtered and simulated data for trial #12.

Contamination Information	**Value**
Quantity of Synthetic Perspiration	5 ml
Regression Constant	1.832
Regression Rate	-3.791e-06 1/s
Signal	**RMS Error**
Bladder Entrance	0.15092
Bladder Exit	0.14539
Reservoir Entrance	0.29532
Reservoir Exit	0.30265
Bypass	0.1765
Cleanliness Equation	0.10397

Table C.13: Contamination conditions and Root-Mean-Squared error results of a standalone astronaut-powered laundry machine for trial #13.

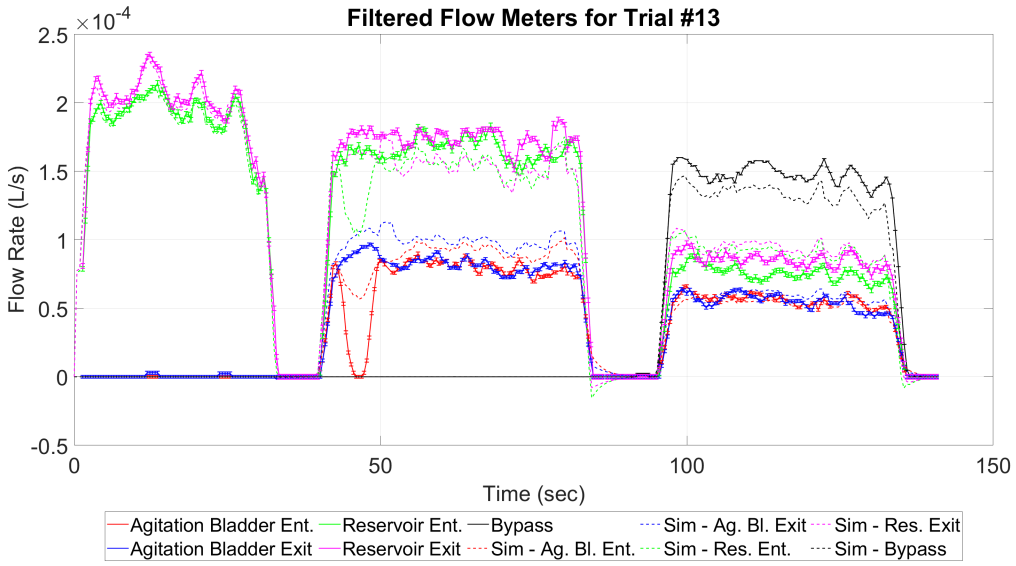

Figure C.37: Standalone astronaut-powered laundry machine prototype experiment flow rate results with filtered and simulated data for trial #13.

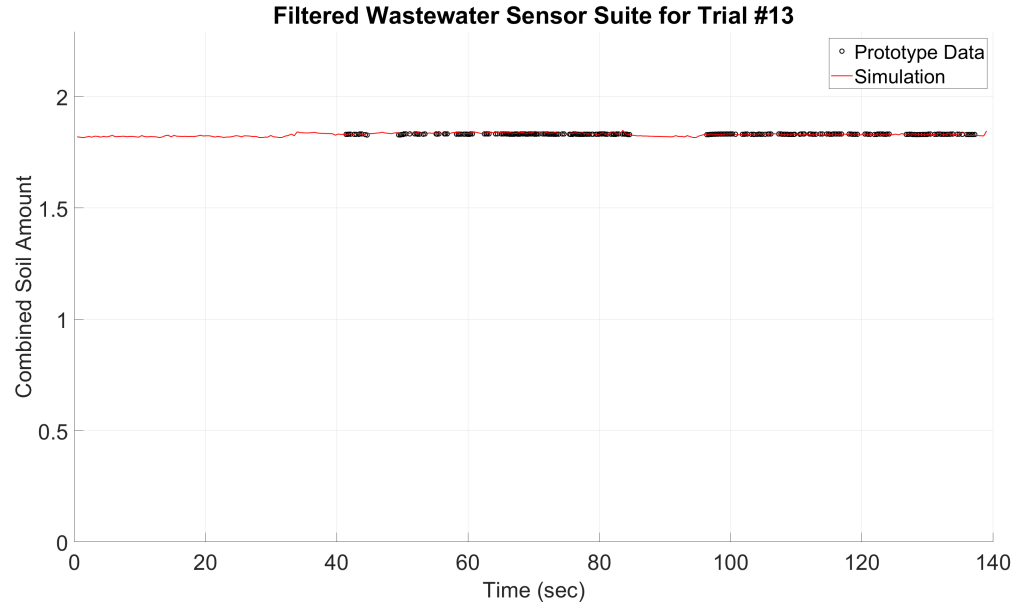

Figure C.38: Standalone astronaut-powered laundry machine prototype experiment wastewater results with filtered and simulated data for trial #13 at scale.

Appendix D

Verification Trial Textile Contamination Procedures

1. **PPE**
   (a) **Don splash goggles and chemical resistance gloves.**
2. **Gather Material**
   (a) **Cotton sheet**
   (b) **Razor blade**
   (c) **Ruler**
   (d) **Cutting surface**
   (e) **Bucket**
   (f) **5mL Pipette**
   (g) **Synthetic Perspiration**
   (h) **Distilled Water**
   (i) **Astronaut powered laundry machine prototype.**
3. **Create Textile Sample**
   (a) **Lay cotton sheet flat on cutting surface.**

(b) Use the ruler to cut four 3” swatches from the cotton with the razor blade.

4. Prepare Machine Bladder

(a) Ensure machine is off (un-powered).

(b) Place machine bladder in bucket.

(c) Remove sealing clips from bladder.

(d) Drain bladder into bucket, including previous cotton swatches.

(e) Rinse bladder with distilled water, emptying into bucket.

(f) Remove bucket and dispose of wastewater. Keep swatch for examination.

5. Prepare Contamination Load

(a) Near the bladder, open synthetic perspiration.

(b) Contaminate each swatch with either 1 mL or 0.5 mL of synthetic perspiration, place into bladder after.

i. Hold Swatch in palm of hand.

ii. Gather synthetic perspiration in pipette.

iii. Drip synthetic perspiration in a spiral pattern over swatch.

(c) Fill bladder with distilled water until valve openings are covered.

(d) Close bladder, remove air, and place both sealing clips back.

(e) Compress bag to remove more air.

6. Return contamination items.

7. Doff PPE

(a) Place splash goggle and chemical resistance gloves back.

Appendix E

Astronaut-Powered Laundry Machine Operation Procedures

1. **PPE**
   (a) **Don UV safety glasses.**
   (b) **Display UV light warning sign and light.**
   (c) **Open drain.**
   (d) **Stow do not touch signs on PPE shelf.**
2. **Check for leaks**
   (a) **Bladder, valves, and pump connections are common areas.**
   (b) **Don appropriate gloves for repairs.**
3. **Open Electronics-Bag (E-Bag)**
   (a) **Insert microSD card.**
   (b) **Reinforce microSD breakout board wires.**
   (c) **Align wire bunch on bike.**
4. **Close E-Bag**
   (a) **Ensure bag is protected from hydraulics.**

5. **Uncoil power cables.**
    (a) **Plug the AC adapter into the protected outlet.**
    (b) **Plug the USB-B cable into a computer.**
6. **Check power lights**
    (a) **LED in E-Bag – Flow meters and UV LEDS**
    (b) **Tachometer – Microcontroller, microSD, and ADC board**
        i. **ADC – Wastewater Sensor Suite**
7. **Prepare Data Collection**
    (a) **Open Thonny on computer**
    (b) **Ensure communication with microcontroller.**
        i. **Stop and Start on Thonny may help, otherwise check cable.**
    (c) **Run "sl.py" for microSD communication.**
        i. **Stop and Start on Thonny may help, otherwise Step 3 and 4.**
8. **Unlock bike**
    (a) **Stow lock on secondary workbench.**
9. **Launder**
    (a) **Run "sl.py" after configurating machine and laundry load.**
    (b) **Power the machine by pedaling.**
        i. **microSD card communication error**
            A. **Data will be saved up to error.**
            B. **Optional - Remove microSD and transfer data to computer followed by Steps 3, 4, 6, and 7.**
            C. **Start "sl.py" or Steps 3 and 4.**
    (c) **Continue pedaling.**

(d) **Once done.**

i. **Stop pedaling and "sl.py".**

ii. **Remove microSD and close E-Bag (Step 4)**

iii. **Transfer data to computer.**

10. **Lock bike**

11. **Coil power cables.**

(a) **Unplug the AC adapter and USB-B cable.**

(b) **Place cable bundle on convenient part of the bike.**

12. **Check for leaks**

(a) **Bladder, valves, and pump connections are common areas.**

(b) **Don appropriate gloves for repairs.**

13. **Doff PPE**

(a) **Place glasses, signs, lights, and drain covers back.**

Appendix F

Data Processing R Code

```
#This code was created by Andrew R. Arends (914009346) for Space Laundry
rm(list=ls())     #Clearing workspace
graphics.off()                          #Closing graphs
#
#LIBRARIES-----------------------------------------------------------------
#
library(Hmisc)
library(RColorBrewer)
#
#STATISTICAL INFORMATION---------------------------------------------------------------------
#
P <- 0.95     #Chosen confidence level for whole analysis
#
#GRAPHING CONTROLS---------------------------------------------------------------------
#
loc <- "C:\\Users\\arare\\Desktop\\HRVIP\\SUDS\\Code\\data\\"
wd <- 3840                          #Width of saved image
ht <- 2160                          #Height of saved image
ps <- 3                             #Scale of saved image
#---Unless otherwise specified, 0 = OFF, 1 = ON
```

```
raw_plot     <- 0   #Raw data graph
outlier_plot <- 0   #Outlier removed data graph
filt_plot    <- 1   #Filtered data graph
cl_plot      <- 0   #Confidence interval with filtered data graph
cals         <- 0   #Calibration Analysis [0= NO, 1= YES]
flows        <- 1   #Graph of all flow rates
wwss         <- 0   #Wastewater Analysis type
#---Sensor Plots
tp           <- 1   #Tachometer
fmp          <- 1   #Flow meters
wssp         <- 1   #Wastewater sensor suite
#
#IMPORTING AND FORMATTING CSV DATA-----------------------------------------------------
#
dl <- list()          #Data directory
plt_title <- c()      #Titles
plt_labels <- c()     #Signal names
dat_nam <- c()        #Data file save name
fil <- c()            #Moving window size for each sensor filter
se <- c()             #Known standard errors for each sensor
qw <- c()             #Quantile window percentage for each sensor
wwi <- length(dl) + 1 # Counter for data management
#TACHOMETER DATA-----------------------------------------------------
if (tp == 1){
tach <- read.csv(paste(loc,"raw\\data_tach.csv",sep=""), sep=',')
plt_title <- c(plt_title, "Tachometer")
plt_labels <- c(plt_labels, "Speed (rps)")
dat_nam <- c(dat_nam, "data_tach")
names(tach) <- c("t","data")
dl[[wwi]] <- tach
```

```
wwi <- wwi + 1
tach_sens <- read.csv(paste(loc,"raw\\sensor_info\\tach.csv",sep=""),header=F,sep=',')
fil <- c(fil, tach_sens[[1]][1])
se <- c(se, tach_sens[[1]][2])
qw <- c(qw, tach_sens[[1]][3])}
#FLOWMETER DATA-----------------------------------------------------
if (fmp == 1){
fwi <- wwi           # Storing length for dyanmic flow meter plotting
if(cals==0){
flow_names <- read.csv(paste(loc,"raw\\data_names
 \\data_fs_names.csv",sep=""),header=F, sep=',')
flow_sens <- read.csv(paste(loc,"raw\\sensor_info
 \\flow.csv",sep=""),header=F,sep=',')
for(i in 1:5)
{ flow <- read.csv(paste(loc,"raw\\data_fs",i,".csv",sep=""),
 sep=',')
plt_title <- c(plt_title, flow_names[[1]][i])
plt_labels <- c(plt_labels, "Flow Rate (L/s)")
dat_nam <- c(dat_nam, paste("data_fs",i,sep=""))
names(flow) <- c("t","data")
dl[[wwi]] <- flow
fwii <- wwi           # Storing length for dyanmic flow meter plotting
wwi <- wwi + 1
fil <- c(fil, flow_sens[[1]][1])
se <- c(se, flow_sens[[1]][2])
qw <- c(qw, flow_sens[[1]][3])
}
plt_title <- c(plt_title, "Total Flow #1")
plt_labels <- c(plt_labels, "Flow Rate (L/s)")
dat_nam <- c(dat_nam, paste("data_fs",i + 1,sep=""))
```

```
dl[[wwi]] <- dl[[wwi - 1]]
dl[[wwi]]$data <- dl[[wwi - 1]]$data + dl[[wwi - 3]]$data + dl[[wwi -
 5]]$data
fwii <- wwi           # Storing length for dyanmic flow meter plotting
wwi <- wwi + 1
fil <- c(fil, flow_sens[[1]][1])
se <- c(se, flow_sens[[1]][2])
qw <- c(qw, flow_sens[[1]][3])
plt_title <- c(plt_title, "Total Flow #2")
plt_labels <- c(plt_labels, "Flow Rate (L/s)")
dat_nam <- c(dat_nam, paste("data_fs",i + 2,sep=""))
dl[[wwi]] <- dl[[wwi - 2]]
dl[[wwi]]$data <- dl[[wwi - 2]]$data + dl[[wwi - 3]]$data + dl[[wwi -
 5]]$data
fwii <- wwi           # Storing length for dyanmic flow meter plotting
wwi <- wwi + 1
fil <- c(fil, flow_sens[[1]][1])
se <- c(se, flow_sens[[1]][2])
qw <- c(qw, flow_sens[[1]][3])

} else {
flow_sens <- read.csv(paste(loc,"raw\\sensor_info
 \\flow.csv",sep=""),header=F,sep=',')
fch <- c(0.175,0.220,0.260)
for(i in 1:3)
{ flow <- read.csv(paste(loc,"raw\\data_fs",i,".csv",sep=""),
 sep=',')
flow_names <- paste("Res. Height = ",fch[i]," m")
plt_title <- c(plt_title, flow_names)
plt_labels <- c(plt_labels, "Flow Sensor (L/s)")
```

```
dat_nam <- c(dat_nam, paste("data_fs",i,sep=""))
names(flow) <- c("t","data")
dl[[wwi]] <- flow
fwii <- wwi           # Storing length for dyanmic flow meter plotting
wwi <- wwi + 1
fil <- c(fil, flow_sens[[1]][1])
se <- c(se, flow_sens[[1]][2])
qw <- c(qw, flow_sens[[1]][3])}
}
}
#WASTEWATER SENSOR SUITE
if (wssp == 1) {
wwii <- wwi            # Storing length for dyanmic wastewater sensor suite plotting
cond_sens <- read.csv(paste(loc,"raw\\sensor_info
\\cond.csv",sep=""),header=F,sep=',')
uv_sens <- read.csv(paste(loc,"raw\\sensor_info
\\uv.csv",sep=""),header=F,sep=',')
wwssxl <- "Time" # WWSS X label
wwsss  <- "A" # First Sensor Suite
if(wwss == 1){
for (wwwss in c(0,1)){
for (csm in seq(from=0, to=160, by=40)){
for (usm in seq(from=0, to=8, by=2)){
cond_dat <- paste(loc,"raw\\wwss_testing\\",wwsss,"
    \\data_cond_",csm,"_",usm,".csv",sep="")
uv_dat <- paste(loc,"raw\\wwss_testing\\",wwsss,"
    \\data_uv_",csm,"_",usm,".csv",sep="")
#CONDUCTIVITY DATA-------------------------------------------------
cond <- read.csv(cond_dat, sep=',')
plt_title <- c(plt_title, paste(csm,"mg-",usm,"%-",wwsss,sep=""))
```

```
plt_labels <- c(plt_labels, "Normalized Conductivity")
dat_nam <- c(dat_nam, paste("data_cond_",csm,"_",usm,"_",wwsss))
names(cond) <- c("t","data")
dl[[wwi]] <- cond
fil <- c(fil, cond_sens[[1]][1])
se <- c(se, cond_sens[[1]][2])
qw <- c(qw, cond_sens[[1]][3])
                  wwi <- wwi + 1
#UV DATA-----------------------------------------------------
uv <- read.csv(uv_dat, sep=',')
plt_title <- c(plt_title, paste(csm,"mg-",usm,"%-",wwsss,sep=""))
plt_labels <- c(plt_labels, "Normalized Absorbance")
dat_nam <- c(dat_nam, paste("data_uv_",csm,"_",usm,"_",wwsss))
names(uv) <- c("t","data")
dl[[wwi]] <- uv
fil <- c(fil, uv_sens[[1]][1])
se <- c(se, uv_sens[[1]][2])
qw <- c(qw, uv_sens[[1]][3])
                  wwi <- wwi + 1
}
}
wwsss  <- "B" # Switching to new sensor suite
}
wwsss <- " "
} else if(wwss == 2){
for (wwwss in c(0,1)){
norm_cond <- 0
norm_uv <- 0
for (csm in seq(from=0, to=160, by=40)){
# create empty vector for new
```

```
new_cond <- c()
new_uv <- c()
per_sal <-c()
for (usm in seq(from=0, to=8, by=2)){
cond_dat <- paste(loc,"raw\\wwss_testing\\",wwsss,"
    \\data_cond_",csm,"_",usm,".csv",sep="")
uv_dat <- paste(loc,"raw\\wwss_testing\\",wwsss,"
    \\data_uv_",csm,"_",usm,".csv",sep="")
cond <- read.csv(cond_dat, sep=',')
uv <- read.csv(uv_dat, sep=',')
new_cond <- c(new_cond, mean(cond[[2]]))
new_uv <- c(new_uv, -mean(uv[[2]]))
per_sal <- c(per_sal, usm)
if (csm == 0 && usm == 0){
norm_cond <- mean(cond[[2]])
norm_uv <- -mean(uv[[2]])
}
}
# Assign new vectors to data set
plt_title <- c(plt_title, paste(csm,"mg-",wwsss,sep=""))
plt_labels <- c(plt_labels, "Normalized Conductivity")
dat_nam <- c(dat_nam, paste("data_cond_",csm,"_avg_",wwsss))
cond <- list(per_sal, new_cond - norm_cond)
names(cond) <- c("t","data")
dl[[wwi]] <- cond
fil <- c(fil, cond_sens[[1]][1])
se <- c(se, cond_sens[[1]][2])
qw <- c(qw, cond_sens[[1]][3])
                  wwi <- wwi + 1
plt_title <- c(plt_title, paste(csm,"mg-",wwsss,sep=""))
```

```
plt_labels <- c(plt_labels, "Normalized Absorbance")
dat_nam <- c(dat_nam, paste(wwsss,"data_uv_",csm,"_avg_",wwsss))
uv <- list(per_sal, new_uv - norm_uv)
names(uv) <- c("t","data")
dl[[wwi]] <- uv
fil <- c(fil, uv_sens[[1]][1])
se <- c(se, uv_sens[[1]][2])
qw <- c(qw, uv_sens[[1]][3])
                  wwi <- wwi + 1
}
wwsss  <- "B" # Switching to new sensor suite
}
wwsss <- " "
wwssxl <- "Volume Percent Saliva" # X label
} else if(wwss == 3){
for (wwwss in c(0,1)){
# create empty vector for new data sets
new_cond <- c()
new_uv   <- c()
per_sp   <- c()
for (spp in seq(from=0, to=20, by=2)){
cond_dat <- paste(loc,"raw\\wwss_sp
   \\data_cond_",wwsss,"_",spp,".csv",sep="")
uv_dat <- paste(loc,"raw\\wwss_sp
   \\data_uv_",wwsss,"_",spp,".csv",sep="")
#CONDUCTIVITY DATA-----------------------------------------------
cond <- read.csv(cond_dat, sep=',')
new_cond <- c(new_cond, mean(cond[[2]]))
      #UV DATA---------------------------------------------------------
uv <- read.csv(uv_dat, sep=',')
```

```
new_uv <- c(new_uv, mean(uv[[2]]))
#PERCENT SALIVA-----------------------------------------------
per_sp <- c(per_sp, spp)
}
# Assign new vectors to data set
plt_title <- c(plt_title, paste(spp,"% - ",wwsss,sep=""))
plt_labels <- c(plt_labels, "Normalized Conductivity")
dat_nam <- c(dat_nam, paste("data_cond_",spp,"_spp_",wwsss))
cond <- list(per_sp, new_cond - new_cond[1])
names(cond) <- c("t","data")
dl[[wwi]] <- cond
fil <- c(fil, cond_sens[[1]][1])
se <- c(se, cond_sens[[1]][2])
qw <- c(qw, cond_sens[[1]][3])
            wwi <- wwi + 1
plt_title <- c(plt_title, paste(spp,"% - ",wwsss,sep=""))
plt_labels <- c(plt_labels, "Normalized Absorbance")
dat_nam <- c(dat_nam, paste("data_uv_",spp,"_spp_",wwsss))
uv <- list(per_sp, new_uv - new_uv[1])
names(uv) <- c("t","data")
dl[[wwi]] <- uv
fil <- c(fil, uv_sens[[1]][1])
se <- c(se, uv_sens[[1]][2])
qw <- c(qw, uv_sens[[1]][3])
            wwi <- wwi + 1
wwsss  <- "B" # Switching to new sensor suite
}
wwsss <- " "
wwssxl <- "Volume Percent Syn. Perspiration" # X label
} else {
```

```
#A-----------------------------------------------------------------
cond_dat_a<- paste(loc,"raw\\data_cda.csv",sep="")
uv_dat_a <- paste(loc,"raw\\data_uva.csv",sep="")
#CONDUCTIVITY DATA-------------------------------------------------
cond_a <- read.csv(cond_dat_a, sep=',')
plt_title <- c(plt_title, "A")
plt_labels <- c(plt_labels, "Normalized Conductivity")
dat_nam <- c(dat_nam, "data_cda")
names(cond_a) <- c("t","data")
dl[[wwi]] <- cond_a
fil <- c(fil, cond_sens[[1]][1])
se <- c(se, cond_sens[[1]][2])
qw <- c(qw, cond_sens[[1]][3])
      wwi <- wwi + 1
#UV DATA-----------------------------------------------------------
uv_a <- read.csv(uv_dat_a, sep=',')
plt_title <- c(plt_title, "A")
plt_labels <- c(plt_labels, "Normalized Absorbance")
dat_nam <- c(dat_nam, "data_uva")
names(uv_a) <- c("t","data")
dl[[wwi]] <- uv_a
fil <- c(fil, uv_sens[[1]][1])
se <- c(se, uv_sens[[1]][2])
qw <- c(qw, uv_sens[[1]][3])
      wwi <- wwi + 1
#B-----------------------------------------------------------------
cond_dat_b <- paste(loc,"raw\\data_cdb.csv",sep="")
uv_dat_b <- paste(loc,"raw\\data_uvb.csv",sep="")
#CONDUCTIVITY DATA-------------------------------------------------
cond_b <- read.csv(cond_dat_b, sep=',')
```

```
plt_title <- c(plt_title, "B")
plt_labels <- c(plt_labels, "Normalized Conductivity")
dat_nam <- c(dat_nam, "data_cdb")
names(cond_b) <- c("t","data")
dl[[wwi]] <- cond_b
fil <- c(fil, cond_sens[[1]][1])
se <- c(se, cond_sens[[1]][2])
qw <- c(qw, cond_sens[[1]][3])
      wwi <- wwi + 1
#UV DATA-------------------------------------------------------
uv_b <- read.csv(uv_dat_b, sep=',')
plt_title <- c(plt_title, "B")
plt_labels <- c(plt_labels, "Normalized Absorbance")
dat_nam <- c(dat_nam, "data_uvb")
names(uv_b) <- c("t","data")
dl[[wwi]] <- uv_b
fil <- c(fil, uv_sens[[1]][1])
se <- c(se, uv_sens[[1]][2])
qw <- c(qw, uv_sens[[1]][3])
      wwi <- wwi + 1
#DIFF----------------------------------------------------------------
#CONDUCTIVITY DATA---------------------------------------------
plt_title <- c(plt_title, "B - A")
plt_labels <- c(plt_labels, "Normalized Conductivity")
dat_nam <- c(dat_nam, "data_cdab")
dl[[wwi]] <- cond_b
dl[[wwi]]$data <- cond_b$data - cond_a$data[1:length(cond_b$data)]
fil <- c(fil, cond_sens[[1]][1])
se <- c(se, cond_sens[[1]][2])
qw <- c(qw, cond_sens[[1]][3])
```

```
      wwi <- wwi + 1
#UV DATA-----------------------------------------------------------
plt_title <- c(plt_title, "B - A")
plt_labels <- c(plt_labels, "Normalized Absorbance")
dat_nam <- c(dat_nam, "data_uvab")
dl[[wwi]] <- uv_b
dl[[wwi]]$data <- uv_b$data - uv_a$data[1:length(uv_b$data)]
fil <- c(fil, uv_sens[[1]][1])
se <- c(se, uv_sens[[1]][2])
qw <- c(qw, uv_sens[[1]][3])
      wwi <- wwi + 1
}}
#
#SENSOR CALIBRATION INFORMATION-------------------------------------------------------------
#
#------TACH CAL
tcal <- c(80,100,120)                    #[rps] tachometer calibration vector
#------FLOW CAL
Ap <- pi*(0.005)^2                  #[m^2] Max area of pipe
Ar <- 0.016129                           #[m^2] Area of reservoir
g <- 9.81                                #[m/s^2] Acceleration due to gravity
h0 <- c(0.175, 0.22, 0.26)               #[m] Inital height of reservoir vector
dh <- 0.125           #[m] Height between bottom of reservoir and sensor
dc <- 0.475                               #Discharge coefficient
flow_cal <- function(t, dat,hw){
fsi <- which(dat != 0)[1]          #Flow start index
Ap <- Ap * (1 + exp(-5*(t-t[fsi]-0.5)))^-1 #Valve opening function
T <- Ar*hw/Ap*sqrt(2/g/hw)                      #Flow time function
htf <- hw*(1-((t-t[fsi])/T))^2                  #Height function
return(dc*Ap*(sqrt(2*g*htf /(1-(Ap/Ar)^2)) + sqrt(2*g*dh)))}
```

```
#
#PLOTTING FUNCTION-----------------------------------------------------------------
#
plt_lab <- 3                                                    #Plot label size
plt_axs <- 2                                                    #Plot axis size
plt_man <- 3                                                    #Plot title size
plt_sub <- 3                                                    #Plot sublabel size
plt_lwd <- 2.5                                                  #Line width
plt_mgp <- c(5,2,0)                                             #Move plot labels
plt_mar <- c(6,8,4,4)                                           #Margin around plot
plot_data <- function(t,dat,dat_name,out,cldat){
windows()
par(mar = plt_mar, mgp=plt_mgp)
title <- plt_title[dat_name]
switch(out,
title <- title,
title <- paste(title," - SOR"),
title <- paste(title," - LPF"),
title <- paste(title," - CI"))
plot(t, dat,
xlim=c(0,max(t)), xlab='Time (s)',
ylim=c(0,max(dat)*1.25), ylab= plt_labels[dat_name],
main= title,
cex.lab=plt_lab, cex.axis=plt_axs, cex.main=plt_man,
  cex.sub=plt_sub, panel.first=grid(lwd=plt_lwd))
lines(t, dat,lwd=plt_lwd)
if (out == 4) {errbar(t, dat, dat + cldat, dat - cldat, add = TRUE,
 errbar.col="red")}
png(paste(paste(loc,"\\graphs\\",sep=""), title, ".png"), width = wd,
 height = ht)
```

```
par(mar = plt_mar*ps, mgp=plt_mgp*ps)
plot(t, dat,
xlim=c(0,max(t)), xlab='Time (s)',
ylim=c(0,max(dat)*1.25), ylab= plt_labels[dat_name],
main= title,
cex.lab=plt_lab*ps, cex.axis=plt_axs*ps, cex.main=plt_man*ps,
  cex.sub=plt_sub*ps, panel.first=grid(lwd=plt_lwd*ps-2))
lines(t, dat,lwd=plt_lwd*ps)
if (out == 4) {errbar(t, dat, dat + cldat, dat - cldat, add = TRUE,
 errbar.col="red")}
dev.off()}
plot_cal <- function(t,dat,sens,out,cldat,cal){
windows()
par(mar = plt_mar, mgp=plt_mgp)
title <- plt_title[sens]
if (cal == 1 & sens == 2){title <- "Flow Rate Sensor"}
if (cal == 1){title <- paste(title, "Calibration")}
switch(out,
title <- title,
title <- paste(title," - SOR"),
title <- paste(title," - LPF"),
title <- paste(title," - CI"))
if (cal == 1 & sens == 1) {
plot(t, dat,
xlim=c(0,max(t)), xlab='Time (s)',
ylim=c(0,max(dat)*1.25), ylab= plt_labels[sens],
main= title,
cex.lab=plt_lab, cex.axis=plt_axs, cex.main=plt_man,
  cex.sub=plt_sub, panel.first=grid(lwd=plt_lwd))
lines(t, dat,lwd=plt_lwd)
```

```
} else {
plot(t[[1]], dat[[1]],
xlim=c(0,max(as.numeric(unlist(t)))), xlab='Time (s)',
ylim=c(0,max(as.numeric(unlist(dat)))*1.25), ylab= plt_labels[sens],
main= title,
cex.lab=plt_lab, cex.axis=plt_axs, cex.main=plt_man,
  cex.sub=plt_sub, panel.first=grid(lwd=plt_lwd))
colors <- c("black","green","blue")
for(i in 1:length(dat)){lines(t[[i]], dat[[i]],lwd=plt_lwd, col=colors[i])}}
if (out == 4) {errbar(t, dat, dat + cldat, dat - cldat, add = TRUE, errbar.col="red")}
if (cal == 1 & sens == 1)
 {for (i in 1:length(tcal)){abline(h=tcal[i],col='red',lw=plt_lwd,lty='dashed')}}
if (cal == 1 & sens == 2)
 {for (i in 1:length(dat))
 {lines(t[[i]], flow_cal(t[[i]],dat[[i]],h0[i]),lwd=plt_lwd, col='red',lty='dashed')}
legend("topright",legend=plt_title[2:4],lwd=plt_lwd, col=colors)}
png(paste(paste(loc,"\\graphs\\",sep=""), title, ".png"), width = wd, height = ht)
par(mar = plt_mar*ps, mgp=plt_mgp*ps)
if (cal == 1 & sens == 1) {
plot(t, dat,
xlim=c(0,max(t)), xlab='Time (s)',
ylim=c(0,max(dat)*1.25), ylab= plt_labels[sens],
main= title,
cex.lab=plt_lab*ps, cex.axis=plt_axs*ps, cex.main=plt_man*ps,
  cex.sub=plt_sub*ps, panel.first=grid(lwd=plt_lwd*ps-2))
lines(t, dat,lwd=plt_lwd)
} else {
plot(t[[1]], dat[[1]],
xlim=c(0,max(as.numeric(unlist(t)))), xlab='Time (s)',
ylim=c(0,max(as.numeric(unlist(dat)))*1.25), ylab= plt_labels[sens],
```

```
main= title,

  cex.lab=plt_lab*ps, cex.axis=plt_axs*ps, cex.main=plt_man*ps,
  cex.sub=plt_sub*ps, panel.first=grid(lwd=plt_lwd*ps-2))
for(i in 1:length(dat)){lines(t[[i]], dat[[i]],lwd=plt_lwd*ps, col=colors[i])}}
if (out == 4) {errbar(t, dat, dat + cldat, dat - cldat, add = TRUE, errbar.col="red")}
if (cal == 1 & sens == 1)
 {for (i in 1:length(tcal)){abline(h=tcal[i],col='red',lw=plt_lwd*ps,lty='dashed')}}
if (cal == 1 & sens == 2)
 {for (i in 1:length(dat))
 {lines(t[[i]], flow_cal(t[[i]],dat[[i]],h0[i]),lwd=plt_lwd*ps,
 col='red',lty='dashed')}
legend("topright",legend=plt_title[2:4],lwd=plt_lwd*ps,
 col=colors,cex=plt_lab*ps-4)}
dev.off()}
plot_flows <- function(frs,out,cldat){
windows()
par(mar = plt_mar, mgp=plt_mgp)
title <- "All Flow Rates"
switch(out,
title <- title,
title <- paste(title," - SOR"),
title <- paste(title," - LPF"),
title <- paste(title," - CI"))
ymax <- 0
for(ym in 1:length(frs)){if (max(frs[[ym]]$data) >
 ymax){ymax <- max(frs[[ym]]$data)}}
plot(frs[[1]]$t, frs[[1]]$data,xlim=c(0,max(frs[[1]]$t)),xlab='Time (s)',
ylim=c(0,ymax*1.25),ylab= "Flow Rate (L/min)",main= title,
cex.lab=plt_lab, cex.axis=plt_axs, cex.main=plt_man,
```

```
  cex.sub=plt_sub, panel.first=grid(lwd=plt_lwd))
colors <- c("black","red","blue","green","purple")
for(pf in 1:length(frs)){lines(frs[[pf]]$t,frs[[pf]]$data,lwd=plt_lwd,col=colors[pf])}
if (out==4){for(pf in 1:length(frs))
{errbar(frs[[pf]]$t,frs[[1]]$data, frs[[pf]]$data+
  cldat[pf], frs[[pf]]$data- cldat[pf], add = TRUE, errbar.col="red")}}
legend("topright",legend=plt_title[fwi:fwii],col=colors,
 lwd=plt_lwd)
png(paste(paste(loc,"\\graphs\\",sep=""), title, ".png"), width = wd, height = ht)
par(mar = plt_mar*ps, mgp=plt_mgp*ps)
plot(frs[[1]]$t, frs[[1]]$data,xlim=c(0,max(frs[[1]]$t)),xlab='Time (s)',
ylim=c(0,ymax*1.25),ylab= "Flow Rate (L/min)",main= title,
cex.lab=plt_lab*ps, cex.axis=plt_axs*ps, cex.main=plt_man*ps,
  cex.sub=plt_sub*ps, panel.first=grid(lwd=plt_lwd*ps-2))
for(pf in 1:length(frs))
 {lines(frs[[pf]]$t,frs[[pf]]$data,lwd=plt_lwd*ps,col=colors[pf])}
if (out==4){for(pf in 1:length(frs))
{errbar(frs[[pf]]$t,frs[[pf]]$data,
  frs[[pf]]$data+ cldat[pf], frs[[pf]]$data- cldat[pf],
  add = TRUE, errbar.col="red")}}
legend("topright",legend=plt_title[fwi:fwii],col=colors,
 lwd=plt_lwd*ps, cex=plt_lab*ps-4)
dev.off()}
plot_wwss_cond <- function(frs,out,cldat,ssl,xl,wssc){
windows()
par(mar = plt_mar, mgp=plt_mgp)
title <- paste("Wastewater Conductivity Suite ",ssl)
switch(out,
title <- title,
title <- paste(title," - SOR"),
```

```
title <- paste(title," - LPF"),
title <- paste(title," - CI"))
ymax <- 0
ymin <- 0
n <- length(frs)
qual_col_pals = brewer.pal.info[brewer.pal.info$category == 'qual',]
col_vector = unlist(mapply(brewer.pal,
 qual_col_pals$maxcolors, rownames(qual_col_pals)))
colors <- sample(col_vector, n)
for(ym in 1:length(frs)){if (max(frs[[ym]]$data) > ymax){ymax <- max(frs[[ym]]$data)}}
for(ym in 1:length(frs)){if (min(frs[[ym]]$data) < ymin){ymin <- min(frs[[ym]]$data)}}
plot(frs[[1]]$t, frs[[1]]$data,xlim=c(0,max(frs[[1]]$t)),xlab=xl,
ylim=c(ymin*1.25,ymax*1.25),ylab= "Normalized Conductivity",main= title,
cex.lab=plt_lab, cex.axis=plt_axs,
  cex.main=plt_man, cex.sub=plt_sub, panel.first=grid(lwd=plt_lwd))
for(pf in 1:length(frs)){lines(frs[[pf]]$t,frs[[pf]]$data,lwd=plt_lwd,
 col=colors[pf])}
if (out==4){for(pf in 1:length(frs))
{errbar(frs[[pf]]$t,frs[[1]]$data,
  frs[[pf]]$data+ cldat[pf], frs[[pf]]$data- cldat[pf],
  add = TRUE, errbar.col="red")}}
legend("topright",legend=plt_title[seq(from=wwii,
 to=length(dl)-1,by=2)],col=colors,lwd=plt_lwd)
png(paste(paste(loc,"\\graphs\\",sep=""), title, ".png"), width = wd, height = ht)
par(mar = plt_mar*ps, mgp=plt_mgp*ps)
plot(frs[[1]]$t, frs[[1]]$data,xlim=c(0,max(frs[[1]]$t)),xlab=xl,
ylim=c(ymin*1.25,ymax*1.25),ylab= "Normalized Conductivity",main= title,
cex.lab=plt_lab*ps, cex.axis=plt_axs*ps,
  cex.main=plt_man*ps, cex.sub=plt_sub*ps, panel.first=grid(lwd=plt_lwd*ps))
for(pf in 1:length(frs))
```

```
 {lines(frs[[pf]]$t,frs[[pf]]$data,col=colors[pf],lwd=plt_lwd*ps)}
if (out==4){for(pf in 1:length(frs))
{errbar(frs[[pf]]$t,frs[[pf]]$data, frs[[pf]]$data+
  cldat[pf], frs[[pf]]$data- cldat[pf], add = TRUE, errbar.col="red")}}
legend("topright",legend=plt_title
 [seq(from=wwii,to=length(dl)-1,by=2)],col=colors,lwd=plt_lwd*ps,cex=plt_lab*ps-4)
dev.off()}
plot_wwss_uv <- function(frs,out,cldat,ssl,xl,wssc){
windows()
par(mar = plt_mar, mgp=plt_mgp)
title <- paste("Wastewater UV Suite ",ssl)
switch(out,
title <- title,
title <- paste(title," - SOR"),
title <- paste(title," - LPF"),
title <- paste(title," - CI"))
ymax <- 0
ymin <- 0
n <- length(frs)
qual_col_pals = brewer.pal.info[brewer.pal.info$category == 'qual',]
col_vector = unlist(mapply(brewer.pal,
 qual_col_pals$maxcolors, rownames(qual_col_pals)))
colors <- sample(col_vector, n)
for(ym in 1:length(frs)){if (max(frs[[ym]]$data) > ymax){ymax <- max(frs[[ym]]$data)}}
for(ym in 1:length(frs)){if (min(frs[[ym]]$data) < ymin){ymin <- min(frs[[ym]]$data)}}
plot(frs[[1]]$t, frs[[1]]$data,xlim=c(0,max(frs[[1]]$t)),xlab=xl,
ylim=c(ymin*1.25,ymax*1.25),ylab= "Normalized Absorbance",main= title,
cex.lab=plt_lab, cex.axis=plt_axs, cex.main=plt_man,
  cex.sub=plt_sub, panel.first=grid(lwd=plt_lwd))
for(pf in 1:length(frs)){lines(frs[[pf]]$t,frs[[pf]]$data,
```

```
 col=colors[pf],lwd=plt_lwd)}
if (out==4){for(pf in 1:length(frs))
{errbar(frs[[pf]]$t,frs[[1]]$data,
  frs[[pf]]$data+ cldat[pf], frs[[pf]]$data- cldat[pf],
  add = TRUE, errbar.col="red")}}
legend("topright",legend=plt_title[seq(from=wwii+1,
 to=length(dl),by=2)],col=colors,lwd=plt_lwd)
png(paste(paste(loc,"\\graphs\\",sep=""), title, ".png"), width = wd, height = ht)
par(mar = plt_mar*ps, mgp=plt_mgp*ps)
plot(frs[[1]]$t, frs[[1]]$data,xlim=c(0,max(frs[[1]]$t)),xlab=xl,
ylim=c(ymin*1.25,ymax*1.25),ylab= "Normalized Absorbance",main= title,
cex.lab=plt_lab*ps, cex.axis=plt_axs*ps, cex.main=plt_man*ps,
  cex.sub=plt_sub*ps, panel.first=grid(lwd=plt_lwd*ps))
for(pf in 1:length(frs)){lines(frs[[pf]]$t,frs[[pf]]$data
 ,col=colors[pf],lwd=plt_lwd*ps)}
if (out==4){for(pf in 1:length(frs))
{errbar(frs[[pf]]$t,frs[[pf]]$data,
  frs[[pf]]$data+ cldat[pf], frs[[pf]]$data- cldat[pf], add = TRUE, errbar.col="red")}}
legend("topright",legend=plt_title[seq(from=wwii+1,to=length(dl),by=2)],col=colors,
 lwd=plt_lwd*ps,cex=plt_lab*ps-4)
dev.off()}
#
#PLOTTING RAW DATA-------------------------------------------------------------------
#
if (raw_plot == 1){
if(cals == 1){for(i in 1:2){if(i==1){plot_cal(dl[[i]]$t, dl[[i]]$data, 1, 1, 0, 1)}else
plot_cal(list(dl[[2]]$t,dl[[3]]$t,dl[[4]]$t),
list(dl[[2]]$data,dl[[3]]$data,dl[[4]]$data), 2, 1, 0, 1)}}}
if(flows == 1 && fmp == 1){plot_flows(dl[fwi:fwii],1,0)}
if(wssp == 1){plot_wwss_cond(dl[seq(from=wwii ,to=length(dl)-
```

```
 1,by=2)],1,0,wwsss,wwssxl,wwss)
  plot_wwss_uv(dl[seq(from=wwii +1,to=length(dl),by=2)],1,0,wwsss,wwssxl,wwss)}
if(tp == 1 || fmp == 1){for(i in 1:length(dl))
 {plot_data(dl[[i]]$t, dl[[i]]$data, i, 1, 0)}}}
#
#SAVING RAW DATA-------------------------------------------------------------------
#
for(i in 1:length(dl))
{write.csv(dl[[i]],file=paste(loc,"\\raw\\",
dat_nam[i],".csv",sep=""),row.names = FALSE)}
#
#SINGLE THOMPSON OUTLIER FOR RAW DATA----------------------------------------------
#
thom_out <- function(P,d_l,j,dat) { #Thompson outlier function
x <- d_l$data                    #Capturing Data Frame column into a vector
N <- length(x) #Number of sample points
tt <- qt(p=(1+P)/2,df=N-2)             #Student's t vaiariable
tau <- (tt*(N-1))/(sqrt(N*(N-2+tt^2)))  #Thompson tau variable
delta <- abs(x-mean(x)) #Outlier criteria baseline
delta_max <- tau*sd(x) #Outlier upper limit
x_out <- which(delta >= delta_max)      #Reporting dataset outliers index
if(dat == 0){cat('out:col-',j,'-id-',x_out,'\n')
return(d_l <- d_l[-c(x_out),])}       #Returning vector with outliers removed
else{return(length(x_out))}}             #Returning number of outliers detected
for(j in 1:length(dl)){
if(thom_out(P,dl[[j]],j,1)!= 0)             #If to detect outliers
dl[[j]] <- thom_out(P,dl[[j]],j,0)}       #Call function to remove
#
#SAVING OUTLIER REMOVED DATA-------------------------------------------------------
#
```

```
for(i in 1:length(dl))
{write.csv(dl[[i]],file=paste(loc,"\\outout\\",
dat_nam[i],".csv",sep=""),row.names = FALSE)}
#
#PLOTTING OUTLIER REMOVED DATA-------------------------------------------------------
#
if (outlier_plot == 1){
if(cals == 1){for(i in 1:2){if(i==1){plot_cal(dl[[i]]$t, dl[[i]]$data, 1, 2, 0, 1)}else
plot_cal(list(dl[[2]]$t,dl[[3]]$t,dl[[4]]$t),
list(dl[[2]]$data,dl[[3]]$data,dl[[4]]$data), 2, 2, 0, 1)}}}
if(flows == 1 && fmp == 1){plot_flows(dl[fwi:fwii],2,0)}
if(wssp == 1){plot_wwss_cond(dl[seq(from=wwii ,to=length(dl)-
 1,by=2)],2,0,wwsss,wwssxl,wwss)
  plot_wwss_uv(dl[seq(from=wwii +1,to=length(dl),by=2)],1,0,wwsss,wwssxl,wwss)}
if(tp == 1 || fmp == 1){for(i in 1:length(dl))
 {plot_data(dl[[i]]$t, dl[[i]]$data, i, 2, 0)}}}
#
#FILTERING DATA----------------------------------------------------------------------
#
for(fli in 1:length(dl)){
if(length(dl[[fli]]$t) == 0){}  # If null data set from outlier removal, do not filter
      else{
dl[[fli]]$data <- filter(dl[[fli]]$data, rep(1/fil[fli],fil[fli]),
 method = "convolution", sides = 2)
dl[[fli]] <- na.omit(dl[[fli]])}}
#
#SAVING FILTERED DATA----------------------------------------------------------------
#
for(i in 1:length(dl))
{write.csv(dl[[i]],file=paste(loc,"\\filtered\\",
```

```
dat_nam[i],".csv",sep=""), row.names = FALSE)}
#
#PLOTTING FILTERED DATA-----------------------------------------------------------------
#
if (filt_plot == 1){
if(cals == 1){for(i in 1:2){if(i==1){plot_cal(dl[[i]]$t, dl[[i]]$data, 1, 3, 0, 1)}else
plot_cal(list(dl[[2]]$t,dl[[3]]$t,dl[[4]]$t),
list(dl[[2]]$data,dl[[3]]$data,dl[[4]]$data), 2, 3, 0, 1)}}}
if(flows == 1 && fmp == 1){plot_flows(dl[fwi:fwii],3,0)}
if(wssp == 1){plot_wwss_cond(dl[seq(from=wwii ,to=length(dl)-1,by=2)],
 3,0,wwsss,wwssxl,wwss)
  plot_wwss_uv(dl[seq(from=wwii +1,to=length(dl),by=2)],3,0,wwsss,wwssxl,wwss)}
if(tp == 1 || fmp == 1){for(i in 1:length(dl)){if(length(dl[[i]]$t) == 0){}
 else{plot_data(dl[[i]]$t, dl[[i]]$data, i, 3, 0)}}}}
#
#CONFIDENCE LEVEL FOR OUTLIER REMOVED DATA----------------------------------------------
#
clc <- c()           #Creating confidence interval list
for(cli in 1:length(dl)){
if(length(dl[[cli]]$t) == 0){clc <- c(clc, 0)}
 # If null data set from outlier removal, do not add confidence intervals
      else{
cl <- 1.96*sqrt((quantile(dl[[cli]]$data, 0.5+qw[cli]/2) -
 quantile(dl[[cli]]$data,0.5- qw[cli]/2))^2 * (1 + se[cli])^2)
clc <- c(clc, cl)}}
#
#SAVING CONFIDENCE LEVEL DATA-----------------------------------------------------------
#
for(i in 1:length(dl))
{write.csv(clc[[i]],file=paste(loc, "\\filtered
```

```
\\",dat_nam[i],"_cl.csv",sep=""), row.names = FALSE)
 write.csv(clc[[i]],file=paste(loc, "\\outout
 \\",dat_nam[i],"_cl.csv",sep=""), row.names = FALSE)
 write.csv(clc[[i]],file=paste(loc, "\\raw
 \\",dat_nam[i],"_cl.csv",sep=""), row.names = FALSE)}
#
#PLOTTING CONFIDENCE INTERVAL DATA-----------------------------------------------------
#
if (cl_plot == 1){
if(cals == 1){for(i in 1:2){if(i==1)
 {plot_cal(dl[[i]]$t, dl[[i]]$data, 1, 4, 0, 1)}else {
plot_cal(list(dl[[2]]$t,dl[[3]]$t,dl[[4]]$t),
list(dl[[2]]$data,dl[[3]]$data,dl[[4]]$data), 2, 4, 0, 1)}}}
if(flows == 1 && fmp == 1){plot_flows(dl[fwi:fwii],4,clc[fwi:fwii])}
if(wssp == 1){plot_wwss_cond(dl[seq(from=wwii ,to=length(dl)-1,by=2)],
 4,0,wwsss,wwssxl,wwss)
  plot_wwss_uv(dl[seq(from=wwii +1,to=length(dl),by=2)],4,0,wwsss,wwssxl,wwss)}
if(tp == 1 || fmp == 1){for(i in 1:length(dl))
 {plot_data(dl[[i]]$t, dl[[i]]$data, i, 4, clc[i])}}}
```